

**CHARGE TRANSFER AND
DIPOLE FORMATION AT
METAL–ORGANIC INTERFACES**

Graduation committee:

prof. dr. J. L. Herek	University of Twente, chairwoman
prof. dr. P. J. Kelly	University of Twente, promotor
dr. G. Brocks	University of Twente, assistant promotor
prof. dr. ing. D. H. A. Blank	University of Twente
prof. dr. ir. H. J. W. Zandvliet	University of Twente
prof. dr. ir. P. W. M. Blom	RU Groningen
dr. P. A. Bobbert	TU Eindhoven
prof. dr. R. Coehoorn	Philips Research
prof. dr. R. A. de Groot	RU Nijmegen

This work was supported by the "Stichting voor Fundamenteel Onderzoek der Materie (FOM)", by the "Prioriteits Programma Materialenonderzoek (PPM)", by the "Nederlandse Organisatie voor Wetenschappelijk Onderzoek (NWO)", and by "NanoNed", a nanotechnology program of the Dutch Ministry of Economic Affairs.

Charge transfer and dipole formation at metal–organic interfaces

P. C. Rusu,

ISBN: 978-90-365-2554-1

Thesis University of Twente, Enschede.

Copyright © P. C. Rusu, 2007

Printed by GILDEPRINT, Enschede

Cover: The interface formed by a monolayer of PTCDA adsorbed on (111) metal surface of Ag.

**CHARGE TRANSFER AND
DIPOLE FORMATION AT
METAL–ORGANIC INTERFACES**

DISSERTATION

to obtain
the doctor's degree at the University of Twente,
on the authority of the rector magnificus,
prof. dr. W. H. M. Zijm,
on the account of the decision of the graduation committee,
to be publicly defended
on Thursday 25th of October 2007 at 15.00

by

Paul Constantin Rusu

born on April 3, 1979
in Cetate, Romania

This doctoral dissertation is approved by:

prof. dr. P. J. Kelly

promotor

dr. G. Brocks

assistant promotor

*This work is dedicated to my girlfriend Luiza
and to my family*

Contents

1	Introduction	1
1.1	Electronic structure of solids	1
1.2	Density Functional Theory (DFT)	3
1.3	Pseudopotential and plane waves approach	6
1.4	Schottky barrier heights at metal-organic interfaces	10
1.5	Thesis outline	14
	Bibliography	15
 Part I Interfaces formed by Self-assembled monolayers on noble metal surfaces		 17
2	Work functions of self-assembled monolayers on metal surfaces	19
	Bibliography	25
3	Surface dipoles and work functions of alkylthiolates and fluorinated alkylthiolates on Au(111)	27
3.1	Introduction	27
3.2	Theoretical section	29
3.3	Results	31
	3.3.1 Structures	31
	3.3.2 Work functions and surface dipoles	35
3.4	Analysis	37
3.5	Conclusions	40
	Bibliography	41
4	Dipole Formation at Interfaces of Alkylthiolate Self-assembled Mono- layers and Ag(111)	45
4.1	Introduction	45
4.2	Theoretical section	47
	4.2.1 Total energy calculations	47

4.2.2	Work functions and interface dipoles	48
4.3	Influence of packing density	50
4.3.1	Structures	50
4.3.2	Work functions and interface dipoles	55
4.4	Summary and conclusions	61
	Bibliography	62
Part II	Interfaces formed by	
	π-conjugated organic monolayers on metal surfaces	65
5	Work function pinning at metal-organic interfaces	67
	Bibliography	74
6	Charge transfer and dipole formation at interfaces between metals	
	and aromatic molecules	77
6.1	Introduction	77
6.2	Computational details	80
6.3	PTCDA	81
6.3.1	Structure of adsorbed monolayers	82
6.3.2	Work functions	86
6.4	Benzene and perylene	88
6.5	Discussion	90
6.5.1	Density of states	90
6.5.2	Charge transfer and interface dipole	95
6.5.3	Model	98
6.6	Summary and conclusions	101
	Bibliography	101
	Summary	107
	List of publications	111
	Acknowledgments	113
	Curriculum Vitae	115

Chapter 1

Introduction

The topic of the thesis is focused on charge injection barriers (Schottky barriers) between metal electrodes and organic materials for use in electronic devices based on organic semiconductors. The thesis encompasses a computational and theoretical study of metal-organic interfaces using electronic structure calculations. In this chapter, some background of the computational method is briefly presented, namely density functional theory using the pseudopotential and plane waves approach. The importance of injection barriers at metal organic interfaces is demonstrated by describing the functionality of an organic light-emitting device, where efficient charge injection is of paramount importance in the device stability and performance.

1.1 Electronic structure of solids

Any solid of macroscopic dimensions contains a large number of atomic nuclei and electrons. The behavior of electrons determine most of the properties of solids. Thus, an important goal of condensed matter theory is the calculation of the electronic properties in solids. It is not only helpful in interpreting experiments, but also to design new molecules and materials and to predict their properties before actually synthesizing them. Moreover, a computational simulation can also provide data on atomic scale properties that are inaccessible experimentally.

The behavior of a system of N electrons in a solid can be predicted by solving the many-body Schrödinger equation:

$$\hat{H}\psi = E\psi, \quad (1.1)$$

where $\psi(\mathbf{r}_1, \mathbf{r}_2, \dots, \mathbf{r}_N)$ is the many-body electron wave function. It is anti-symmetric in order to satisfy the Fermi statistics of electrons. The Hamiltonian is given by the equation:

$$\hat{H} = -\frac{\hbar^2}{2m} \sum_i \nabla_{\mathbf{r}_i}^2 + V_{ext}(\{\mathbf{r}_i\}) + \sum_{i \neq j} \frac{e^2}{|\mathbf{r}_i - \mathbf{r}_j|}, \quad (1.2)$$

where the first term in the Hamiltonian describes the kinetic energy of the system, V_{ext} describes the Coulomb interaction between the electrons and a given configuration of nuclei and the last term gives the electron-electron Coulomb interaction. Analytic solution of the Schrödinger equation is possible only for few simple systems, whereas numerically exact solutions can be found for a small number of atoms and molecules.

A straightforward separation of the many-body wave function would make the solution of the problem simple computationally, but it neglects the complicated effects of the interactions between the electrons. Such scheme was introduced by Hartree [1] who approximated the many-electron wave function by a product of single particle wave functions:

$$\psi(\mathbf{r}_1, \mathbf{r}_2, \dots, \mathbf{r}_N) = \psi_1(\mathbf{r}_1) \cdot \psi_2(\mathbf{r}_2) \cdot \dots \cdot \psi_N(\mathbf{r}_N), \quad (1.3)$$

where each of the single electron wave functions is satisfying a one-electron Schrödinger equation

$$\left[-\frac{\hbar^2}{2m}\nabla^2 + V_{ext} + V_H^{(i)}\right]\psi_i(\mathbf{r}) = \epsilon_i\psi_i(\mathbf{r}), \quad (1.4)$$

where $V_H^{(i)}$ is the Hartree potential of the i -th electron and is given by the expression:

$$V_H^{(i)} = e^2 \int \frac{\rho^{(i)}(\mathbf{r}')d^3\mathbf{r}'}{|\mathbf{r}' - \mathbf{r}|}, \quad (1.5)$$

and the density ρ is given by:

$$\rho^{(i)}(\mathbf{r}) = \sum_{\substack{j=1 \\ i \neq j}}^N |\psi_j(\mathbf{r})|^2, \quad (1.6)$$

with the sum over the N lowest one-electron energy states. The Hartree approximation describes the electron as interacting only with the field obtained by averaging over the position of the remaining electrons. The Hartree potential replaces the electron-electron interaction and the many-electron wave function is given by the product of the one-electron wave functions, eq. (1.3). One has to solve these equations by iteration until self-consistency is reached, since the Hartree potential determines the one-electron wave functions through eq. (1.4) and the charge distribution is given by the same wave functions through eq. (1.6). In practice, one starts by guessing the electron density ρ and then constructing the Hartree potential $V_H^{(i)}$ for each electron through eq. (1.5). Once the Hartree potential is known, the Schrodinger equation can be solved for each of the electrons using eq. (1.4) and the one-electron wave functions determined. Using eq. (1.6) the electron density is reevaluated. The procedure continues until further iterations do not change the electronic density. In practice a convergence parameter is introduced. The iteration stops if the difference in total energies between two successive cycles drops below the value of this parameter. The parameter determines the accuracy of the calculation. The procedure described above is rather general, and is known as the self consistent field procedure (SCF). It applies also to the Hartree-Fock approximation or density functional theory described below.

Fock [2] showed that the Hartree approximation neglects an important contribution arising from the anti-symmetry of the many-electron wave functions which is called exchange. The wave function must be anti-symmetric under the exchange of any 2 electrons because the electrons are fermions. This is called Hartree-Fock approximation (HFA) and leads to an additional, non-local exchange term in the Schrödinger equation, replacing the product wave function by a single determinantal wave function:

$$\left[-\frac{\hbar^2}{2m}\nabla^2 + V_{ext} + V_H^{(i)}\right]\psi_i(\mathbf{r}) + \int V_x(\mathbf{r}, \mathbf{r}')\psi_i(\mathbf{r}')d^3\mathbf{r}' = \epsilon_i\psi_i(\mathbf{r}) \quad (1.7)$$

and

$$\psi(\mathbf{r}_1, \mathbf{r}_2, \dots, \mathbf{r}_N) = \frac{1}{\sqrt{N!}}\det[\psi_1(\mathbf{r}_1) \cdot \psi_2(\mathbf{r}_2) \cdots \psi_N(\mathbf{r}_N)], \quad (1.8)$$

which is an anti-symmetrized product of the one-electron wave functions. Moreover, the electron-electron interactions cause additional energy terms besides those described by the HFA, called correlation energy. As an electron moves, the other electrons "feel" its Coulomb potential, experience a force field and move in response. Hence the motion of the electrons is correlated.

With the use of modern computers, the Hartree-Fock equations can be solved for systems consisting of tens of atoms. The computational efficiency can be increased by using density functional theory, which enables calculations on systems that are larger by at least an order of magnitude.

1.2 Density Functional Theory (DFT)

Density functional theory was formulated by Hohenberg and Kohn [3]. They introduced the concept of electronic density $\rho(\mathbf{r})$ as a basic variable and proved that the total energy of an electron gas, including exchange and correlation, is a unique functional of the electron density:

$$E[\rho(\mathbf{r})] = F[\rho(\mathbf{r})] + \int V_{ext}(\mathbf{r})\rho(\mathbf{r})d^3\mathbf{r}, \quad (1.9)$$

where $F[\rho(\mathbf{r})]$ is a universal functional. The universal functional can be expressed in terms of kinetic energy T , Hartree energy E_H due to Coulomb electron-electron interaction and E_{XC} , which comes from non-classical electron-electron interaction and represents the exchange-correlation energy:

$$F[\rho(\mathbf{r})] = T[\rho(\mathbf{r})] + E_H[\rho(\mathbf{r})] + E_{XC}[\rho(\mathbf{r})]. \quad (1.10)$$

The minimum of the functional with respect to $\rho(\mathbf{r})$ gives the ground state energy of the system. In this form DFT is of little practical use since the functional is not known. Later Kohn and Sham [4] supposed that there exists a non-interacting reference system with the Hamiltonian described by:

$$\hat{H}_S = \sum_{i=1}^N \left[-\frac{\hbar^2}{2m}\nabla_i^2 + V_{eff}(\mathbf{r}_i)\right], \quad (1.11)$$

where the effective potential V_{eff} is given by:

$$V_{eff}(\mathbf{r}_i) = V_{ext}(\mathbf{r}_i) + V_H(\mathbf{r}_i) + V_{XC}(\mathbf{r}_i), \quad (1.12)$$

for which the ground state density is exactly $\rho(\mathbf{r})$ of the true interacting system. For this system there will be an exact determinantal ground-state wave function

$$\phi(\mathbf{r}_1, \mathbf{r}_2, \dots, \mathbf{r}_N) = \frac{1}{\sqrt{N!}} \det[\phi_1(\mathbf{r}_1) \cdot \phi_2(\mathbf{r}_2) \cdot \dots \cdot \phi_N(\mathbf{r}_N)], \quad (1.13)$$

where ϕ_i are the lowest eigenstates of the one electron Hamiltonian \hat{H}_S satisfying

$$\hat{H}_S \phi_i = \varepsilon_i \phi_i, \quad (1.14)$$

and the ground state electron density given by:

$$\rho(\mathbf{r}) = \sum_{i=1}^N |\phi_i(\mathbf{r})|^2 \quad (1.15)$$

The Kohn-Sham equations represent a mapping of the interacting many-electron system onto a system of non interacting electrons moving in an effective potential due to the other electrons. The Kinetic energy

$$T_S = - \sum_{i=1}^N \frac{\hbar^2}{2m} \int \phi_i^* \nabla^2 \phi_i d^3 \mathbf{r} \quad (1.16)$$

is not equal to the true electronic kinetic energy of the system, but it is of similar magnitude and it can be computed exactly. The Hartree energy is given by expression:

$$E_H = \frac{e^2}{2} \iint \frac{\rho(\mathbf{r})\rho(\mathbf{r}')}{|\mathbf{r} - \mathbf{r}'|} d^3 \mathbf{r} d^3 \mathbf{r}'. \quad (1.17)$$

Until now, the terms in the total energy have been defined to be exact. An exact expression for the exchange and correlation energy E_{XC} , which accounts for the difference between $T_S + E_H$ and the true functional F , is unknown however and here approximations have to be made. The operator \hat{H}_S defined by eq. (1.11) and eq. (1.12) is called the Kohn-Sham Hamiltonian and its eigenvalues ε_i and eigenstates ϕ_i do not represent the elementary excitations and single-electron wave functions respectively. They are auxiliary quantities used to determine the ground state energy of the system. The eigenvalues contribute to the ground state energy through the following expression:

$$E = \sum_{i=1}^N \varepsilon_i - \frac{e^2}{2} \iint \frac{\rho(\mathbf{r})\rho(\mathbf{r}')}{|\mathbf{r} - \mathbf{r}'|} d^3 \mathbf{r} d^3 \mathbf{r}' - \int V_{XC}(\mathbf{r})\rho(\mathbf{r})d^3 \mathbf{r} + E_{XC}(\mathbf{r}), \quad (1.18)$$

with

$$V_{XC}(\mathbf{r}) = \frac{\delta E_{XC}[\rho]}{\delta \rho(\mathbf{r})}. \quad (1.19)$$

As described above, the only approximation in the Kohn-Sham equations refer to the exchange and correlation energy functional. An improvement to E_{XC} will lead to a better prediction of ρ and the ground-state energy E . In solid state calculations, the most common approximation to E_{XC} is the local density approximation (LDA) [4] given by:

$$E_{XC}^{(LDA)} = \int \varepsilon_{XC}(\rho(\mathbf{r}))\rho(\mathbf{r})d^3\mathbf{r}, \quad (1.20)$$

where $\varepsilon_{XC}(\rho(\mathbf{r}))$ is the exchange-correlation energy per electron of a uniform electron gas of density ρ . ε_{XC}^{LDA} is usually split in two parts, the exchange part and the correlation part $\varepsilon_{XC}^{LDA} = \varepsilon_X^{LDA} + \varepsilon_C^{LDA}$. The exchange energy density of the uniform electron gas is an exact quantity, given by equation:

$$\varepsilon_X^{LDA}(r_s) = -\frac{3}{4\pi} \frac{(9\pi/4)^{1/3}}{r_s}, \quad (1.21)$$

where $r_s = (\frac{3\rho}{4\pi})^{1/3}$. An analytical expression of the correlation energy density is now known. Ceperley and Alder [5] performed accurate quantum Monte Carlo calculations on the electron gas. The results were fitted to a parametrized expression by Perdew and Zunger, for instance [6]. Although LDA is expected to be valid for systems in which the charge density is slowly varying, experience has shown that LDA gives good results for a large variety of systems. Other examples of exchange and correlation functionals widely used today are the generalized gradient approximation (GGA) [7] which takes into account the gradient of the density at the same coordinate

$$E_{XC}^{GGA}(\rho(\mathbf{r})) = \int f(\rho(\mathbf{r}), \nabla(\rho(\mathbf{r})))\rho(\mathbf{r})d^3\mathbf{r}. \quad (1.22)$$

Hybrid functionals, which are a linear combination of the Hartree-Fock exchange (E_X^{HF}) and LDA/GGA functionals, are commonly used by the chemistry community. An example is the B3LYP functional [8, 9]

$$E_{XC}^{B3LYP} = E_{XC}^{LDA} + a_0(E_X^{HF} - E_X^{LDA}) + a_x(E_X^{GGA} - E_X^{LDA}) + a_c(E_C^{GGA} - E_C^{LDA}), \quad (1.23)$$

where $a_0 = 0.20$, $a_x = 0.72$ and $a_c = 0.81$ are the three empirical parameters.

DFT as summarized above is strictly a ground state formalism. In particular, the DFT eigenvalues ε_i formally do not represent electronic excitations. If they are nevertheless interpreted as such, one finds for instance that LDA or GGA calculations severely underestimate the band gaps of semiconductors and insulators. The eigenvalue spectrum can be calculated properly using Green function techniques and the *GW* approximation to the electronic self-energy [10].

The work done in the last decades proved that DFT describes well the ground state properties of the systems. The results obtained using these functionals are sufficiently accurate for most of many systems, but there is no systematic way of improving them. The current DFT approach does not estimate the error of the calculations without comparing the results to other methods or experiment. It is then important to have a direct comparison with experimental studies.

1.3 Pseudopotential and plane waves approach

In this section a short description of the pseudopotential and plane waves formalism is presented, for use in electronic properties calculations of solids. We make use of the simplest pseudopotentials, Troullier-Martins norm-conserving pseudopotentials, to explain the principles behind the pseudopotential approach.

Bloch's theorem states that whatever the complicated form of the effective potential is, eq. (1.12), if the crystal is perfectly periodic, the potential has a lattice periodicity $U(\mathbf{r}) = U(\mathbf{r} + \mathbf{R})$ and the eigenstates of the one electron Hamiltonian can be chosen to have the form:

$$\psi_{\mathbf{k}}^n(\mathbf{r}) = e^{i\mathbf{k}\mathbf{r}} u_{\mathbf{k}}^n(\mathbf{r}), \quad (1.24)$$

for all \mathbf{R} , where \mathbf{R} is a lattice vector and $u_{\mathbf{k}}^n(\mathbf{r})$ is a function which has periodicity of the lattice: $u_{\mathbf{k}}^n(\mathbf{r}) = u_{\mathbf{k}}^n(\mathbf{r} + \mathbf{R})$. The wave function $\psi_{\mathbf{k}}^n$ then has the property:

$$\psi_{\mathbf{k}}^n(\mathbf{r} + \mathbf{R}) = e^{i\mathbf{k}\mathbf{R}} \psi_{\mathbf{k}}^n(\mathbf{r}), \quad (1.25)$$

with wave vector \mathbf{k} real. The index n that appears in Bloch's theorem stands for the band index, because for each of the \mathbf{k} vectors there are many solutions to the Schrödinger equation. Making use of the form of the eigenstates given by eq. (1.24) in eq. (1.14) a new set of equations for $u_{\mathbf{k}}^n(\mathbf{r})$ is found for each of the wave vectors \mathbf{k} . Thus the problem of studying, for instance, a system of an infinite number of electronic wave functions is mapped onto solving a finite number of bands at an infinite number of \mathbf{k} points. However, the electronic wave functions at \mathbf{k} points that are very close together are almost identical, thus many integrals are approximated by a finite number of \mathbf{k} points.

In order to solve the Kohn-Sham equations (1.14) numerically, one needs to represent the wave functions ϕ_i on some basis set. In principle all basis sets give the same accuracy if they are complete. The main basis sets used in calculations are: localized atomic orbitals and plane waves. Mathematically and numerically a plane wave basis set formalism is one of the easiest to implement for a crystal. However, expanding the oscillatory core wave functions (see Fig. 1.1) into plane waves needs a very large number (i.e. thousands) of plane waves. For this reason, a plane wave basis set is used only in combination with pseudopotentials, which reduces the number of plane waves required to represent the wave function substantially, to about ~ 100 per bulk atom. This number is roughly 10 times larger than that used to represent the wave function using localized atomic orbitals.

The electrons in atoms are divided into two types: core and valence electrons. It is well known that most properties of a solid depend on the valence electrons, the core electron wave functions remaining unchanged when placed into a different chemical environment. The atomic orbitals are more used for systems describing nearly localized core electrons whereas the plane waves and pseudopotential method is more appropriate to nearly free valence electrons.

A major contribution to the pseudopotentials and plane wave method was given by Troullier and Martins in 1991 by generating smooth norm-conserving pseudopotentials [11]. In the pseudopotential approach only the valence electrons are treated

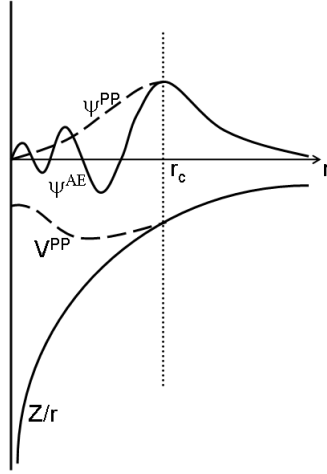


Figure 1.1: Schematic representation of the pseudopotential and the pseudo-wave function (dashed lines) as compared to all-electron potential and wave function (solid lines). Indicated is the r_c cutoff radius beyond which the pseudo and all electron potentials and wave functions coincide.

explicitly, the core electrons are included with the nucleus. The norm-conserving pseudopotentials are constructed such that they satisfy four general conditions:

a) The valence pseudo wave functions generated from the pseudopotentials are altered within a chosen cutoff radius r_c to remove all the nodes (see Fig. 1.1). The smaller the radius size the greater the transferability of the pseudopotential to different chemical environments. Nevertheless, this affects the smoothness of the pseudopotential. A typical value of the cutoff radius ranges from one to two core radius distances of the atom. Moreover one has to keep in mind that the cutoff radius of neighboring atoms in the crystal must not overlap.

b) The radial pseudo wave functions (PP) and all electron wave functions (AE) must coincide beyond the chosen cutoff r_c (see Fig. 1.1).

$$R_l^{PP}(r) = R_l^{AE}, \text{ for } r \geq r_c. \quad (1.26)$$

c) The charge enclosed within the radius r_c for the two wave functions must be equal:

$$\int_0^{r_c} |R_l^{PP}(r)|^2 r^2 dr = \int_0^{r_c} |R_l^{AE}(r)|^2 r^2 dr. \quad (1.27)$$

d) The valence all-electron and pseudopotential eigenvalues must be equal:

$$\varepsilon_l^{PP} = \varepsilon_l^{AE}. \quad (1.28)$$

In practice, the pseudopotential is constructed as follows:

- An all electron DFT calculation using a given form of the exchange and correlation

density functional is performed solving the radial Schrodinger equation for an isolated atom. This provides the all electron valence wave functions and eigenvalues.

$$\left[-\frac{1}{2} \frac{d^2}{dr^2} + \frac{l(l+1)}{2r^2} + V[\rho; r] \right] rR_{nl}(r) = \varepsilon_{nl} rR_{nl}(r), \quad (1.29)$$

where R_{nl} are the radial wave functions.

- The radial pseudo wave function is constructed inside the cutoff radius so that it satisfies condition (a).

Troullier and Martins proposed the following expression of the pseudo wave function:

$$R_l^{PP}(r) = \begin{cases} R_l^{AE} & , r \geq r_c \\ r^{l \text{exp}[p(r)]} & , r < r_c \end{cases},$$

with the polynomial $p(r)$ having the following form:

$$p(r) = c_0 + c_2 r^2 + c_4 r^4 + c_6 r^6 + c_8 r^8 + c_{10} r^{10} + c_{12} r^{12}, \quad (1.30)$$

with 7 coefficients determined from 7 conditions regarding norm-conservation of charge within the core radius and the continuity of the pseudo wave function and its first four derivatives at core radius r_c .

- Next, the radial Schrödinger is inverted to determine the screened pseudopotential:

$$V_{scr,l}^{PP}(r) = \begin{cases} V^{AE} & , r \geq r_c \\ \varepsilon_l + \frac{l+1}{r} \frac{p'(r)}{2} + \frac{p''(r) + [p'(r)]^2}{2} & , r < r_c \end{cases}.$$

The screening from the valence electrons depends on the environment in which they are placed. The index l is used because the pseudopotential must reproduce the right phase shift when scattering at the core region. An ionic pseudopotential can be defined from the screened pseudopotential by subtracting the Hartree and the exchange-correlation potentials calculated from the valence pseudo wave functions:

$$V_{ion,l}^{PP}(r) = V_{scr,l}^{PP}(r) - V_H^{PP}(r) - V_{XC}^{PP}(r) \quad (1.31)$$

Each angular momentum component of the wave function will see a different potential so the pseudopotential is nonlocal with different projectors for each of the angular momentum components. The ionic pseudopotential operator is then given by:

$$\hat{V}_{ion}^{PP}(r) = V_{ion,local}^{PP}(r) + \sum_l V_{nonlocal,l}(r) \hat{P}_l, \quad (1.32)$$

where $V_{ion,local}^{PP}(r)$ is the local potential and $V_{nonlocal,l}(r) = V_{ion,l}^{PP} - V_{ion,local}^{PP}(r)$ is the nonlocal potential for angular momentum l and \hat{P}_l projects out the l -th angular momentum component from the wave function.

- The parameterized form of the pseudopotential is then adjusted so that the calculated pseudo wave functions and pseudo eigenvalues using the same exchange-correlation functional will coincide to the all-electron valence wave functions and valence eigenvalues outside the cutoff radius r_c (see (b) and (d)).
- The pseudopotential obtained in this way will be used for the atom placed in any environment.

The Kohn-Sham eigenstates are given by an expansion of plane waves at each \mathbf{k} point:

$$\Psi_{\mathbf{k}}^n(\mathbf{r}) = \sum_{\mathbf{G}} c_{\mathbf{k}}^n(\mathbf{G}) e^{i(\mathbf{k}+\mathbf{G})\mathbf{r}}, \quad (1.33)$$

where the sum is over the reciprocal lattice vectors \mathbf{G} and $c_{\mathbf{k}}^n$ are the coefficients of the plane wave Fourier expansion. In practice, the basis set is truncated. The coefficients of the plane waves with small kinetic energy are more important than those with a larger kinetic energy. For this reason a cutoff energy is defined as: $E_{cut} = \hbar \frac{|\mathbf{k}+\mathbf{G}|^2}{2}$ and only the \mathbf{G} vectors that have energy smaller than E_{cut} are used in calculations. Nevertheless, test calculations regarding the convergence of the calculations with respect to the cutoff energy need to be performed to validate the basis set.

The Schrodinger equation for a crystal using pseudopotentials and a plane wave basis set is written in reciprocal space as:

$$\sum_{\mathbf{G}'} H_{\mathbf{G}\mathbf{G}'}(\mathbf{k}) c_{\mathbf{k}}^n(\mathbf{G}') = \varepsilon c_{\mathbf{k}}^n(\mathbf{G}), \quad (1.34)$$

with the Hamiltonian matrix for the point \mathbf{k} in the Brillouin zone having the form:

$$H_{\mathbf{G}\mathbf{G}'}(\mathbf{k}) = \frac{1}{2} \delta_{\mathbf{G}\mathbf{G}'} |\mathbf{G} + \mathbf{k}|^2 + V_{local}(\mathbf{G} - \mathbf{G}') + \sum_l V_{nonlocal,l}(\mathbf{G} + \mathbf{k}, \mathbf{G}' + \mathbf{k}), \quad (1.35)$$

where the first term is the kinetic operator and V_{local} and $V_{nonlocal,l}$ are the local and nonlocal potential Fourier-transformed in reciprocal space.

Here we have described briefly general ideas behind the pseudopotential and plane waves method. Other known examples of pseudopotentials provided with modern DFT codes are: ultra-soft Vanderbilt (US-PP) [12] or projector-augmented wave (PAW) pseudopotentials [13, 14]. Generation of such pseudopotentials to suit each problem at hand is a complicated task. Moreover, it is preferable for large communities to make use of the same set of pseudopotentials to different problems because ill-behaved pseudopotentials can then be spotted and improved. In our calculations we use the PAW pseudopotentials provided with the Vienna ab-initio simulation package (VASP) code. Such pseudopotentials allow a considerable reduction of the number of plane waves per atom, generally 50 to 100 plane waves are required for a good description of bulk materials.

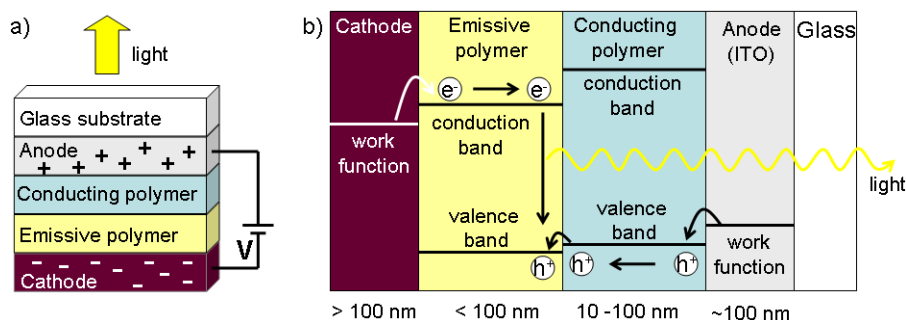


Figure 1.2: The OLED device; (a) the structure; (b) the energy diagram. Indicated are the work functions of the cathode and the anode and the valence and conduction bands of the polymers.

1.4 Schottky barrier heights at metal-organic interfaces

Recent developments in molecular electronics, where organic semiconductors constitute active layers in various electronic devices such as thin-film transistors [15, 16], solar cells [17], photovoltaic devices [18] or light-emitting diodes (LEDs) [19, 20] for use in flat panel applications are presently receiving great interest.

To highlight the importance of Schottky barriers or dipole formation at metal-organic interfaces, the functionality of a light emitting device is briefly presented. The active layers in such LEDs that are used in display applications can be made from organic molecules or polymers. They are called organic light emitting diodes (OLEDs) or polymer light emitting devices (polyLEDs). Figure 1.2 (a) shows the main parts of a polyLED. The following description also holds for OLEDs based on molecules, if one substitutes “polymer” by “molecule”.

A polyLED consists from a low work function cathode like Ba or Ca, a light emitting polymer, a hole transporting layer (PEDOT:PPS), a transparent anode (indium-tin oxide) and a glass substrate. Applying a small voltage across the device results in charge carriers that drift through the light-emitting polymer under the influence of the applied field. In the emissive polymer layer, charge carriers can recombine producing photons that are emitted through the transparent anode. The process occurs very many times per second and gives the device brightness. The type of the light-emitting polymer gives the color of the emitted light. Tailoring the material properties of the polymer through chemistry, light can be emitted in all colors of the spectrum. An alternative method can be used by adding a suitable dye to the polymer, or using multilayers of different light-emitting materials. In this way the light is emitted only from the dye and the color of the device can be tuned. Full color displays can be made from an array of such polyLEDs and the LED pixels can be accessed individually.

One of the critical points in the device performance is the interface between the metal contacts and the organic materials, whose properties determine the balance of

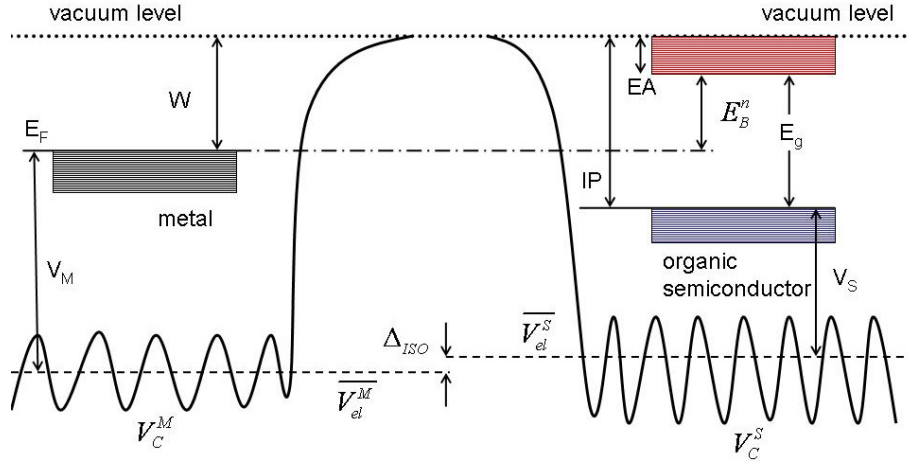


Figure 1.3: Schematic representation of an isolated metal and organic semiconductor. The electrostatic Coulomb energy potential of the metal and semiconductor V_C^M and V_C^S are aligned to a common vacuum level. The figure shows the n-type interface Schottky barrier E_B^n given by the Schottky-Mott rule.

electrons and holes injected into the device. Figure 1.2 (b) shows the energy level diagram of a polyLED device. For good charge injection at metal-organic interfaces, Ohmic behavior at these contacts is preferable. In practice energy barriers at interfaces are formed which influence the charge flow from metallic contacts into the organic materials. Thus, the energy level alignment of the semiconductor with respect to the metal Fermi level is of paramount importance. The n-type Schottky barrier of a metal organic interface is defined as the minimum energy required to extract an electron from the Fermi level of the metal and place it across the interface at the bottom of the conduction band of the semiconductor.

Figure 1.3 shows schematically the Coulomb electrostatic energy and the energy levels of a metal and a semiconductor far apart from each other.

Relevant quantities indicated in the figure are:

- the bulk reference energy of the metal V_M that we define as:

$$V_M = E_F + \overline{V}_{el}^M, \quad (1.36)$$

where E_F is the Fermi energy of the metal and \overline{V}_{el}^M is the long range average potential energy in the metal.

- the bulk reference energy of the semiconductor V_S that we define as:

$$V_S = E_{VB} + \overline{V}_{el}^S, \quad (1.37)$$

where E_{VB} is the energy of the top of the valence band and \overline{V}_{el}^S is the average potential energy in the semiconductor.

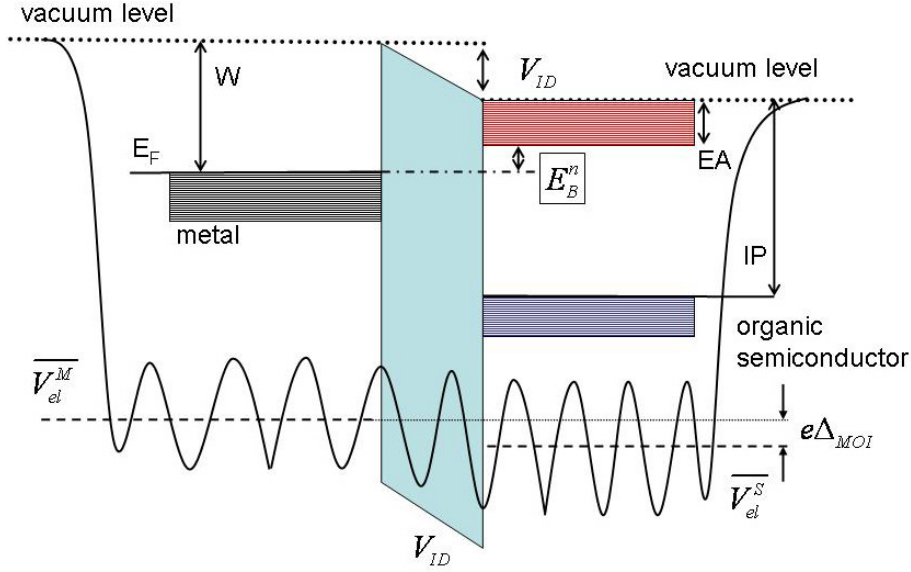


Figure 1.4: Schematic representation of a metal-organic interface. At the interface, charge redistribution takes place which creates an interface dipole layer that shifts the molecular levels with respect to the Fermi level of the metal, implicitly affecting the charge injection barrier.

- the metal surface work function W defined as the minimum energy to extract an electron from the metal far away into the vacuum.
- the electron affinity EA and ionization potential IP defined as the difference between the bottom of the conduction band, respectively the top of the valence band, with respect to the energy in the vacuum.

It was generally assumed that electronic properties at a metal-organic interface follow the simple rule of vacuum alignment, known as the Schottky-Mott rule:

$$E_B^n = W - EA, \quad (1.38)$$

or calculated with respect to the isolated bulk reference energy of the metal and the semiconductor:

$$E_B^n = (V_S + E_g) - V_M + \Delta_{ISO}, \quad (1.39)$$

with E_g the band gap energy of the semiconductor and Δ_{ISO} the difference between the average electrostatic energy in bulk metal and organic crystal, \overline{V}_{el}^M and \overline{V}_{el}^S respectively, with the two materials far apart from each other. Basically the rule states that when the materials are placed into contact no charge rearrangement is taking place. This idea was initially accepted for organic molecules since they are closed-shell molecules supposed not to undergo major modifications when interacting

with a metal surface. Experimentally, the work done on a variety of metal-organic interfaces in the last years proves the invalidity of the model [21–23].

At metal-organic interfaces the wave functions of the two parts interact with each other and new wave functions are produced at the interface region. This is shown schematically in Fig. 1.4. The electrostatic Coulomb potential at the interface is continuous and it satisfy the Poisson equation:

$$\nabla^2\Phi = 4\pi e^2\rho(r). \quad (1.40)$$

Due to the overlap of the metal and semiconductor wave functions, charge reordering takes place at the interface which produces an interface dipole layer that shifts the molecular energy levels with respect to the Fermi level of the metal.

Metal-organic interfaces are different from interfaces between metals and conventional semiconductors (such as Si) in the sense that band bending effects are rarely observed, at least on the thickness scale relevant to thin film devices (≤ 100 nm) and in nominally undoped layers [22]. Metal-organic interface dipoles are produced mainly between the top metal layer and the first organic monolayer [22, 24, 25]. Away from the interface specific region into the bulk, the long range average energy potential converges rapidly to the metal or semiconductor internal values \bar{V}_{el}^M and \bar{V}_{el}^S .

The n-type Schottky barrier is expressed by adding the effect of the interface dipole layer to the Schottky Mott expression in eq. (1.38), leading to:

$$E_B^n = W - EA - V_{ID}, \quad (1.41)$$

where V_{ID} represent the energy potential energy drop at the interface. Expressed in terms of internal reference energies of the metal and semiconductor, the Schottky barrier becomes:

$$E_B^n = (V_S + E_g) - V_M + \Delta_{ISO} - V_{ID} = (V_S + E_g) - V_M + \Delta_{MOI}, \quad (1.42)$$

where Δ_{MOI} is the difference between the long-range averaged internal energy of the metal and semiconductor after the contact is made.

In expression (1.41), besides the V_{ID} term, the other two quantities refer only to the isolated materials. Therefore in order to evaluate energy barriers at metal-organic interfaces, one has to evaluate the energy drop that takes place upon the deposition of the organic materials on top of metal surfaces. Since in many cases the interface dipole is localized at the metal-organic interface one can calculate the potential drop by monitoring the shift in the metal work function produced upon adsorption of a single molecular layer.

The thesis aims at understanding and modeling dipole formation and charge transfer at metal-organic interfaces.

1.5 Thesis outline

The thesis is organized into two main parts.

In **Part I** we focus on interfaces formed by strongly interacting systems, namely chemisorbed self-assembled monolayers (SAMs) on metal surfaces. We study short chain alkylthiolate molecules CH_3S , $\text{C}_2\text{H}_5\text{S}$ and partially fluorinated thiolate molecules CF_3S and $\text{CH}_2\text{CF}_3\text{S}$ on (111) noble surfaces of Ag, Au and Pt. Since such metals have the same crystal structure, namely face centered cubic (FCC) with similar surface lattice parameters, one would expect that such metal surfaces form SAMs that have similar structures. A good starting point is the $(\sqrt{3} \times \sqrt{3})\text{R}30^\circ$ structure used in **Chapter 2**. By varying the relative electronegativity of the surface and molecules, one can introduce electron transfer and create an interface dipole without rearranging the interface structure. The sign of the dipole moments of fluorinated alkylthiolate molecules is opposite to those of nonfluorinated ones. Therefore, modifying the molecular tails allows one to vary the size of the work function. The spread in the work functions of these SAMs on metal surfaces can be as large as 2 eV. A model based on bond and individual molecular dipoles is presented and can be used for the estimation of SAMs on metal surfaces work functions. **Chapters 3** and **4** focus on SAMs on Au(111) and Ag(111) respectively, by investigating several structures with different packing densities.

Motivated by the use of π -conjugated organic thin molecular layers in electronic devices, **Part II** is focused on interfaces formed by monolayers of PTCDA ($\text{C}_{22}\text{H}_8\text{O}_6$), perylene ($\text{C}_{20}\text{H}_{12}$) and benzene (C_6H_6) adsorbed on close-packed metal surfaces of Ca, Mg, Al, Ag and Au. The choice of these metal surfaces gives a substantially large spread in the work functions. Correlated to the different energy level position of the lowest unoccupied molecular orbital, which increases from benzene to PTCDA, they make up suitable systems to analyze dipole formation at interfaces. Such molecules are closed-shell molecules and moreover since they do not exhibit a permanent dipole moment, it is interesting to see that upon molecular adsorption, the work functions can be substantially altered. A qualitative model based on charge transfer is discussed in **Chapter 5** and, in more detail, in **Chapter 6**. We find that the size and the sign of the interface dipole produced upon molecular adsorption to be the result of two competing effects. In the presence of the molecular layer near the metal surface, Pauli repulsion between molecular and surface electrons leads to a compression of the electronic tail that spills from the metal surface into the vacuum. Electrons are pushed from the molecular region into the metal, implicitly creating an interface dipole which decreases the metal work function. The work functions can be also increased for interfaces where donation of electrons from the metal surface to the molecular levels occurs. **Chapter 5** and **6** treat interfaces formed by PTCDA and perylene monolayers on metal surfaces. In the last chapter, we evaluate the influence of packing density on the metal work function and we compare the work function results using LDA and GGA exchange and correlation functionals. The calculations are extended and compared to benzene monolayers adsorbed on metal surfaces.

Bibliography

- [1] D. R. Hartree, Proc. Cambridge Philos. Soc. **24**, 89 (1928).
- [2] V. Fock, Z. Phys. **61**, 126 (1930).
- [3] P. Hohenberg and W. Kohn, Phys. Rev. **136**, B864 (1964).
- [4] W. Kohn and L. J. Sham, Phys. Rev. **140**, A1133 (1965).
- [5] D. M. Ceperley and B. J. Alder, Phys. Rev. Lett. **45**, 566 (1980).
- [6] J. P. Perdew and A. Zunger, Phys. Rev. B **23**, 5048 (1981).
- [7] J. P. Perdew *et al.*, Phys. Rev. B **46**, 6671 (1992).
- [8] A. D. Becke, J.Chem. Phys **98**, 5648 (1993).
- [9] C. Lee, W. Yang, and R. G. Parr, Phys. Rev. B **37**, 785 (1988).
- [10] L. Hedin, Phys. Rev. **139**, A796 (1965).
- [11] N. Troullier and J. L. Martins, Phys. Rev. B **43**, 1993 (1991).
- [12] D. Vanderbilt, Phys. Rev. B **41**, 7892 (1990).
- [13] G. Kresse and D. Joubert, Phys. Rev. B **59**, 1758 (1999).
- [14] P. E. Blöchl, Phys. Rev. B **50**, 17953 (1994).
- [15] D. Gundlach, Y. Lin, T. Jackson, S. Nelson, and D. Schlom, IEEE Electron Device Lett. **18**, 87 (1997).
- [16] A. Tsumura, H. Koezuka, and T. Ando, Appl. Phys. Lett. **49**, 1210 (1986).
- [17] N. S. Sariciftci, L. Smilowitz, A. J. Heeger, and F. Wudl, Science **258**, 1474 (1992).
- [18] P. Peumans, S. Uchida, and S. R. Forrest, Nature **425**, 158 (2003).
- [19] C. W. Tang and S. A. VanSlyke, Appl. Phys. Lett. **51**, 913 (1987).
- [20] J. H. Burroughes *et al.*, Nature **347**, 539 (1990).
- [21] I. G. Hill, A. Rajagopal, A. Kahn, and Y. Hu, Appl. Phys. Lett. **73**, 662 (1998).
- [22] A. Kahn, N. Koch, and W. Gao, J. Polym. Sci. Part B **41**, 2529 (2003).
- [23] N. Koch, S. Duhm, J. P. Rabe, A. Vollmer, and R. L. Johnson, Phys. Rev. Lett. **95**, 237601 (2005).
- [24] N. J. Watkins, L. Yan, and Y. Gao, Appl. Phys. Lett **80**, 4384 (2002).
- [25] E. V. Tsiper, Z. G. Soos, W. Gao, and A. Kahn, Chem. Phys. Lett. **360**, 47 (2002).

Part I

Interfaces formed by
Self-assembled monolayers on
noble metal surfaces

Chapter 2

Work functions of self-assembled monolayers on metal surfaces

Using first-principles calculations we show that the work function of noble metals can be decreased or increased by up to 2 eV upon the adsorption of self-assembled monolayers of organic molecules. We identify the contributions to these changes for several (fluorinated) thiolate molecules adsorbed on Ag(111), Au(111) and Pt(111) surfaces. The work function of the clean metal surfaces increases in this order, but adsorption of the monolayers reverses the order completely. Bonds between the thiolate molecules and the metal surfaces generate an interface dipole, whose size is a function of the metal, but it is relatively independent of the molecules. The molecular and bond dipoles can then be added to determine the overall work function.

Recent advances in molecular electronics, where organic molecules constitute active materials in electronic devices, have created a large interest in metal organic interfaces [1]. Transport of charge carriers across the interfaces between metal electrodes and the organic material often determines the performance of a device [2]. Organic semiconductors differ from inorganic ones as they are composed of molecules and intermolecular forces are relatively weak. In a bulk material this increases the importance of electron-phonon and electron-electron interactions [3]. At a metal organic interface the energy barrier for charge carrier injection into the organic material is often determined by the formation of an interface dipole localized at the first molecular layer. The interface dipole can be extracted by monitoring the change in the metal surface work function after deposition of an organic layer [1, 4].

Atoms and molecules that are physisorbed on a metal surface usually decrease the work function, as the Pauli repulsion between the molecular and surface electrons decreases the surface dipole [5, 6]. Chemisorption can give an increase or

a decrease of the work function, and can even lead to counterintuitive results [7, 8]. Self-assembled monolayers (SAMs) are exemplary systems to study the effect of chemisorbed organic molecules upon metal work functions [9]. More specifically, alkylthiolate ($C_nH_{2n+1}S$) SAMs on the gold (111) surface are among the most extensively studied systems [10–14]. The sulphur atoms of the thiolate molecules form stable bonds to the gold surface and their alkyl tails are close packed, which results in a well ordered monolayer. SAMs with similar structures are formed by alkylthiolates on a range of other (noble) metal surfaces [10, 14, 15].

Often the change in work function upon adsorption of a SAM is interpreted mainly in terms of the dipole moments of the individual thiolate molecules, whereas only a minor role is attributed to the change induced by chemisorption [9, 11, 12, 16]. This assumption turns out to be reasonable for adsorption of methyl thiolate (CH_3S) on Au(111) [13], but for CH_3S on Cu(111) it is not [14]. In this chapter we apply first-principles calculations to study the interface dipoles and the work function change induced by adsorption of thiolate SAMs.

In particular, we analyze the contributions of chemisorption and of the molecular dipoles to uncover the effects of charge reordering at the interface. The chemical bonds between the thiolate molecules and the metal surfaces generate an interface dipole. We find that this dipole strongly depends upon the metal, but it is nearly independent of the electronegativity of the molecules. The size and direction of the interface dipole are such that it overcompensates for the difference between the clean metal work functions. This results in the SAM adsorbed on the highest work function metal having the lowest work function and vice versa. Modifying the molecular tails allows one to vary the absolute size of the work function over a range of more than 2 eV.

Since alkylthiolate molecules form SAMs with a similar structure on (111) surfaces of several noble metals, they are ideal model systems for studying metal organic interfaces. By varying the relative electronegativity of surface and molecules one can induce electron transfer and create an interface dipole, without completely rearranging the interface structure. The electronegativity of a metal substrate is given by its work function. We consider the (111) surfaces of three metals that have a substantially different work function, but the same crystal structure and a similar lattice parameter: Ag (4.5 eV, 2.89 Å), Au (5.3 eV, 2.88 Å) and Pt (6.1 eV, 2.77 Å).

One would also like to vary the molecule’s electronegativity without changing the structure of the SAM. This can be achieved by fluorinating the alkyl tails of thiolate molecules, which increases their electronegativity [10]. However, fluorinating the alkyl tails also reverses the polarity of the thiolate molecules and one has to separate this electrostatic effect from the charge reordering caused by chemisorption. In this chapter we study the short chain thiolates CH_3S , C_2H_5S , CF_3S , and CF_3CH_2S .

Density functional theory (DFT) calculations are carried out using the projector augmented wave (PAW) method [17, 18], a plane wave basis set and the PW91 generalized gradient approximation (GGA) functional, as implemented in the VASP program [19, 20]. We use supercells containing a slab of at least five layers of metal atoms with a SAM adsorbed on one side of the slab and a vacuum region of ~ 12 Å. The Brillouin zone of the $(\sqrt{3} \times \sqrt{3})R30^\circ$ surface unit cell is sampled by a 11×11

k-point grid. The plane wave kinetic energy cutoff is 450 eV. To avoid interactions between periodic images of the slab we apply a dipole correction [21]. The geometry of the SAM is optimized, as well as the positions of the top two layers of metal atoms. The atoms in the remaining metal layers are fixed at their bulk positions. The optimized bulk lattice parameters are 2.93, 2.94 and 2.79 Å for Ag, Au and Pt, respectively.

The work function is given by $W = V(\infty) - E_F$, where $V(\infty)$ is the asymptotic electrostatic potential in vacuum, and E_F is the Fermi energy of the bulk metal. $V(\infty)$ is extracted from the plane averaged potential $\bar{V}(z) = A^{-1} \iint_A V(x, y, z) dx dy$, with A the area of the surface unit cell. In practice, $\bar{V}(z)$ reaches an asymptotic value within a distance of 5 Å from the surface. Accurate values of the Fermi energy are obtained following the procedure outlined in Ref. [22]. By varying the computational parameters discussed above we estimate that the work functions are converged to within 0.05 eV. Typically DFT calculations give work functions that are within ~ 0.1 – 0.2 eV of the experimental values, although occasionally somewhat larger deviations are found.

The $(\sqrt{3} \times \sqrt{3})R30^\circ$ structure of CH_3S on Au(111) has been studied in several first-principles calculations [13, 14, 23–25]. We find basically the same optimized geometry as obtained in those calculations. Several structures exist that have a slightly different geometry, but are very close in energy, such as a $c(4 \times 2)$ superstructure [24]. We find that the work functions of these structures are within 0.1 eV of that of the simpler structure, so we will not discuss these superstructures here.

The $(\sqrt{3} \times \sqrt{3})R30^\circ$ structure is also a good starting point for studying other systems. Thiolates with longer alkyl tails on Au(111) adopt this structure, as does CH_3S on Pt(111), as well as alkylthiolates on Au(111) whose end groups are fluorinated [10, 15]. Thiolates with long alkyl tails on Ag(111) form a somewhat denser packing, whereas long fluorinated alkylthiolates form a somewhat less dense packing [10]. To analyze the work function we use optimized $(\sqrt{3} \times \sqrt{3})R30^\circ$ structures for all our SAMs. We find that varying the packing density only introduces a scaling factor to the work function change [13].

Table 2.1 lists the calculated work functions. The work functions of the clean Au and Ag surfaces agree with the experimental values [26, 27], but that of Pt is ~ 0.3 eV too low [28]. The latter can be attributed to the GGA functional. Using the local density approximation (LDA) the calculated work function of Pt(111) is 6.14 eV, which agrees with experiment. In other cases the difference between the work functions calculated with GGA and LDA functionals is much smaller. For

	clean	CH_3S	$\text{C}_2\text{H}_5\text{S}$	CF_3S	$\text{CF}_3\text{CH}_2\text{S}$
Ag	4.50	3.95	4.13	6.14	6.30
Au	5.25	3.81	3.93	5.97	6.27
Pt	5.84 (6.14 ^a)	3.45	3.47	5.68	5.87

Table 2.1: Calculated work functions W (eV) of clean (111) surfaces and of surfaces covered by SAMs in a $(\sqrt{3} \times \sqrt{3})R30^\circ$ structure. ^a LDA value.

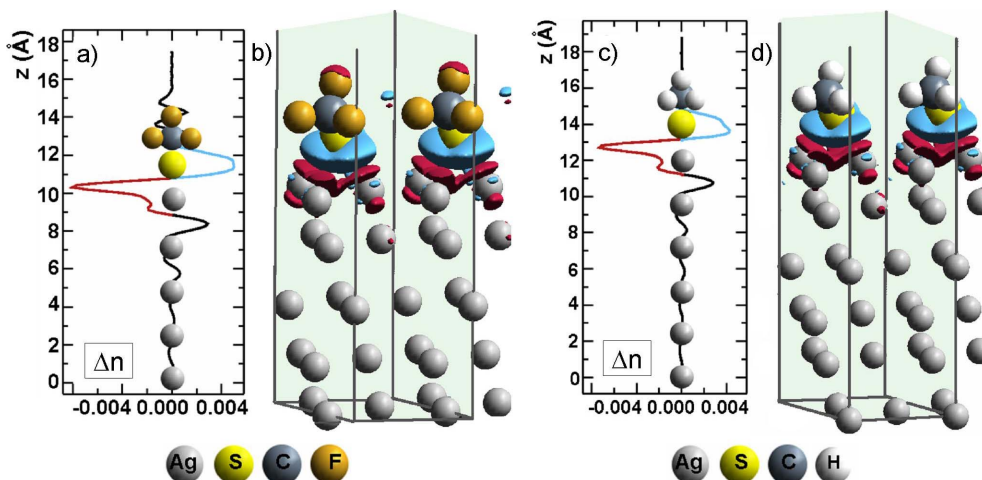


Figure 2.1: Difference electron density $\Delta n = n_{\text{tot}} - n_{\text{surf}} - n_{\text{SAM}}$ for CF₃S on Ag(111), (a) as function of z , averaged over the xy plane, in units of \AA^{-3} ; (b) as an isodensity surface; (c), (d) the same for CH₃S on Ag(111).

instance, the GGA and LDA work functions of the SAMs on Pt are within 0.02 eV of one another. We will use the GGA values throughout this chapter. The trend in the work functions of the SAM covered surfaces agrees well with experimental observations [9, 11, 12]. The experimental work function shifts with respect to the clean surface are sometimes somewhat smaller than the calculated ones [29].

The first observation one can make by comparing the numbers in Table 2.1 within columns is that on SAM covered surfaces the work function *decreases* in the order Ag, Au, Pt. This is striking, since the work function of the clean metal surfaces clearly *increases* in this order. Secondly, comparing the numbers within rows one finds that the work functions of the fluorinated alkylthiolate covered surfaces are 2 – 2.5 eV higher than of the non-fluorinated ones. We will argue that the first observation can be ascribed to the interface dipole formed upon chemisorption. This interface dipole is independent of the molecular tails. The second observation will be interpreted in terms of the individual molecular dipoles.

In order to visualize the charge reordering at the surface upon adsorption of the SAM, we calculate the difference electron density Δn . It is obtained by subtracting from the total electron density n_{tot} of the SAM on the surface, the electron density n_{surf} of the clean surface and that of the free standing SAM n_{SAM} . n_{surf} and n_{SAM} are obtained in two separate calculations of a clean surface and a free standing SAM, respectively, with their structures frozen in the adsorbed geometry. As an example, Fig. 2.1 shows Δn for SAMs of CF₃S and CH₃S on Ag(111).

Fig. 2.1 illustrates that Δn is localized mainly at the metal-SAM interface, i.e. near the sulphur atoms and the metal atoms in the first surface layers. In case of adsorption on Ag, electrons are transferred from the metal to the molecule, which

substrate		CH ₃ S	C ₂ H ₅ S	CF ₃ S	CF ₃ CH ₂ S
Ag	$\Delta\mu$	-0.32	-0.22	0.97	1.07
	μ_{SAM}	-0.88	-0.79	0.44	0.50
	μ_{chem}	0.56	0.57	0.53	0.57
Au	$\Delta\mu$	-0.86	-0.79	0.43	0.61
	μ_{SAM}	-0.88	-0.81	0.44	0.53
	μ_{chem}	0.02	0.02	-0.01	0.08
Pt	$\Delta\mu$	-1.28	-1.27	-0.08	0.02
	μ_{SAM}	-0.86	-0.80	0.37	0.47
	μ_{chem}	-0.42	-0.47	-0.45	-0.45

Table 2.2: Dipole per molecule $\Delta\mu$, from the change in work function upon adsorption. The (perpendicular) molecular dipole moment μ_{SAM} in a free standing SAM. The chemisorption dipole moment is $\mu_{\text{chem}} = \Delta\mu - \mu_{\text{SAM}}$. All values are in D.

results in an increase of the electron density on the sulphur atoms and a decrease on the surface metal atoms. The charge transfer does not depend strongly on the molecule, compare Figs. 2.1 (a,b) to (c,d). This is somewhat surprising since the electronegativity of CF₃S is much higher than that of CH₃S.

Very often a charge transfer between two systems is interpreted in terms of their relative electronegativity. For a metal surface the latter is simply the work function W_{clean} . For a molecule the Mulliken electronegativity χ_M is defined as the average of the ionization potential and the electron affinity and considered to be the molecular equivalent of a chemical potential [30]. We find $\chi_M = 5.4$ eV for the CH₃S and CH₃CH₂S molecules. Since χ_M is close to W_{clean} for Au(111), this would explain the lack of electron transfer upon adsorption of these molecules [13, 14]. However, the calculated χ_M for CF₃S and CF₃CH₂S are much higher, i.e. 6.9 eV and 6.1 eV, respectively. Yet this does not result in a markedly increased electron transfer to these molecules, as Fig. 2.1 indicates. It means that χ_M is not a generally suitable parameter to predict the amount of charge transfer between surface and molecules. χ_M reflects the relative stability of charged molecular states. In particular, for the thiolates χ_M reflects the ability of the (fluorinated) alkyl chains to stabilize or screen charge that resides on the sulphur atom. We suggest that this is not important in case of adsorbed molecules, as the metal surface takes over this role.

Meanwhile, Fig. 2.1 suggests the following analysis. From the change in the work function upon adsorption of the SAM, $\Delta W = W - W_{\text{clean}}$, see Table 2.1, one can obtain the change of the surface dipole upon adsorption, $\Delta\mu = \varepsilon_0 A \Delta W / e$ (with ε_0 the permittivity of vacuum and A the area of the surface unit cell). Since the unit cell contains one molecule, $\Delta\mu$ is the change in the surface dipole per adsorbed molecule. The results are shown in Table 2.2. $\Delta\mu$ contains contributions from the charge reordering at the interface due to chemisorption, as well as from the dipole moments of the individual molecules.

The latter can be accounted for by calculating the dipole moment μ_{SAM} per

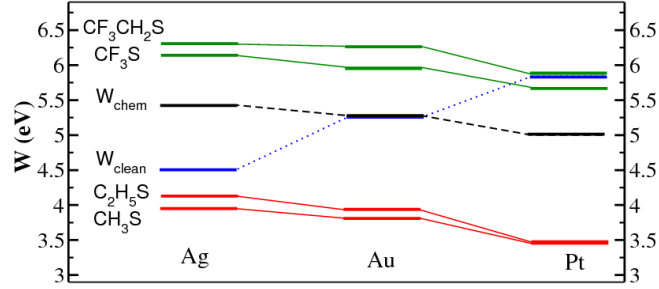


Figure 2.2: Work functions W_{clean} of the clean surfaces, W_{chem} of the surfaces including the chemisorption dipole, and of the SAM covered surfaces.

molecule of free standing SAMs, i.e. without the presence of a metal surface. We focus upon the component of the dipole that is perpendicular to the surface, since the other components do not contribute to the work function. As the calculation uses a full monolayer of molecules, it incorporates the effect on each molecule of the depolarizing field caused by the dipoles of all surrounding molecules. The calculated μ_{SAM} are given in Table 2.2. The structure of a SAM is fixed in its adsorption geometry, which is similar for the three metal surfaces. Therefore the μ_{SAM} values for adsorption on Ag, Au, and Pt in Table 2.2 differ only slightly. Of course μ_{SAM} depends upon the molecule. In CH_3S and $\text{CH}_3\text{CH}_2\text{S}$ the dipole points from the sulphur atom to the alkyl group. The large electronegativity of fluor causes a reversal of the dipole in CF_3S and $\text{CF}_3\text{CH}_2\text{S}$.

We define the contribution to the interface dipole resulting from chemisorption as $\mu_{\text{chem}} = \Delta\mu - \mu_{\text{SAM}}$. The results shown in Table 2.2 clearly demonstrate that μ_{chem} is nearly independent of the molecule and strongly dependent on the metal substrate. As an independent check we have also calculated the dipole on the basis of the electron density redistribution, see Fig. 2.1, $\mu_{\Delta n} = -e \iiint_{\text{cell}} z \Delta n(\mathbf{r}) dx dy dz$. We find that $\mu_{\Delta n} \approx \mu_{\text{chem}}$, which indicates the consistency of this analysis.

The results obtained allow for a simple qualitative picture. The chemisorption dipole μ_{chem} is very small for all SAMs on Au(111), indicating that the charge transfer between the Au surfaces and the molecules is small. This generalizes previous results obtained for methyl thiolate SAMs on Au(111) [13, 14]. Since the work function of Ag(111) is substantially lower than that of Au(111), a significant electron transfer takes place from the surface to the molecules for SAMs on Ag. This is confirmed by the values of μ_{chem} for Ag in Table 2.2. Fig. 2.1 shows that the electrons are transferred mainly to the sulphur atoms. Integrating the positive peak of Δn on the sulphur atom gives a charge of $(0.11 \pm 0.01)e$. The sign of the charge transfer is such that μ_{chem} increases the work function with respect to clean Ag(111). By a similar argument, since the work function of Pt(111) is much higher than that of Au(111), an electron transfer takes place from the molecules to the surface for adsorption on Pt. The values of μ_{chem} for Pt in Table 2.2 confirm this. In this case the net charge on the sulphur atom is positive and μ_{chem} decreases the work function with respect

to clean Pt(111).

The size of the charge transfer is remarkable. Chemisorption creates an interface dipole μ_{chem} that overcompensates for the difference between the metal work functions. We define a work function that includes the contribution from the chemisorption dipoles as $W_{\text{chem}} = W_{\text{clean}} + e\mu_{\text{chem}}/(\epsilon_0 A)$. The results shown in Fig. 2.2 demonstrate that W_{chem} decreases in the order Ag, Au and Pt, whereas W_{clean} increases in that order. The work function of the SAM covered surfaces can then be expressed as $W = W_{\text{chem}} + e\mu_{\text{SAM}}/(\epsilon_0 A)$. From the polarity of the molecules discussed above, it is clear that SAMs of CH_3S and $\text{CH}_3\text{CH}_2\text{S}$ decrease the work function, whereas SAMs of CF_3S and $\text{CF}_3\text{CH}_2\text{S}$ increase it.

Acknowledgments

We thank G. Giovannetti for the molecular calculations and B. de Boer, P. W. M. Blom and P. J. Kelly for very helpful discussions. This work is part of the research program of the "Stichting voor Fundamenteel Onderzoek der Materie" (FOM) and the use of supercomputer facilities was sponsored by the "Stichting Nationale Computer Faciliteiten" (NCF), both financially supported by the "Nederlandse Organisatie voor Wetenschappelijk Onderzoek" (NWO).

Bibliography

- [1] A. Kahn, N. Koch, and W. Gao, *J. Polym. Sci., Part B: Polym. Phys.* **41**, 2529 (2003).
- [2] V. D. Mihailetschi, L. J. A. Koster, and P. W. M. Blom, *Appl. Phys. Lett.* **85**, 970 (2004).
- [3] G. Brocks, J. van den Brink, and A. F. Morpurgo, *Phys. Rev. Lett.* **93**, 146405 (2004).
- [4] O. Tal, W. Gao, C. K. Chan, A. Kahn, and Y. Rosenwaks, *Appl. Phys. Lett.* **85**, 4148 (2004).
- [5] P. S. Bagus, V. Staemmler, and C. Wöll, *Phys. Rev. Lett.* **89**, 096104 (2002).
- [6] J. L. F. D. Silva, C. Stampfl, and M. Scheffler, *Phys. Rev. Lett.* **90**, 066014 (2003).
- [7] A. Michaelides, P. Hu, M.-H. Lee, A. Alavi, and D. A. King, *Phys. Rev. Lett.* **90**, 246103 (2003).
- [8] T. C. Leung, C. L. Kao, W. S. Su, Y. J. Feng, and C. T. Chan, *Phys. Rev. B* **68**, 195408 (2003).
- [9] I. H. Campbell *et al.*, *Phys. Rev. B* **54**, 14321 (1996).

- [10] F. Schreiber, *Prog. Surf. Sci.* **65**, 151 (2000).
- [11] D. M. Alloway *et al.*, *J. Phys. Chem. B* **107**, 11690 (2003).
- [12] B. de Boer, A. Hadipour, M. M. Mandoc, T. van den Woudenbergh, and P. W. M. Blom, *Adv. Mater.* **17**, 621 (2005).
- [13] V. D. Renzi *et al.*, *Phys. Rev. Lett.* **95**, 046804 (2005).
- [14] M. Konôpka, R. Rousseau, I. Štich, and D. Marx, *Phys. Rev. Lett.* **95**, 096102 (2005).
- [15] J. J. Lee *et al.*, *Surf. Sci.* **516**, 1 (2002).
- [16] G. Heimel, L. Romaner, J.-L. Brédas, and E. Zojer, *Phys. Rev. Lett.* **96**, 196806 (2006).
- [17] P. E. Blöchl, *Phys. Rev. B* **50**, 17953 (1994).
- [18] G. Kresse and D. Joubert, *Phys. Rev. B* **59**, 1758 (1999).
- [19] G. Kresse and J. Hafner, *Phys. Rev. B* **47**, (R)558 (1993).
- [20] G. Kresse and J. Furthmüller, *Phys. Rev. B* **54**, 11169 (1996).
- [21] J. Neugebauer and M. Scheffler, *Phys. Rev. B* **46**, 16067 (1992).
- [22] C. J. Fall, N. Binggeli, and A. Baldereschi, *J. Phys.: Condens. Matter.* **11**, 2689 (1999).
- [23] Y. Yourdshahyan, H. K. Zhang, and A. M. Rappe, *Phys. Rev. B* **63**, (R)081405 (2001).
- [24] M. C. Vargas, P. Giannozzi, A. Selloni, and G. Scoles, *J. Phys. Chem. B* **105**, 9500 (2001).
- [25] T. Hayashi, Y. Morikawa, and H. Nozoye, *J. Chem. Phys.* **114**, 7615 (2001).
- [26] G. V. Hansson and S. A. Flodstrom, *Phys. Rev. B* **18**, 1572 (1978).
- [27] R. C. Monreal, L. Guillemot, and V. A. Esaulov, *J. Phys.: Condens. Matter.* **15**, 1165 (2003).
- [28] G. N. Derry and Z. Ji-Zhong, *Phys. Rev. B* **39**, 1940 (1989).
- [29] This could be due to a number of reasons. The experiments are not performed in UHV, which might introduce impurities. Moreover, since in experiment longer molecules with a larger polarizability are used, the effect of the depolarizing field of the molecular dipoles is larger, which reduces the interface dipole.
- [30] R. G. Parr and W. Yang, *Density-Functional Theory of Atoms and Molecules* (Clarendon Press, Oxford, 1989).

Chapter 3

Surface dipoles and work functions of alkylthiolates and fluorinated alkylthiolates on Au(111)

We study the dipole formation at the surface formed by $-CH_3$ and $-CF_3$ terminated short-chain alkylthiolate monolayers on Au(111). In particular, we monitor the change in work function upon chemisorption using density functional theory calculations. We separate the surface dipole into two contributions, resulting from the gold-adsorbate interaction and the intrinsic dipole of the adsorbate layer, respectively. The two contributions turn out to be approximately additive. Adsorbate dipoles are defined by calculating dipole densities of free-standing molecular monolayers. The gold-adsorbate interaction is to a good degree determined by the Au–S bond only. This bond is nearly apolar and its contribution to the surface dipole is relatively small. The surface dipole of the self-assembled monolayer is then dominated by the intrinsic dipole of the thiolate molecules. Alkylthiolates increase the work function of Au(111), whereas fluorinated alkylthiolates decrease it.

3.1 Introduction

Self-assembled monolayers (SAMs) of organo-thiolate molecules on gold are studied for a wide range of applications, such as supramolecular assembly, biosensors, molecular electronics and microelectronic devices [1–4]. Using organic semiconducting materials as the active components of opto-electronic devices, often the energy barriers for charge injection from metal electrodes into the organic material form a limiting factor for the device performance [5, 6]. It has been shown that chemisorption of a SAM on the surface of the metal electrode can alter its work function substantially. By tailoring the SAM's chemical structure this effect can be used advantageously to lower

the energy barrier for charge injection and increase the device performance [7–9].

The work function change of the surface is directly proportional to the change in the surface electric dipole caused by adsorption of the SAM. Therefore, in order to understand the relation between the work function change and the SAM’s chemical structure one has to focus on the dipoles formed in the SAM–metal interface region. One obvious contribution to the surface dipole stems from the permanent dipoles of the molecules within the SAM. It has been demonstrated experimentally that a strong correlation exists between the molecular dipole moments and the work function changes induced by SAMs on gold and silver surfaces [7–10]. The dense packing of molecular dipoles in a SAM, however, causes a sizable depolarizing electric field, which polarizes the molecules such as to effectively reduce their dipole. This effect is often modeled empirically by using an effective dielectric constant for the molecular layer.

A second major contribution to the surface dipole results from the charge reordering associated with the formation of the chemical bonds between the metal surface and the adsorbate molecules. This contribution is foremost determined by the nature of the chemical bonds, but can also be modified by the packing density of the molecules. Thiolate molecules on gold surfaces are among the best studied systems, but it is still debated whether there is a sizable charge transfer between the surface and the molecules upon chemisorption.

In this chapter we want to elucidate the role played by the different contributions to the surface dipole of a SAM on gold and study the interplay between them. We calculate the dipole contributions and the work function change from first principles using density functional theory (DFT). In particular, we study alkylthiolates on the Au(111) surface, since these are among the best characterized systems, experimentally as well as theoretically [1, 11–21]. The common functionals used within DFT are very well suited to describe chemisorption, but lack an accurate description of the van der Waals interactions between the alkyl chains that determine the structure of long-chain alkylthiolate SAMs. This inter-chain interaction is relatively unimportant in short-chain alkylthiolates and, since we are mainly interested in surface dipole formation, we study the short-chain alkylthiolates CH_3S and $\text{CH}_3\text{CH}_2\text{S}$.

The basic building block of the structure of an alkylthiolate SAM on Au(111) is well-known. It consists of one thiolate molecule per $(\sqrt{3} \times \sqrt{3})\text{R}30^\circ$ surface unit cell [1, 11]. Superstructures of this basic pattern have been reported that contain up to four molecules in the same overall packing density. Experimentally, the positions of the adsorption sites of the thiolate molecules on the surface and the exact structure of the thiolate layers are still hotly debated. Theoretically, the energy differences between several of these structures are very small and are within the error bar of DFT calculations (using common functionals). We examine these structures such as to elucidate as to what extent structural variations lead to a difference in surface dipole.

The sign of the dipole moment of a fluorinated alkylthiolate molecule is opposite to that of a non-fluorinated one. Therefore, SAMs of molecules with fluorinated alkyl tails give work function changes that are opposite to those that consist of molecules with normal alkyl tails [7–10]. We analyze the surface dipoles of SAMs containing molecules with $-\text{CF}_3$ end groups, in particular CF_3S and $\text{CF}_3\text{CH}_2\text{S}$. The structure

of such SAMs is much less well characterized than that of their alkyl counterparts. Long-chain alkylthiolates having only $-\text{CF}_3$ end groups are believed to have basically the same structure and packing as those with $-\text{CH}_3$ end groups, although the $-\text{CF}_3$ end groups lead to a larger degree of surface disorder [22]. If long alkyl chains are largely fluorinated, then alkylthiolates form a less densely packed SAM [23, 24]. A priori it is not clear what SAM structure the molecules CF_3S and $\text{CF}_3\text{CH}_2\text{S}$ would form. Therefore we discuss a couple of possible structures and packings.

3.2 Theoretical section

DFT calculations are performed with the VASP (Vienna ab initio simulation package) program [25, 26] using the PW91 functional for electronic exchange and correlation [27]. The projector augmented wave (PAW) method is used to represent the electron wave functions [28, 29]. For gold atoms, 6s and 5d electrons are treated as valence electrons, for carbon and fluor 2s and 2p, and for sulfur 3s and 3p, respectively. The valence wave functions are expanded in a basis set consisting of plane waves. All plane waves up to a kinetic energy cutoff of 450 eV have been included.

The Au(111) surface is modeled in a supercell containing a slab of typically five or six layers of gold atoms. The SAM is adsorbed on one side of the slab. A vacuum region of about 13 Å is used, and periodic boundary conditions are applied in all three dimensions. The surface unit cell depends upon the monolayer structure and coverage. Our reference point is a $(\sqrt{3} \times \sqrt{3})\text{R}30^\circ$ surface unit cell, which contains three gold atoms in the surface layer.

The electronic structure is calculated using a uniform \mathbf{k} -point sampling grid in the surface Brillouin zone (SBZ) and a Methfessel-Paxton broadening of 0.2 eV [30]. A typical \mathbf{k} -point grid consists of a 8×8 division of the SBZ of the $(\sqrt{3} \times \sqrt{3})\text{R}30^\circ$ cell. SBZ samplings of other surface cells are chosen such that they have a similar density of grid points. Periodic boundary conditions can lead to spurious interactions between the dipoles of repeated slabs. To avoid such interactions the Neugebauer-Scheffler dipole correction is applied [31]. The electronic structure and the geometry are optimized self-consistently, where typically the positions of the atoms in the SAM and those in the first two layers of the gold slab are allowed to vary. The cell parameter of the Au(111) 1×1 surface unit cell is fixed at the bulk optimized value of 2.94 Å.

The surface work function W is defined as the minimum energy required to move an electron from the bulk to the vacuum outside the surface and it is given by the expression:

$$W = V(\infty) - E_F, \quad (3.1)$$

where $V(\infty)$ is the electrostatic potential in the vacuum, at a distance where the microscopic potential has reached its asymptotic value; E_F is the Fermi energy of the bulk metal. A self-consistent electronic structure calculation using a plane wave basis set produces the electrostatic potential $V(x, y, z)$ on a grid in real space. Assuming

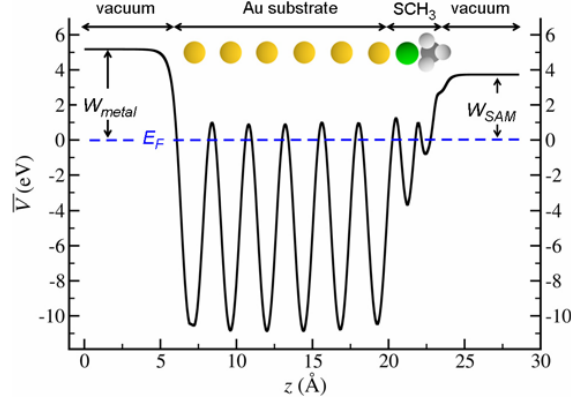


Figure 3.1: Plane averaged electrostatic potential $\bar{V}(z)$ of a slab comprising six layers of gold atoms and one layer of methylthiolate CH_3S . The z -axis is along the 111 direction. Indicated are the Fermi energy E_F , the work function W_{SAM} of the SAM and of the clean metal W_{metal} . In this chapter we use the colors yellow for Au atoms, green for S, dark grey for C, light grey for H, and light blue for F.

that the surface normal is along the z -axis, one can define a plane averaged potential

$$\bar{V}(z) = \frac{1}{A} \iint_{cell} V(x, y, z) dx dy, \quad (3.2)$$

where A is the area of the surface unit cell. Plotting $\bar{V}(z)$ as function of z is then a convenient way of extracting the value of $V(\infty)$. In practice, $\bar{V}(z)$ reaches its asymptotic value already within a distance of 5 Å from the surface. An example resulting from a calculation of a SAM of methylthiolate CH_3S on Au(111) is shown in Fig. 3.1.

In order to calculate surface work functions according to eq. (3.1) one needs an accurate value of the Fermi energy inside the metal. Whereas the value obtained from a slab calculation is quite reasonable, provided a slab of sufficient thickness is used, a better value can be obtained from a separate bulk calculation, following the procedure outlined by Fall et al [32]. Typically DFT calculations give work functions that are within 0.1 – 0.2 eV of the experimental values, although occasionally somewhat larger deviations are found [33–35].

In order to estimate the convergence of the numbers given in this chapter, we perform test calculations in which we vary the \mathbf{k} -point sampling grid and broadening parameter, the thickness of the slab and of the vacuum region, and the number of layers in which the gold atoms are allowed to relax their positions. From these tests we estimate that the energy differences quoted in this chapter are converged to within 1 kJ/mol and the work functions to within 0.05 eV.

3.3 Results

3.3.1 Structures

In this section we discuss the possible structures of alkylthiolate SAMs on Au(111). Our main goal is to study the link between the structure and the work function, which we will discuss in the next section. The earliest experimental (He) diffraction studies established a $(\sqrt{3} \times \sqrt{3})R30^\circ$ structure for alkylthiolate SAMs on Au(111) with one molecule per surface unit cell [36, 37], see Fig. 3.2. Somewhat later a $c(4 \times 2)$ superstructure was found, which contains four thiolate molecules per surface unit cell in the same packing density as the simpler $(\sqrt{3} \times \sqrt{3})R30^\circ$ structure [38], see Fig. 3.3. From infrared data it was concluded that there are two different orientations in the alkyl chains [39] and from grazing incidence X-ray diffraction data, a model was proposed for the superstructure based upon thiolate dimers [40]. Evidence against the dimer model was presented by scanning tunneling microscopy [41] and by electron spectroscopy experiments [42]; in the latter, thiolate dimers were found only at temperatures above 375 K. In recent He and X-ray diffraction experiments it was concluded that in the $c(4 \times 2)$ superstructure alkylthiolate molecules adsorb as monomers on the Au(111) surface [43, 44]. Experimentally the $c(4 \times 2)$ and $(\sqrt{3} \times \sqrt{3})R30^\circ$ structures seem to be close in energy; in scanning tunneling microscopy experiments, domains of both structures have been shown to coexist [22]. Moreover, larger and more complex superstructures such as (3×4) could also be close in energy [45].

Regarding the exact binding sites of thiolate molecules, diffraction and time of flight scattering studies emphasize the hollow sites on the Au(111) surface, where the sulfur atoms are threefold coordinated by Au atoms of the substrate [44, 46]. From recent photoelectron diffraction data and X-ray standing wave analysis it was concluded, however, that thiolate molecules favor the on-top adsorption sites, where a sulfur atom is positioned on top of a single Au atom of the substrate [47, 48].

The adsorption of Methylthiolate CH_3S on Au(111) has been studied intensively by first-principles calculations in recent years. Most of these calculations consider the basic $(\sqrt{3} \times \sqrt{3})R30^\circ$ structure [12–18], and a number of them have addressed the $c(4 \times 2)$ superstructure [14–20]. Earlier calculations give the threefold hollow sites on the Au(111) surface as the most stable sites for adsorption of the thiolate molecules [12, 13, 18], but more accurate recent calculations distinctly prefer the twofold bridge sites [14–17, 20]. The S-atom of the adsorbate molecule is bonded to two Au atoms of the surface, see Fig 3.2. The on-top adsorption site is clearly unfavorable; in most calculations it not even represents a metastable structure, but a maximum on the energy surface. To achieve converged computational results it has become evident from these calculations that the number of Au layers representing the substrate has to be sufficiently large, and that relaxation of the surface atoms is significant. Moreover, it is important to have a sufficiently dense Brillouin zone sampling.

Different density functionals give somewhat different values for the adsorption energy of alkylthiolates on Au(111), but they favor the same order in preferential binding sites, i.e. the bridge site is much more stable than the hollow site, which is more stable than the on-top site. In addition, calculations on small clusters indicate that DFT

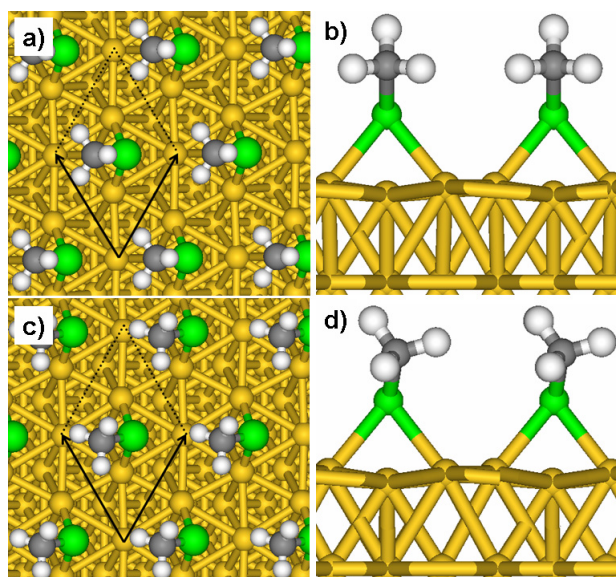


Figure 3.2: The $(\sqrt{3} \times \sqrt{3})R30^\circ$ structure of the CH_3S SAM on Au(111) with the molecules adsorbed at bridge sites; (a), (b) top and side view of the bridge (s, symmetric) structure; (c), (d) top and side view of the bridge (bs, broken symmetry) structure.

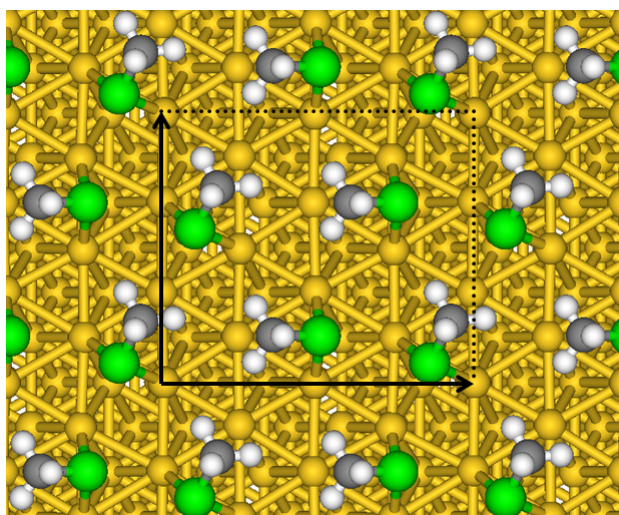


Figure 3.3: Top view of the $c(4 \times 2)$ structure of the CH_3S SAM on Au(111), which contains 4 molecules per surface unit cell [14].

and Hartree-Fock (plus many-body perturbation or coupled cluster corrections) give essentially the same stable structures [49]. Calculations on the $c(4 \times 2)$ superstructure clearly favor adsorption of thiolate molecules as monomers instead of dimers, in agreement with recent experimental results. Because of the strong preference for the bridge adsorption site, most $c(4 \times 2)$ superstructures that have been proposed from calculations are based upon molecules adsorbed at different bridge sites [14, 16, 17], see Fig. 3.3. However, the calculated total energy differences between such $c(4 \times 2)$ and $(\sqrt{3} \times \sqrt{3})R30^\circ$ structures are ≤ 5 kJ/mol. Such energy differences are too small to be reproduced accurately by common density functionals.

In view of these computational and experimental results we consider only structures in which the alkylthiolates are adsorbed as monomers on the Au(111) surface. First we focus upon CH_3S on Au(111) in the $(\sqrt{3} \times \sqrt{3})R30^\circ$ structure as shown in Fig. 3.2 (a),(b). As in previous calculations we find that the bridge site is more stable than the hollow site and that the on-top position is unstable. The relative energies associated with these adsorption sites are given in Table 3.1, in the columns marked by "bridge(s)", "fcc hollow", and "on-top". Table 3.1 also presents some structural data. Energies and structures are in fair agreement with the results obtained in previous calculations [14,16,17]. The spread in the results obtained in different calculations reflect the use of different density functionals, as well as slightly different computational parameters.

The $(\sqrt{3} \times \sqrt{3})R30^\circ$ structure of CH_3S adsorbed at the bridge site on Au(111) as shown in Fig. 3.2 (a),(b), has mirror and glide plane symmetry (this structure has the two-dimensional space group Cm). Rotating the CH_3 -group around the CS bond breaks the mirror and glide plane symmetry. Breaking the symmetry and optimizing the geometry results in a structure shown in Fig. 3.2 (c),(d). The structural data of CH_3S at the bridge site in this 'broken symmetry' structure, bridge(bs), are also given in Table 3.1. This structure is quite similar to the symmetric bridge(s) structure. The most significant change in the bridge(bs) structure, besides the CH_3 rotation already mentioned, are that the two Au-S bonds have become slightly inequivalent; moreover, the azimuthal angle ϕ of the CS bond has changed. The calculated total energies of the bridge(s) and bridge(bs) structures are very close, the latter being actually 1.7 kJ/mol lower in energy. However, this is within the error bar associated with the PW91 functional we used.

Since the bridge site is much more stable than other adsorption sites, it is reasonable to base a $c(4 \times 2)$ superstructure entirely upon molecules adsorbed at bridge sites. Fig. 3.3 shows the $c(4 \times 2)$ superstructure proposed by Vargas et al. [14], which contains four molecules per cell. The inequivalent molecules have a similar tilt angle of the CS bond with respect to the surface normal, but differ by $\sim 60^\circ$ in the azimuthal angle ϕ of that bond. We optimized this structure using the same computational parameters as for the $(\sqrt{3} \times \sqrt{3})R30^\circ$ unit cell calculations (in particular the k-point grid for the Brillouin zone integration). The results are listed in Table 3.1. The local geometries of all molecules in the $c(4 \times 2)$ structure are quite similar, so we only give the average geometric parameters. The structural parameters are actually similar to those of the bridge(s) structure. The largest difference is in the C-S-normal angle, where the molecules in the $(\sqrt{3} \times \sqrt{3})R30^\circ$ structure are tilted

	$(\sqrt{3} \times \sqrt{3})R30^\circ$				c(4 × 2)
	bridge(s)	bridge(bs)	fcc hollow	on-top	
Energy (kJ/mol)	0.0	-1.7	25.3	34.9	1.0
Au-S (Å)	2.50 /2.50	2.52 /2.49	2.63/2.60 /2.50	2.39	2.52 /2.50
S-C (Å)	1.84	1.84	1.85	1.82	1.83
Au-S-Au (°)	77.0	76.5	74.6/76.7 /76.3	—	73.2
C-S-normal (°)	45.3	46.3	14.4	64.6	57.2
ϕ (°)	30.0	38.4	—	—	31.8
W (eV)	3.81	3.85	3.39	4.73	4.04

Table 3.1: Total energies, bond lengths, bond angles, and work functions of SAMs of CH₃S on Au(111). The columns indicate the possible adsorption sites in the $(\sqrt{3} \times \sqrt{3})R30^\circ$ or c(4 × 2) structures. For geometries in the c(4 × 2) structure only averages over the four molecules are given.

	bridge(s)	bridge(bs)		bridge(s)	bridge(bs)
	Energy (kJ/mol)	0.0		-1.0	Au-S-Au (°)
Au-S (Å)	2.54	2.52/2.48	C-S-normal (°)	54.6	52.4
S-C (Å)	1.85	1.85	ϕ (°)	30.0	26.2
C-C (Å)	1.53	1.52	W (eV)	3.93	3.83

Table 3.2: Total energies, bond lengths, bond angles, and work functions of SAMs of CH₃CH₂S on Au(111) in the $(\sqrt{3} \times \sqrt{3})R30^\circ$ structure. The columns bridge(s) and bridge(bs) indicate the 'symmetric' and 'broken symmetry' bridge sites, respectively.

somewhat more upright. The total energy of the c(4 × 2) structure is only 1.0 kJ/mol per molecule higher than that of the $(\sqrt{3} \times \sqrt{3})R30^\circ$ bridge(s) structure, so again it is hardly possible to distinguish between these two structures energetically on the DFT level.

In conclusion, from a computational point of view there are several structures of a CH₃S SAM on Au(111) that are very close in energy and are based upon adsorption of CH₃S molecules on bridge sites. They differ in the azimuthal angle ϕ of the CS bond and the rotation angle of the CH₃-group around the CS bond. The spread in the tilt angle C-S-Au of the CS bond with respect to the surface is smaller. The possible structures of an ethylthiolate (CH₃CH₂S) SAM on Au(111) very much resemble those of a methylthiolate SAM. Table 3.2 gives the energy and geometry of CH₃CH₂S in the $(\sqrt{3} \times \sqrt{3})R30^\circ$ structure with the molecule adsorbed on a bridge site in the symmetric (bridge(s)), as well as in the broken symmetry (bridge(bs)) structure. A comparison to the data shown in Table 3.1 shows that indeed the geometries of the adsorbed alkylthiolates are very similar.

The structure of (partially) fluorinated alkylthiolates on gold is much less well-established than that of their alkyl counterparts, both experimentally and theoretically. SAMs of long-chain alkylthiolates with fluorinated (-CF₃) end groups show a large degree of surface disorder, although their basic structure remains similar to

	CF ₃ S			CF ₃ CH ₂ S		
	bridge(s)	bridge(bs)	p(2 × 2)	bridge(s)	bridge(bs)	p(2 × 2)
Au-S (Å)	2.50	2.51/2.47	2.52/2.53	2.52	2.54/2.50	2.52/2.50
S-C (Å)	1.85	1.86	1.85	1.85	1.84	1.85
C-F (Å)	1.36	1.36	1.36	1.37	1.36	1.37
Au-S-Au (°)	77.0	78.4	73.4	76.4	75.6	74.6
C-S-normal (°)	45.7	37.8	49.8	43.3	52.0	50.6
ϕ (°)	30.0	21.1	29.6	30.0	24.2	29.5
W (eV)	5.97	5.98	6.00	6.27	6.35	6.21

Table 3.3: Bond lengths, bond angles, and work functions of SAMs of CF₃S and CF₃CH₂S on Au(111) in the ($\sqrt{3} \times \sqrt{3}$)R30° and p(2 × 2) structures. The columns bridge(s) and bridge(bs) indicate the 'symmetric' and 'broken symmetry' bridge sites in the structure, respectively.

that of SAMs of alkylthiolates with -CH₃ end groups [22]. Our calculations on trifluoromethylthiolate (CF₃S) on Au(111) show that within a $\sqrt{3} \times \sqrt{3}$ packing of molecules similar variations in structure are possible as for CH₃S on Au(111), with similar small energy differences between these structures.

Thiolates with a longer fluorinated alkyl chain form SAMs with a less denser packing, because of the bulkier fluorinated alkyl tails. Whereas in a $\sqrt{3} \times \sqrt{3}$ packing the nearest neighbor distance between the sulfur atoms on the surface is 5.0 Å, see Fig. 3.2, in fluorinated alkylthiolates this distance is 5.8 Å, leading to a 30% less dense surface packing [11, 23, 24]. This distance is twice the nearest neighbor distance between the gold atoms in the surface and a p(2 × 2) structure has been proposed for fluorinated alkylthiolate SAMs on Au(111) [23]. More complex superstructures, such as a c(7 × 7), or even an incommensurate structure have also been proposed [24, 50]. For the short-chain fluorinated molecules we are considering, i.e. CF₃S and CF₃CH₂S, it is not a priori clear whether the dense $\sqrt{3} \times \sqrt{3}$ or the less dense p(2 × 2) packing is favored. Therefore we have also optimized the geometries of these molecules in a p(2 × 2) unit cell. An example of an optimized structure is shown in Fig. 3.4. Also in this structure the (displaced) bridge site is the most favorable site for adsorption. The local geometry of the adsorbed molecules is in fact quite similar to that in the $\sqrt{3} \times \sqrt{3}$ packing, as is demonstrated by Table 3.3. We will consider both possible packings in discussing the work functions.

3.3.2 Work functions and surface dipoles

We now focus upon the distribution of dipole moments at the SAM-gold surface. A sensitive technique for characterizing a surface dipole, experimentally or theoretically, is to determine the work function of the surface. For the clean Au(111) surface we calculate a work function of 5.25 eV. Reported experimental values are 5.26 eV [51] and 5.35 eV [21] and previously reported calculated values are 5.23 eV [52], 5.27 eV [53], 5.31 eV [54] and 5.35 eV [21]. All these values are within the experimental and computational error bars.

The calculated work functions of the SAM-Au(111) surfaces in the different ge-

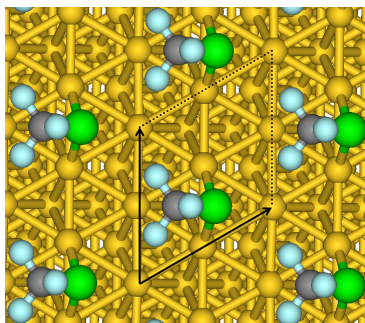


Figure 3.4: Top view of the $p(2 \times 2)$ structure of the CF_3S SAM on Au(111).

ometries are given in Tables 3.1–3.3. It can be observed that structures whose total energies are close, also have similar work functions. For instance, the total energies of the bridge(s) and the bridge(bs) $(\sqrt{3} \times \sqrt{3})\text{R}30^\circ$ structures of CH_3S on Au(111), as well as that of the $c(4 \times 2)$ structure, are within 2 kJ/mol of one another, see Table 3.1. The work functions of the bridge(s) and bridge(bs) structures differ by 0.04 eV, which is close to the (convergence) error bar of the DFT calculations. The work function of the $c(4 \times 2)$ structure is ~ 0.2 eV higher. As compared to the clean Au(111) surface, the work function is shifted to a substantially lower value for these three structures.

The latter involve a similar bonding of molecules at bridge sites and also the local geometry of the adsorbed CH_3S molecules is very similar. Comparing the geometries of the bridge and the $c(4 \times 2)$ structures in Table 3.1, one observes that the bond lengths are similar, as well as the Au–S–Au bond angle. The C–S–normal tilt angle in the $c(4 \times 2)$ structure is $11 - 12^\circ$ higher than in the $(\sqrt{3} \times \sqrt{3})\text{R}30^\circ$ structures, which means that in the latter the thiolate molecules are standing somewhat more upright. As a result the component of the molecular dipole moment along the surface normal is somewhat larger in the $(\sqrt{3} \times \sqrt{3})\text{R}30^\circ$ structures. The work function shift, i.e. the difference between the work functions of the SAM covered surface and that of the clean Au(111) surface, is sensitive to this normal component; see also the analysis below. The fact that the work function shift of both $(\sqrt{3} \times \sqrt{3})\text{R}30^\circ$ structures is ~ 0.2 eV larger than that of the $c(4 \times 2)$ structure can be attributed to a larger normal component of the molecular dipoles.

The azimuthal angle ϕ and the rotation angle around the CS bond are substantially different in the three structures, see Figs. 3.2 and 3.3. However, these angles do not affect the normal molecular dipole component and hence they do not affect the work function. The same geometrical arguments also hold for the other molecules. As can be observed from Tables 3.1 to 3.3, one obtains similar work functions in the bridge(s) and bridge(bs) $(\sqrt{3} \times \sqrt{3})\text{R}30^\circ$ structures for all molecules. In conclusion, for the SAMs we have studied, the structures that have nearly the same total energy also have a very similar local geometry and hence a very similar work function.

Comparing in Table 3.1 the work functions of $(\sqrt{3} \times \sqrt{3})\text{R}30^\circ$ structures that

correspond to adsorption of CH_3S at different sites, one observes that the fcc hollow site leads to a work function that is ~ 0.4 eV lower than that of the bridge site, whereas that of the on-top site is ~ 0.9 eV higher. Following the arguments presented above, this can be partly understood from the difference in the C–S–normal tilt angle between these structures. A small (large) tilt angle gives a large (small) normal molecular dipole component and a large (small) shift in work function with respect to the clean Au(111) surface. In addition, the bonding between the molecules and the surface, which is different for the different adsorption sites, contributes to the work function shift. We suggest that work function measurements might contribute to settle the issue of the adsorption site of CH_3S on Au(111) from an experimental point of view.

From Table 3.3 one can also observe that the work functions of the fluorinated alkylthiolate SAMs on Au(111) do not depend strongly upon the packing density of the molecules. Both the $(\sqrt{3} \times \sqrt{3})\text{R}30^\circ$ and the $\text{p}(2 \times 2)$ structures, whose packing density differs by 33 %, have a similar work function. This is slightly surprising since one expects the shift in the work function upon adsorption of the SAM to depend upon the packing density of the molecules. On the one hand, one would expect a higher packing density to result in a larger work function shift because of a higher density of molecular dipoles. On the other hand, increasing the packing density of the molecular dipoles also enlarges the depolarizing field in the SAM, which acts to decrease the dipoles and therefore the work function shift. Apparently in the range of packing densities that are relevant to the $(\sqrt{3} \times \sqrt{3})\text{R}30^\circ$ and $\text{p}(2 \times 2)$ structures, these two effects tend to cancel one another.

3.4 Analysis

We will use the bridge(s) $(\sqrt{3} \times \sqrt{3})\text{R}30^\circ$ structure to analyze the work functions and begin by noticing that the latter fall into two groups. Adsorption of the two alkylthiolates CH_3S and $\text{CH}_3\text{CH}_2\text{S}$ gives one work function, compare Tables 3.1 and 3.2, whereas adsorption of fluorinated CF_3S and $\text{CF}_3\text{CH}_2\text{S}$ molecules gives another value for the work function, see Table 3.3. It makes sense to use the work function of the clean Au(111) surface, 5.25 eV, as a reference point and analyze changes of the work functions upon adsorption of the molecules. We define the change in work function caused by the SAM with respect to the clean Au(111) surface as $\Delta W = W_{\text{SAM}} - W_{\text{metal}}$. The results are collected in Table 3.4, which shows that SAMs of CH_3S and $\text{CH}_3\text{CH}_2\text{S}$ lower the work function by 1.3–1.4 eV, whereas SAMs of CF_3S and $\text{CF}_3\text{CH}_2\text{S}$ increase the work function by 0.7–1.0 eV.

These work function changes ΔW can be interpreted in terms of changes in the surface dipole $\Delta\mu$ due to adsorption of the SAM. Simple electrostatics gives the relation [55]

$$\Delta W = \frac{e\Delta\mu}{\epsilon_0 A}, \quad (3.3)$$

where A is the surface area taken up by one molecule and $\Delta\mu$ is the change in surface dipole that occurs upon adsorption of the SAM, normalized per molecule. Note

molecule	W	ΔW	$\Delta\mu$	μ_{SAM}	μ_{chem}
CH ₃ S	3.81	-1.44	-0.86	-0.88	0.02
CH ₃ CH ₂ S	3.93	-1.32	-0.79	-0.81	0.02
CF ₃ S	5.97	0.72	0.43	0.44	-0.01
CF ₃ CH ₂ S	6.27	1.02	0.61	0.53	0.08

Table 3.4: Work functions of SAMs on Au(111) in eV in the bridge(s) $\sqrt{3} \times \sqrt{3}$ structure; absolute values (W) and relative to clean Au(111) (ΔW). The surface dipole moment ($\Delta\mu$) relative to that of clean Au(111), the dipole moment of a free-standing SAM (μ_{SAM}) and that of the adsorbate-surface bonds ($\mu_{chem} = \Delta\mu - \mu_{SAM}$); all in D.

that $\Delta\mu$ corresponds to the component of the dipole moment directed along the surface normal, since it is only this component that affects the work function. The values of $\Delta\mu$ calculated according to eq. (3.3) are also given in Table 3.4. The sign of $\Delta\mu$ is such that for CH₃S and CH₃CH₂S the dipoles point from the surface into the gold crystal, whereas for CF₃S and CF₃CH₂S they point from the surface into the vacuum. Intuitively one would like to interpret $\Delta\mu$ in terms of molecular dipole moments and indeed the size of $\Delta\mu$ is of the order of a molecular dipole moment [7–10]. One should bear in mind however that upon adsorption on a metal surface, even molecules that have a zero dipole moment can alter the surface dipole considerably [56, 57].

Therefore we divide $\Delta\mu$ into a part that results from the molecules only and a part that results from the formation of chemical bonds between the molecules and the surface:

$$\Delta\mu = \mu_{SAM} + \mu_{chem}. \quad (3.4)$$

We define μ_{SAM} as the dipole moment along the surface normal of a molecule embedded in a free-standing SAM, i.e. without the presence of the metal substrate. This definition takes care of the geometry of the molecule in the SAM. In addition, this definition automatically incorporates the effect of the depolarizing electric field that is caused by the molecular dipoles surrounding each molecule in the SAM. The effect of this depolarizing field is sometimes introduced phenomenologically as an effective dielectric constant in the molecular layer [7–10]. Using a computational technique in which periodic boundary conditions are applied, there is no need for a phenomenological dielectric constant, since the calculation is done automatically on a full monolayer.

One places the molecule in a unit cell in the correct SAM geometry and performs a self-consistent DFT calculation while keeping the geometry fixed. Electrostatics then relates μ_{SAM} to the step in the electrostatic potential as [55]

$$V_{SAM}(\infty) - V_{SAM}(-\infty) = \frac{e\mu_{SAM}}{\epsilon_0 A}, \quad (3.5)$$

where $V_{SAM}(\infty)$, $V_{SAM}(-\infty)$ are the asymptotic electrostatic potentials on both sides of the SAM. These are easily obtained from the calculation, since the potential

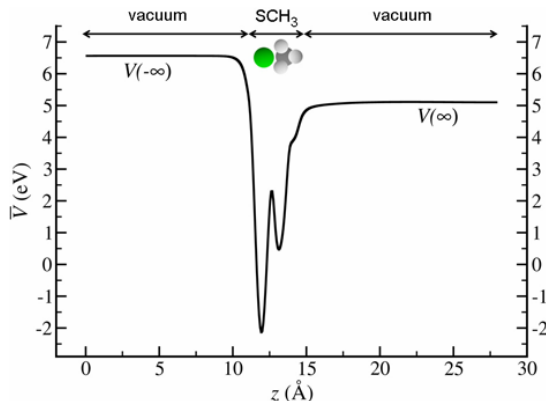


Figure 3.5: Plane averaged electrostatic potential $\bar{V}(z)$ of a free-standing monolayer of methylthiolate CH_3S . Indicated are the asymptotic electrostatic potentials $V(\infty)$, $V(-\infty)$ on both sides of the layer.

reaches its asymptotic values within a distance of few Å from the molecular layer, as is illustrated in Fig. 3.5. The calculated μ_{SAM} are listed in Table 3.4.

Having calculated $\Delta\mu$ and μ_{SAM} from eqs. (3.3) and (3.5), respectively, we then define μ_{chem} by eq. (3.4) and interpret it as the change in the surface dipole due to chemisorption of the molecule on the metal surface. It reflects the charge reordering in the molecule and in the metal surface that takes place upon formation of a chemical bond. The calculated μ_{chem} are given in Table 3.4 for the four molecules. Two main conclusions can be drawn from these numbers. First, μ_{chem} shows relatively little variation within this range of molecules. Apparently the charge reordering is mainly confined to the chemical bond formed at the surface, which for all four molecules is the gold–sulfur bond, and it does not depend much on the (fluorinated) alkyl tail of the molecules. Second, the absolute value of μ_{chem} is very small as compared to the absolute value of μ_{SAM} . This means that the charge reordering in the gold–sulfur bond is such that it does not give rise to a substantial dipole moment. In other words, the gold–sulfur bond is nearly apolar. This result agrees with that obtained in a previous calculation on CH_3S on Au(111) [21]. Similar results on SAMs of conjugated thiols on Au(111) would indicate that this conclusion is quite general [58].

Kelvin probe measurements of the work functions of SAMs of the long chain thiols $\text{C}_{16}\text{H}_{33}\text{S}$ and $\text{C}_8\text{F}_{17}\text{C}_2\text{H}_4\text{S}$ on Au(111) have been reported by de Boer et al. [9]. Work function changes upon SAM adsorption on Au(111) have been deduced from photoemission measurements by De Renzi et al. [21] for CH_3S , and by Alloway et al. [10] for alkylthiolates ranging from $\text{C}_3\text{H}_7\text{S}$ to $\text{C}_{18}\text{H}_{37}\text{S}$ and for fluorinated alkylthiolates ranging from $\text{CF}_3\text{C}_{12}\text{H}_{24}\text{S}$ to $\text{CF}_3\text{C}_{15}\text{H}_{30}\text{S}$, and from $\text{CF}_3\text{C}_{15}\text{H}_{30}\text{S}$ to $\text{C}_{10}\text{F}_{21}\text{C}_6\text{H}_{12}\text{S}$. The trends in these measurements are clear; alkylthiolates lead to a substantial lowering of the work function relative to the clean gold surface, whereas (partially) fluorinated alkylthiolates give an increase of the work function. For alkylthiolates photoemission gives a ΔW of -1.2 eV for CH_3S [21], and a ΔW ranging from

-1.0 eV for C_3H_7S to -1.4 eV for $C_{16}H_{33}S$ [10]. The Kelvin probe gives a ΔW of -0.8 eV for $C_{16}H_{33}S$ [9].

Our calculated value for CH_3S is in good agreement with the experimental value, see Table 3.4. Also the value we find for CH_3CH_2S is within the range determined by the photoemission experiments. The work function shows only little variation for alkylthiolates because both μ_{SAM} and μ_{chem} only weakly depend upon the length of the alkyl tail. The dipole μ_{chem} resulting from chemisorption of the alkylthiolate is mainly determined by the gold-sulfur bond. Both the dipole moment of an alkylthiolate molecule and the orientation of the molecule in the SAM do not vary strongly with the size of the alkyl tail. Therefore, μ_{SAM} only weakly depends upon the size of the alkyl group. The Kelvin probe measurement gives a somewhat lower value for ΔW than the photoemission experiments. This could be due to a number of reasons. The experiments are not performed in UHV, which might introduce impurities. Under ambient conditions the work function of a clean gold surface becomes 4.9 eV instead of the 5.3 eV obtained under UHV conditions [9]. Incorporating this difference would give a ΔW of -1.2 eV, which would bring it close to the photoemission and to the calculated results.

A direct comparison to the experimental results on fluorinated alkylthiolates is more difficult. The dipoles μ_{SAM} of fluorinated alkylthiolates vary more widely than those of unsubstituted alkylthiolates. The molecular dipoles depend on which and how many of the hydrogens on the alkyl tail are substituted by fluor. The substitution also affects the structure of the SAM, and hence the depolarizing field. Moreover, SAMs of fluorinated alkylthiolates tend to show more intrinsic disorder than their unsubstituted counterparts. Photoemission gives a maximum ΔW of +0.5 eV for $C_{10}F_{21}C_6H_{12}S$ and the Kelvin probe gives +0.6 eV for $C_8F_{17}C_2H_4S$. The calculations on short-chain fluorinated alkylthiolates give somewhat larger ΔW 's as can be observed from Table 3.4.

3.5 Conclusions

We have studied the surface dipoles and work functions of SAMs of self-assembled monolayers of CH_3S , CH_3CH_2S , CF_3S and CF_3CH_2S on the Au(111) by means of density functional theory calculations. Several structures exist that have almost the same total energy, but also give very similar work functions. By performing separate calculations on the free-standing SAMs we can calculate the dipole moments of the molecules as they are embedded in the SAMs. This allows us to define dipole moments that result from chemisorption of the molecules on the Au(111) surface. The latter are almost independent of the molecule, indicating that they mainly result from the gold-sulfur bond. Moreover, the gold-sulfur bond turns out to be apolar and give only a small contribution to the surface dipoles. The main contributions to the latter stems from the molecular dipole moments. The direction of these is such that adsorption of CH_3S and CH_3CH_2S lowers the work function as compared to the clean Au(111) surface, whereas adsorption of CF_3S and CF_3CH_2S increases the work function.

Acknowledgments

We thank B. de Boer for introducing us to this topic and for showing us his experimental data prior to publication. P. J. Kelly is acknowledged for useful discussions and G. de Wijs and M. Uijtewaal are thanked for help with the VASP program. This work is supported by the "Prioriteits Programma Materialenonderzoek" (PPM), and is part of the research program of the "Stichting voor Fundamenteel Onderzoek der Materie" (FOM), financially supported by the "Nederlandse Organisatie voor Wetenschappelijk Onderzoek" (NWO). The use of supercomputer facilities was sponsored by the "Stichting Nationale Computer Faciliteiten" (NCF), financially supported by NWO.

Bibliography

- [1] A. Ulman, *Chem. Rev* **96**, 1533 (1996).
- [2] C. S. Chen, M. Mrksich, S. Huang, G. M. Whitesides, and D. E. Ingber, *Biotechnol. Prog.* **14**, 356 (1998).
- [3] L. A. Bumm *et al.*, *Science* **271**, 1705 (1996).
- [4] R. E. Holmlin *et al.*, *J. Am. Chem. Soc.* **123**, 5075 (2001).
- [5] T. van Woudenbergh, P. W. M. Blom, M. C. J. M. Vissenberg, and J. N. Huiberts, *Appl. Phys. Lett.* **79**, 1697 (2001).
- [6] T. van Woudenbergh, P. W. M. Blom, and J. N. Huiberts, *Appl. Phys. Lett.* **82**, 985 (2003).
- [7] I. H. Campbell *et al.*, *Phys. Rev. B* **54**, R14321 (1996).
- [8] I. H. Campbell *et al.*, *J. Appl. Phys* **71**, 3528 (1997).
- [9] B. de Boer, A. Hadipour, M. M. Mandoc, T. van Woudenbergh, and P. W. M. Blom, *Adv. Mater.* **17**, 621 (2005).
- [10] D. M. Alloway *et al.*, *J. Phys. Chem. B.* **107**, 11690 (2003).
- [11] F. Schreiber, *Prog. Surf. Sci.* **65**, 151 (2000).
- [12] H. Sellers, A. Ulman, Y. Shnidman, and J. E. Eilers, *J. Am. Chem. Soc.* **115**, 9389 (1993).
- [13] H. Grönbeck, A. Curioni, and W. Andreoni, *J. Am. Chem. Soc.* **122**, 3839 (2000).
- [14] M. C. Vargas, P. Giannozzi, A. Selloni, and G. Scoles, *J. Phys. Chem. B.* **105**, 9509 (2001).
- [15] T. Hayashi, Y. Morikawa, and H. Nozoye, *J. Chem. Phys.* **114**, 7615 (2001).

- [16] Y. Morikawa, T. Hayashi, C. C. Liew, and H. Nozoye, *Surf. Sci.* **507**, 46 (2002).
- [17] Y. Yourdshahyan and A. M. Rappe, *J. Chem. Phys.* **117**, 825 (2002).
- [18] L. Zhang, W. A. Goddard, and S. Jiang, *J. Chem. Phys.* **117**, 7342 (2002).
- [19] L. M. Molina and B. Hammer, *Chem. Phys. Lett.* **360**, 264 (2002).
- [20] D. Fischer, A. Curioni, and W. Andreoni, *Langmuir* **19**, 3567 (2003).
- [21] V. De Renzi *et al.*, *Phys. Rev. Lett.* **95**, 046804 (2005).
- [22] J. Pflaum *et al.*, *Surf. Sci.* **89**, 498 (2002).
- [23] C. A. Alves and M. D. Porter, *Langmuir* **9**, 3507 (1993).
- [24] G. yu Liu *et al.*, *J. Chem. Phys.* **101**, 4301 (1994).
- [25] G. Kresse and J. Hafner, *Phys. Rev. B.* **47**, (R)558 (1993).
- [26] G. Kresse and J. Furthmüller, *Phys. Rev. B.* **54**, 11169 (1996).
- [27] J. P. Perdew *et al.*, *Phys. Rev. B* **46**, 6671 (1992).
- [28] P. E. Blöchl, *Phys. Rev. B.* **50**, 17953 (1994).
- [29] G. Kresse and D. Joubert, *Phys. Rev. B.* **59**, 1758 (1999).
- [30] M. Methfessel and A. T. Paxton, *Phys. Rev. B* **40**, 3616 (1989).
- [31] J. Neugebauer and M. Scheffler, *Phys. Rev. B.* **46**, 16067 (1992).
- [32] C. J. Fall, N. Binggeli, and A. Baldereschi, *J. Phys.* **11**, 2689 (1999).
- [33] A. Michaelides, P. Hu, M.-H. Lee, A. Alavi, and D. A. King, *Phys. Rev. Lett.* **90**, 246103 (2003).
- [34] F. Favot, A. D. Corso, and A. Baldereschi, *J. Chem. Phys.* **114**, 483 (2001).
- [35] M. Gajdoš, A. Eichler, and J. Hafner, *Surf. Sci.* **531**, 272 (2003).
- [36] N. Camillone, C. E. D. Chidsey, G. yu Liu, T. M. Putvinski, and G. Scoles, *J. Chem. Phys.* **94**, 8493 (1991).
- [37] C. E. D. Chidsey, G. yu Liu, P. Rowntree, and G. Scoles, *J. Chem. Phys.* **91**, 4421 (1989).
- [38] N. Camillone, C. E. D. Chidsey, G. yu Liu, and G. Scoles, *J. Chem. Phys.* **98**, 3503 (1993).
- [39] R. G. Nuzzo, E. M. Korenic, and L. H. Dubois, *J. Chem. Phys.* **93**, 767 (1990).
- [40] P. Fenter, A. Eberhardt, and P. Eisenberger, *Science* **266**, 1216 (1994).

-
- [41] G. E. Poirier and M. J. Tarlov, *Langmuir* **10**, 2853 (1994).
- [42] G. J. Kluth, C. Carraro, and R. Maboudian, *Phys. Rev. B* **59**, R10449 (1999).
- [43] M. F. Danişman, L. Casalis, G. Bracco, and G. Scoles, *J. Phys. Chem. B.* **106**, 11771 (2002).
- [44] X. Torrelles *et al.*, *Langmuir* **20**, 9396 (2004).
- [45] V. De Renzi *et al.*, *J. Phys. Chem. B.* **108**, 16 (2004).
- [46] L. Houssiau *et al.*, *J. Chem. Phys.* **109**, 9134 (1998).
- [47] H. Kondoh *et al.*, *Phys. Rev. Lett.* **90**, 066102 (2003).
- [48] M. G. Roper *et al.*, *Chem. Phys. Lett* **389**, 87 (2004).
- [49] D. Krüger, H. Fuchs, R. Rousseau, D. Marx, and M. Parrinello, *J. Chem. Phys.* **115**, 4776 (2001).
- [50] K. Tamada *et al.*, *Langmuir* **17**, 1913 (2001).
- [51] G. V. Hansson and S. A. Flodstrom, *Phys. Rev. B* **18**, 1572 (1978).
- [52] A. Bilic, J. R. Reimers, N. S. Hush, and J. Hafner, *J. Chem. Phys.* **116**, 8981 (2002).
- [53] S. Piccinin, A. Selloni, S. Scandolo, R. Car, and G. Scoles, *J. Chem. Phys.* **119**, 6729 (2003).
- [54] Y. Xue, S. Datta, and M. A. Ratner, *J. Chem. Phys.* **115**, 4292 (2001).
- [55] J. D. Jackson, *Classical Electrodynamics*, Wiley, New York (1975).
- [56] X. Crispin *et al.*, *J. Am. Chem. Soc.* **124**, 8131 (2002).
- [57] P. S. Bagus, V. Staemmler, and C. Wöll, *Phys. Rev. Lett.* **89**, 096104 (2002).
- [58] G. Heimel, L. Romaner, J.-L. Brédas, and E. Zojer, *Phys. Rev. Lett.* **96**, 196806 (2006).

Chapter 4

Dipole Formation at Interfaces of Alkylthiolate Self-assembled Monolayers and Ag(111)

The formation of interface dipoles in self-assembled monolayers (SAMs) of $-CH_3$ and $-CF_3$ terminated short-chain alkylthiolates on Ag(111) is studied by means of density functional theory calculations. The interface dipoles are characterized by monitoring the change in the surface work function upon adsorption of the SAM. We compare results obtained for SAMs in structures with a different packing density of molecules, i.e. $(\sqrt{7} \times \sqrt{7})R19.1^\circ$, $(\sqrt{3} \times \sqrt{3})R30^\circ$, and $p(2 \times 2)$. The work function of alkylthiolate SAMs on silver depends weakly on the packing density; that of fluorinated alkylthiolates shows a stronger dependence. The results are analyzed in terms of two nearly independent contributions to the interface dipole. These originate respectively from the molecular dipoles and from a charge transfer between the metal surface and the molecules. The charge transfer is determined by the silver-sulfur bond and it is independent of the electronegativity of the molecules.

4.1 Introduction

Self-assembled monolayers (SAMs) of organothiolates on metal surfaces are studied for a wide range of technological applications running from catalysis, biosensors to micro-electronic devices [1–3]. In organic light-emitting diodes, the interfaces between the metal contacts and the organic material are critical in the device performance, since they control the injection of electrons and holes into the device [4]. Chemisorption of a SAM on a metal surface can alter its work function substantially. Depending on the SAM, the work function can be manipulated advantageously to lower the energy barrier for electron and hole injection [5–7].

Self-assembled monolayers have also become attractive for fundamental studies in metal–organic interfaces and molecular electronics. They represent stable and ordered structures, which can be prepared experimentally in air, in solution, or in vacuum [8, 9]. SAMs of alkylthiolates, $C_nH_{2n+1}S$, on Au(111) are among the most extensively studied systems. Alkylthiolate SAMs on Au(111) adopt a $(\sqrt{3} \times \sqrt{3})R30^\circ$ structure or superstructures thereof [10, 11]. Alkylthiolates form SAMs on a wide range of (noble) metal surfaces, which have a similar structure as on Au(111). Variations on the packing density are possible, however, and on Ag(111) a somewhat denser packed $(\sqrt{7} \times \sqrt{7})R19.1^\circ$ structure has been reported [9].

The change in work function of the surface upon adsorption of the SAM is directly proportional to the dipole moment density generated at the SAM–metal interface. For SAMs on Au(111) it has been shown that this dipole moment density is mainly determined by the permanent dipoles in the thiolate molecular layer. The sulfur–gold bonds that are formed upon adsorption, are nearly apolar and give a very small contribution to the interface dipole [12–15]. However, a small sulfur–metal bond dipole is typical of gold and the existence of a much larger bond dipole is indicated by experiments of alkylthiolate SAMs on silver [7]. In a previous computational study on model structures we have shown that large bond dipoles can be formed in the adsorption of SAMs on Ag and Pt surfaces, see Chapter 2.

In this chapter we study the interface dipole formation resulting from adsorption of SAMs on Ag(111) by first-principles density functional theory (DFT) calculations. In particular we examine the influence of the structure and the packing density of the molecules in the SAM. The $(\sqrt{7} \times \sqrt{7})R19.1^\circ$ packing, which is observed experimentally for alkylthiolate SAMs on Ag(111) [9], is our starting point. We consider several low energy structures [16, 17]. The results are compared to the $(\sqrt{3} \times \sqrt{3})R30^\circ$ structure, where the surface area per adsorbed molecule is 29% larger, which is the most common structure of alkylthiolate SAMs on other noble metal (111) surfaces. We also consider the less densely packed $p(2 \times 2)$ structure, which has a 71% higher surface area per molecule. Fluorinated alkylthiolate SAMs on Au(111) can be observed in this structure [9], and it might be possible that this structure is also formed by such molecules adsorbed on Ag(111). We show that although the interface dipole density is smaller for less densely packed structures, it is not simply proportional to the packing density due to dielectric screening in the molecular layer.

The commonly used DFT functionals describe the formation of chemical bonds and the resulting charge distribution very well, but they fail to capture the van der Waals interactions between the alkyl chains. Van der Waals interactions are relatively unimportant in short chain alkylthiolates, which is why we focus on the short chain thiolates CH_3S and C_2H_5S . To elucidate the influence of the polarity of the molecules on the SAM–metal interface dipole, we also study the fluorinated thiolates CF_3S and CF_3CH_2S . Since the directions of the dipole moment of fluorinated and of nonfluorinated thiolates are roughly opposite, this leads to an obvious difference in the interface dipole between SAMs of the two types of molecules. In addition, fluorinated thiolates have a much higher electronegativity. One would expect that by varying the relative electronegativity of the surface and the molecules, one can modify the electron transfer between surface and molecules, which would give an additional

contribution to the interface dipole.

In this chapter we will show that increasing the electronegativity by fluorinating the alkyl tails does however not lead to a change in charge transfer. We will arrive at this conclusion by analyzing the interface dipole and separating it into a contribution from the molecular dipoles and from the charge reordering at the metal–SAM interface. By comparing these results to those obtained for SAMs on Au(111) and Pt(111) interfaces, it can be concluded that the charge transfer depends on the metal surface and the nature of the sulfur–metal bond, but not on the molecular tails.

The chapter is organized as follows. In the next section we describe the techniques we use for calculating and analyzing the interface dipoles and give details on the parameters used in the calculations. Subsequently the results on the SAM–Ag(111) interfaces are discussed. First we discuss the possible structures and then we analyze the interface dipoles. The last section contains a short summary and the conclusions.

4.2 Theoretical section

4.2.1 Total energy calculations

The Ag(111) metal surface is represented by a slab of layers of metal atoms stacked according to an *fcc* ABC sequence. A typical slab consists of four layers. The SAM is adsorbed on one side of the slab. The surface unit cell depends upon the monolayer structure and coverage. The cells used in our calculations are $(\sqrt{7} \times \sqrt{7})R19.1^\circ$, $(\sqrt{3} \times \sqrt{3})R30^\circ$, and $p(2 \times 2)$, which contain 7, 3 and 4 metal atoms per layer, respectively. Periodic boundary conditions are applied in all three directions. This means that not only are the cells repeated along the surface (the *xy*-plane), but also the slabs are repeated in the *z*-direction. The atoms in neighboring cells are separated along the *z*-direction by a vacuum region of ~ 12 Å. To cancel the artificial interaction between the dipoles of the repeated slabs, the Neugebauer-Scheffler dipole correction is applied [18].

The electronic structure is treated within density functional theory (DFT) [19] using the PW91 functional [20] to describe the electronic exchange and correlation. The calculations are performed with the program VASP (Vienna *ab initio* simulation package) [21, 22] using the projector augmented wave (PAW) method [23, 24]. For noble metal atoms the outer shell *s* and *d* electrons are treated as valence electrons, and for first and second row elements the outer shell *s* and *p* electrons. The valence pseudo wave functions are expanded in a basis set consisting of plane waves. All plane waves up to a kinetic energy cutoff of 500 eV are included.

The geometries are optimized by allowing the atoms in the top two metal layers and the atoms in the SAMs to relax. The (1×1) surface unit cell parameter is fixed at its optimized bulk value of 2.93 Å. The calculations use a **k**-point sampling mesh of 7×7 for the $\sqrt{7} \times \sqrt{7}$ structure, 11×11 for the $\sqrt{3} \times \sqrt{3}$ and 9×9 for the $p(2 \times 2)$ structures, according to the Monkhorst-Pack scheme. For geometry optimization a Methfessel-Paxton smearing is used with a broadening parameter of 0.2 eV [25]. The energies of the optimized geometries are recalculated using the tetrahedron scheme [26]. Tests regarding the slab thickness, vacuum thickness, **k**-point sampling grid, and plane

wave kinetic energy cutoff are performed, from which we estimate that total energy differences are converged to within ~ 0.05 eV.

The adsorption energy of the SAM is calculated by comparing the total energy of the slab (with the adsorbed SAM), with that of the clean slab (with the top surface in its relaxed Ag(111) structure), and the free alkylthiolate (radical) molecules. If SAM adsorption results in a reconstruction of the surface that involves metal adatoms [17, 27], we assume that these adatoms are supplied by the bulk metal. The adsorption energy per molecule E_{ads} associated with a surface structure that contains M molecules, N_s metal atoms per layer and N_{ad} adatoms is then given by

$$E_{\text{ads}} = \frac{1}{M} [E_{\text{slab}} - N_s E_{\text{clean}} - N_{\text{ad}} E_{\text{bulk}}] - E_{\text{mol}}, \quad (4.1)$$

where E_{slab} is the total energy of the slab, E_{clean} is the total energy of the clean slab per surface atom (top surface in optimized Ag(111) structure), E_{bulk} is the total energy of bulk Ag per atom, and E_{mol} is the total energy of an alkylthiolate molecule. Note that E_{ads} is negative if the adsorption is exothermic.

To analyze the results we have also calculated several properties of isolated thiolate molecules: dipole moments, ionization potentials, electron affinities and electronegativities. For these calculations we use the GAMESS program [28], and treat the electronic structure within DFT using the B3LYP functional [29, 30]. We use the aug-cc-pVTZ basis set. Calculations with the smaller 6-311G** basis set give dipole moments that are up to ~ 0.15 D smaller, and ionization potentials, electron affinities that differ by ~ 0.1 eV.

4.2.2 Work functions and interface dipoles

Interface dipoles can be extracted from the change in the surface work function upon adsorption of a SAM on a metal surface, as will be described below. Surface work functions are evaluated from the expression:

$$W = V(\infty) - E_F, \quad (4.2)$$

where $V(\infty)$ is the electrostatic potential in vacuum and E_F is the Fermi energy of the bulk metal. $V(\infty)$ is extracted by calculating the average electrostatic potential in the xy -planes of the slab:

$$\bar{V}(z) = \frac{1}{C} \iint_{\text{cell}} V(x, y, z) dx dy, \quad (4.3)$$

where C is the area of the surface unit cell and $V(x, y, z)$ is the total electrostatic potential. The latter is generated on an equidistant real space grid and the integral is obtained by straightforward numerical integration. In practice $\bar{V}(z)$ reaches an asymptotic value $V(\infty)$ within a distance of $\sim 5\text{\AA}$ from the surface into the vacuum.

An example of $\bar{V}(z)$ is shown in Fig. 4.1 for CF_3S on the Ag(111) surface. W_{metal} is the work function of the clean Ag surface and $W_{\text{SAM-Ag}}$ is the work function of surface covered by the SAM. Slab calculations produce a reasonable value for the bulk Fermi

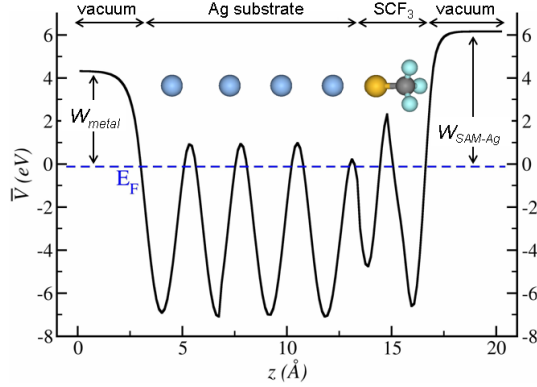


Figure 4.1: Plane averaged electrostatic potential $\bar{V}(z)$ of a slab consisting of four layers of silver atoms and one layer of CF_3S molecules on top. The z axis is normal to the (111) surface.

energy E_F , but a more accurate value is obtained from a separate bulk calculation. We follow the procedure described by Fall et al. [31]. From the convergence tests discussed in the previous section we estimate that calculated work functions are converged to within ~ 0.05 eV. Typically, DFT/PW91 calculations give work functions that are within 0.1 – 0.2 eV of the experimental values, although occasionally larger deviations of ~ 0.3 eV can be found [32, 33].

Upon adsorption of a SAM the work function of a metal surface usually changes considerably. The work function change ΔW can be interpreted in terms of a change in the surface dipole $\Delta\mu$:

$$\Delta W = W_{\text{SAM-metal}} - W_{\text{metal}} = \frac{e\Delta\mu}{\epsilon_0 A}, \quad (4.4)$$

where A is the surface area per adsorbed molecule [34]. Note that $\Delta\mu$ corresponds to the component of the dipole moment directed along the surface normal, since only this component affects the work function. $\Delta\mu$ is the result of the interface formation between the SAM and the metal surface, and we call it the *interface dipole* in the following.

We split the interface dipole into a contribution μ_{SAM} from the molecular dipoles in the SAM, and a contribution μ_{chem} from the charge transfer between the metal surface and the molecule, which occurs upon chemisorption of the SAM. The latter contribution is then defined by:

$$\mu_{\text{chem}} = \Delta\mu - \mu_{\text{SAM}}. \quad (4.5)$$

μ_{SAM} is obtained from a separate calculation on a free-standing SAM without the presence of a metal slab, but with the molecules frozen in their adsorbed geometry. In the following we will show that μ_{chem} is nearly independent of the (fluorinated)

alkyl tail of the thiolate molecule. This means that μ_{chem} is mainly determined by the sulfur–metal bond and the charge transfer associated with this bond.

Note that the calculation of μ_{SAM} is done for a full monolayer. In practice μ_{SAM} is obtained from the expression:

$$\mu_{\text{SAM}} = \frac{\varepsilon_0 A \Delta V}{e}, \quad (4.6)$$

where $\Delta V = V(\infty) - V(-\infty)$ is the potential drop over the SAM, and $V(\infty), V(-\infty)$ are the asymptotic electrostatic potentials on both sides of the SAM. These are easily obtained, since the potential reaches its asymptotic values within a distance of few Å of the SAM.

This calculation incorporates the effect of the depolarizing electric field within the SAM that is generated by the close-packed molecular dipoles. Often this effect is modeled phenomenologically by introducing an effective dielectric constant ε for the SAM:

$$\mu_{\text{SAM}} = \frac{\mu_z}{\varepsilon}, \quad (4.7)$$

where μ_z is the z -component of the permanent dipole of the isolated molecule. By obtaining μ_z from a separate calculation we will extract the effective dielectric constant as a function of the packing density of the molecules in the SAM.

4.3 Influence of packing density

We will first discuss the possible structures of thiolate SAMs on the Ag(111) surface and then study the influence of the packing density on the work function.

4.3.1 Structures

From early scanning tunneling microscopy (STM) experiments it was concluded that SAMs of alkylthiolates on the Ag(111) surface form a commensurate $(\sqrt{7} \times \sqrt{7})\text{R}10.9^\circ$ structure [35, 36]. Normal incident X-ray standing wave (NIXSW) experiments have confirmed the $\sqrt{7} \times \sqrt{7}$ structure, but have corrected the registry of the SAM on the underlying substrate to $(\sqrt{7} \times \sqrt{7})\text{R}19.1^\circ$ [16]. The proposed model of this structure has the molecules in the SAM arranged in a hexagonal lattice with a nearest neighbor distance between the sulfur atoms of 4.41 Å, see Fig. 4.2 (a). Long chain alkylthiolates adopt an expanded incommensurate $(\sqrt{7} \times \sqrt{7})\text{R}19.1^\circ$ structure with a nearest neighbor distance of 4.6 – 4.8 Å [37, 38], whereas short chain alkylthiolates keep the commensurate structure [16]. Recently a new model has been proposed for the $(\sqrt{7} \times \sqrt{7})\text{R}19.1^\circ$ structure of CH_3S SAMs on Ag(111) on the basis of NIXSW and medium energy ion scattering (MEIS) experiments [17, 39, 40]. It involves a surface reconstruction consisting of a 3/7 monolayer of Ag adatoms, which are bonded to the methylthiolate molecules, Fig. 4.2 (c).

The $(\sqrt{7} \times \sqrt{7})\text{R}19.1^\circ$ structure proposed first consists of three molecules per surface unit cell with two of the molecules adsorbed on hollow sites and one on a top site [16]. Starting from this structure we have relaxed the geometry of CH_3S on Ag(111)

and the result is shown in Fig. 4.2 (a) and (b). The molecules labeled 1 and 3 change their position only slightly and remain adsorbed in a hollow site. The molecule labeled 2 moves away from the top site towards a bridge site. The angle between the surface normal and the C–S bond is 42° , whereas that angle for molecules 1 and 3 is only $9 - 10^\circ$. The latter molecules are almost standing upright, as can be observed in Fig. 4.2 (b). We call this structure the “1,3 hollow” structure in the following. The most important bond distances and angles of this structure are given in Table 4.1. The adsorption energy (averaged, per molecule) according to eq. (4.1) is -1.97 eV.

In our previous calculations for alkylthiolate SAMs on Au(111) the molecules show a strong preference for adsorption on bridge sites, instead of on hollow or top sites [15]. Starting with CH_3S molecules 1 and 3 on bridge positions we obtain the optimized geometry that is shown in Figs. 4.2 (e) and (f). In this structure the CH_3S molecule 2 also moves closer to the bridge position, as compared to the 1,3 hollow structure, see Table 4.1. The new structure, which we call the “bridge” structure, is 0.10 eV/molecule lower in energy than the 1,3 hollow structure. The bridge structure is energetically favored over the 1,3 hollow structure. The calculated adsorption energy in the bridge structure is -2.07 eV/molecule. The geometries of the three molecules in the bridge structure are more similar than in the 1,3 hollow structure. For instance, the angle between the surface normal and the C–S bond is in the range $43 - 51^\circ$ for all three molecules, see Table 4.1. The work functions of the 1,3 hollow and the bridge structures are substantially different as will be discussed below.

We have also optimized the geometry in the $(\sqrt{7} \times \sqrt{7})\text{R}19.1^\circ$ reconstructed structure [17, 40]. The reconstruction involves a commensurate layer of Ag adatoms at a $3/7$ monolayer coverage. The sulfur atoms of the adsorbed thiolate molecules are threefold coordinated by adatoms. The optimized geometry is shown in Figs. 4.2 (c) and (d) and bond distances and angles of this structure are given in Table 4.1. The resulting structure has the CH_3S molecules standing upright with the C–S bond pointing along the surface normal in agreement with previous calculations [27, 41]. The distance of the S atoms of the different molecules to the surface is the same within ~ 0.1 Å, which represents a very small “rumpling” in agreement with the latest experimental results [40]. The work function of the reconstructed structure is substantially different from that of the unreconstructed structures as will be discussed below. The calculated adsorption energy in the reconstructed structure is -2.07 eV/molecule. This number is very close to the adsorption energy in the (unreconstructed) bridge structure. Within the intrinsic error bar of DFT calculations the two structures are degenerate in energy. It has recently been suggested that the two structures, i.e. reconstructed and unreconstructed, might coexist on the surface [41].

The optimized unreconstructed $(\sqrt{7} \times \sqrt{7})\text{R}19.1^\circ$ structure of a $\text{CH}_3\text{CH}_2\text{S}$ SAM also has the molecules adsorbed on or near bridge sites, as shown in Fig. 4.2 (g). The three molecules in the unit cell have a similar geometry. For instance, the C–S–normal angle is $42 - 45^\circ$, see Table 4.2, which is similar to the experimental value reported for $\text{CH}_3(\text{CH}_2)_7\text{S}$ on Ag(111) [16]. The chain angles are in the range $12 - 17^\circ$, which is similar to experimental results for long-chain alkylthiolates [42].

We have also studied $(\sqrt{3} \times \sqrt{3})\text{R}30^\circ$ and $\text{p}(2 \times 2)$ structures, where the surface area per adsorbed molecule is 29% and 71% larger, respectively, see Fig. 4.3. Experi-

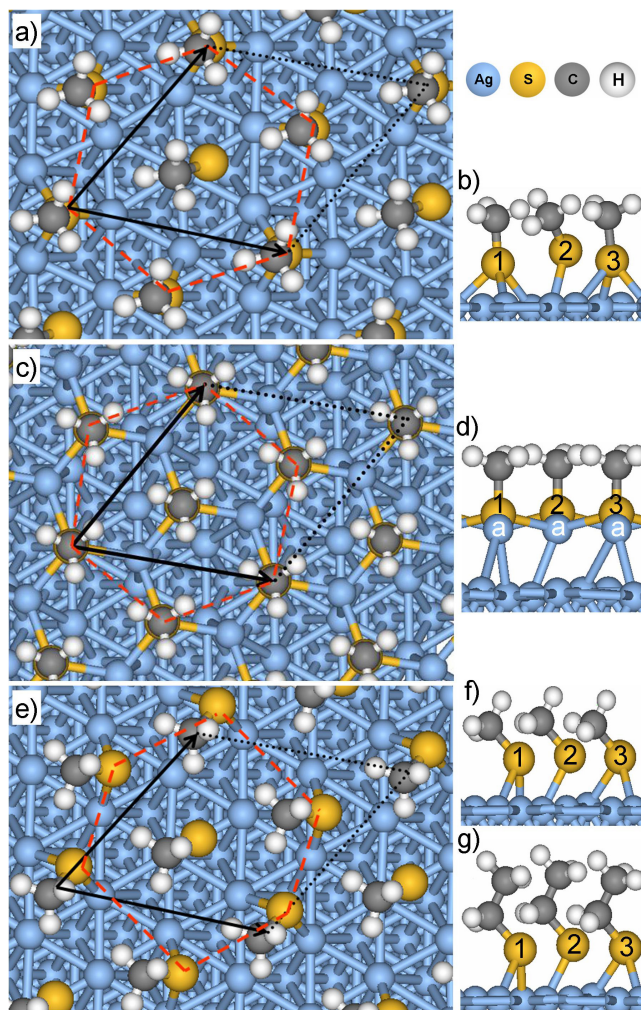


Figure 4.2: Possible $(\sqrt{7} \times \sqrt{7})R19.1^\circ$ structures of CH_3S SAMs on $\text{Ag}(111)$; (a), (b) top and side view of the 1,3 hollow structure; (c), (d) of the reconstructed structure; (e), (f) of the bridge structure; (g) of a $\text{CH}_3\text{CH}_2\text{S}$ SAM in the bridge structure. “1, 2, 3” label the molecules, “a” labels the Ag adatoms.

mentally it is not likely that alkylthiolates on $\text{Ag}(111)$ form these structures, but they enable us to model the influence of the packing density of the molecules in the SAM on the work function and the interface dipoles. In both these structure the bridge site is the favored adsorption site and the local geometry of the molecules is similar to that in the $(\sqrt{7} \times \sqrt{7})R19.1^\circ$ bridge structure.

The structure of (partially) fluorinated alkylthiolates is much less established than that of their nonfluorinated counterparts. On $\text{Au}(111)$ thiolates with long fluorinated

	molecule 1	2	3
	1,3 hollow		
C-H (Å)	1.10	1.10	1.10
S-C (Å)	1.83	1.84	1.84
Ag-S (Å)	2.52/2.50/2.50	2.47/3.01	2.63/2.54/2.54
C-S-normal (°)	9.0	42.0	9.7
Ag-S-Ag (°)	78.7/77.5/77.4	–	76.2/71.3/72.5
	bridge		
C-H (Å)	1.10	1.10	1.10
S-C (Å)	1.83	1.84	1.83
Ag-S (Å)	2.56/2.49	2.46/2.82	2.58/2.48
C-S-normal (°)	51.4	43.0	46.6
Ag-S-Ag (°)	72.3	–	72.5
	reconstructed		
C-H (Å)	1.10	1.10	1.10
S-C (Å)	1.84	1.84	1.84
Ag-S (Å)	2.65	2.66	2.64
C-S-normal (°)	0	0	0
Ag-S-Ag (°)	114.9	115.3	115.9
d_z (Å)	2.47	2.56	2.47

Table 4.1: Bond lengths and bond angles of the $(\sqrt{7} \times \sqrt{7})R19.1^\circ$ 1,3 hollow, bridge and reconstructed structures of CH_3S SAMs on $\text{Ag}(111)$. The columns indicate the three molecules in the supercell, see Fig. 4.2. d_z is the distance along the surface normal between a Ag adatom and the top Ag layer.

	molecule 1	2	3
C-H (Å)	1.10	1.10	1.10
C-C (Å)	1.52	1.53	1.52
S-C (Å)	1.85	1.85	1.84
Ag-S (Å)	2.57/2.50	2.47/2.90	2.58/2.49
C-C-normal (°)	25.5	26.3	26.8
C-S-normal (°)	44.2	41.9	45.0
chain (°)	14.7	12.0	17.1
Ag-S-Ag (°)	72.1	–	72.5

Table 4.2: Bond lengths and bond angles of the $(\sqrt{7} \times \sqrt{7})R19.1^\circ$ bridge structure of $\text{CH}_3\text{CH}_2\text{S}$ SAMs on $\text{Ag}(111)$. The chain angle represents the angle made by the line connecting the top C and S atoms with the surface normal.

alkyl tails have a less dense packing because of their relatively bulky tails [9, 43]. For such SAMs a $p(2 \times 2)$ structure has been proposed, where the spacing between the adsorbate molecules is 5.87 Å [44]. SAMs of long-chain alkylthiolates with fluorinated end groups on Au(111) have a $(\sqrt{3} \times \sqrt{3})R30^\circ$ structure [45]. The spacing between the adsorbate molecules is then 5.08 Å.

We did not find reports on the structural details of fluorinated alkylthiolate SAMs on silver in the literature. We optimized the structure of CF_3S and $\text{CF}_3\text{CH}_2\text{S}$ SAMs on Ag(111) in three different packing densities, i.e., $\sqrt{7} \times \sqrt{7}$, $\sqrt{3} \times \sqrt{3}$ and $p(2 \times 2)$. For the $(\sqrt{7} \times \sqrt{7})R19.1^\circ$ structure of a CF_3S SAM, which represents the most dense packing, we used the 1,3 hollow and the bridge structures of CH_3S as starting points and optimized the geometry. The bridge structure of CF_3S is more stable than the 1,3 hollow structure, albeit by less than 0.02 eV/molecule. However, even in the bridge structure only molecules 1 and 3 are actually adsorbed on bridge sites, whereas molecule 2 is adsorbed on a hollow site. This results in a distorted hexagonal packing of the CF_3S molecules.

For the $(\sqrt{3} \times \sqrt{3})R30^\circ$ and $p(2 \times 2)$ structures of fluorinated alkylthiolate SAMs on Au(111) we have found a preference for the molecules to adsorb on bridge sites

	$\sqrt{7} \times \sqrt{7}$	$\sqrt{3} \times \sqrt{3}$	$p(2 \times 2)$
	CF_3S		
C-F (Å)	1.35/1.36/1.35	1.36	1.36
S-C (Å)	1.85/1.83/1.87	1.84	1.84
Ag-S (Å)	2.51/2.41/2.57	2.56	2.54
C-S-normal ($^\circ$)	6.5/35.5/5.0	43.2	47.7
Ag-S-Ag ($^\circ$)	79/-/72	73.4	71.5
E_{ads} (eV)	-1.98	-2.32	-2.39
	$\text{CF}_3\text{CH}_2\text{S}$		
C-F (Å)	1.35	1.36	1.36
C-C (Å)	1.52	1.52	1.52
C-H (Å)	1.10	1.09	1.09
S-C (Å)	1.84	1.85	1.85
Ag-S (Å)	2.53/2.45/2.52	2.56	2.56
C-C-normal ($^\circ$)	25.9/25.7/29.0	25.8	21.0
C-S-normal ($^\circ$)	44.0/42.4/42.7	42.8	46.7
chain ($^\circ$)	13.9/12.9/15.1	12.3	16.7
Ag-S-Ag ($^\circ$)	72.5/-/73.5	72.1	72.0
E_{ads} (eV)	-2.01	-2.27	-2.24

Table 4.3: Bond lengths, bond angles and adsorption energies of CF_3S and $\text{CF}_3\text{CH}_2\text{S}$ SAMs adsorbed on Ag(111) surface in $(\sqrt{7} \times \sqrt{7})R19.1^\circ$, $(\sqrt{3} \times \sqrt{3})R30^\circ$ and $p(2 \times 2)$ structures. The chain angle represents the angle made in the $\text{CF}_3\text{CH}_2\text{S}$ SAM by the top C atom and the sulfur atom with the surface normal.

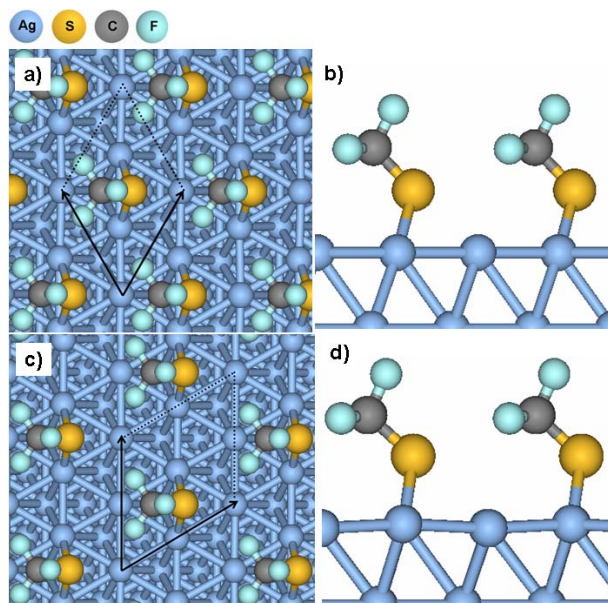


Figure 4.3: CF_3S SAM on $\text{Ag}(111)$ with the molecules adsorbed on bridge sites; (a),(b) top and side view of the $(\sqrt{3} \times \sqrt{3})\text{R}30^\circ$ structure; (c),(d) of the $\text{p}(2 \times 2)$ structure.

[15]. The calculated nearest neighbor distance between the metal atoms on $\text{Au}(111)$ and $\text{Ag}(111)$ is very similar, i.e., 2.94 and 2.93 Å respectively. Moreover, since even in the $(\sqrt{7} \times \sqrt{7})$ structure the molecules show a tendency to adsorb on bridge sites, we only consider bridge sites for the $(\sqrt{3} \times \sqrt{3})$ and $\text{p}(2 \times 2)$ structures of SAMs on Ag, see Fig. 4.3.

Table 4.3 lists the molecular geometries of CF_3S and $\text{CF}_3\text{CH}_2\text{S}$ SAMs on $\text{Ag}(111)$ adsorbed in bridge structures for the different packings. The geometries are in fact very similar, with S–Au bond lengths in the range 2.5 – 2.6 Å, and angles of the C–S bond with the surface normal around 45° . In the case of $\text{CF}_3\text{CH}_2\text{S}$ the chain angle is $13 - 15^\circ$, which is similar to that found in $\text{CH}_3\text{CH}_2\text{S}$, see Table 4.1.

The calculated adsorption energies indicate that a less dense packing of the fluorinated alkylthiolate SAMs is favorable, see Table 4.3. The $\text{p}(2 \times 2)$ structure is most stable for CF_3S , whereas for $\text{CF}_3\text{CH}_2\text{S}$ the $(\sqrt{3} \times \sqrt{3})\text{R}30^\circ$ is slightly more stable. Some of the energy differences are quite small, but the calculations correspond to the experimental trend observed in fluorinated alkylthiolates on $\text{Au}(111)$ [44, 45].

4.3.2 Work functions and interface dipoles

The change in work function upon adsorption of a SAM is defined by eq. (4.4). For the clean $\text{Ag}(111)$ surface we calculate a work function of 4.50 eV, using a 25×25 k-point Brillouin zone sampling grid. This is in good agreement with the experimen-

	$\sqrt{7} \times \sqrt{7}$	$\sqrt{3} \times \sqrt{3}$	p(2×2)
CH ₃ S	-0.52 (-0.84 ^a , -0.99 ^b)	-0.61	-0.34
CH ₃ CH ₂ S	-0.59	-0.52	-0.46
CF ₃ S	1.80 (1.79 ^a)	1.61	1.48
CF ₃ CH ₂ S	2.09	1.75	1.75

Table 4.4: Work functions shifts in eV with respect to the clean surface of SAMs on Ag(111) in the bridge structure; ^{a,b} in the 1,3 hollow and the reconstructed structure, respectively.

tal results of 4.5 eV [46] and 4.4 eV [7], and with a previously reported theoretical value of 4.42 eV, which was extracted from DFT-GGA calculations and a 15×15 **k**-point sampling [47]. The calculated work function changes upon adsorption of the (fluorinated) alkylthiolate SAMs are given in Table 4.4.

The results clearly show that alkylthiolates decrease the work function, whereas fluorinated alkylthiolates increase it significantly. Depending on the structure, a difference of 2–2.5 eV is found between the work functions of alkylthiolates and partially fluorinated alkylthiolates adsorbed on the silver surface. The work function is thus tunable over a large range by adsorption of a suitable SAM, as is observed experimentally [5, 7]. The absolute change in the work function upon adsorption of fluorinated alkylthiolates is 3–4 times larger than the change upon adsorption of nonfluorinated molecules. This result is quite different from our previous findings for SAMs on Au(111), where fluorinated and nonfluorinated molecules give a change in the work function that is similar in size (but of opposite sign, of course) [15]. We conclude that the interaction between the molecules and the silver surface differs from that between the molecules and the gold surface.

Kelvin probe measurements of the work function changes induced by adsorption of long-chain thiolate SAMs on Ag(111) have been reported by Campbell et al. [5], and by de Boer et al. [7]. The values reported for CH₃(CH₂)₉S and CH₃(CH₂)₁₅S are -0.7 eV [5], and -0.6 eV [7], respectively, and 0.9 eV [5] and 1.1 eV [7] for CF₃(CF₂)₇(CH₂)₂S. Our calculated value of -0.59 eV for CH₃CH₂S in the ($\sqrt{7} \times \sqrt{7}$)R19.1° bridge structure is close to the experimental values for alkylthiolates. The calculated values for the fluorinated molecules are higher than the experimental values even for the less densely packed p(2×2) structure. One explanation might be that the effective dipole moment of a long-chain fluorinated molecule embedded in a SAM is smaller than that of a short-chain molecule; in other words, the effective dielectric constant in a long-chain fluorinated thiolate SAM is larger, see eq. (4.7). In addition, SAMs of fluorinated alkylthiolates may show more intrinsic disorder than their nonfluorinated counterparts [45], which also reduces the average dipole moment perpendicular to the surface.

The three $\sqrt{7} \times \sqrt{7}$ structures for CH₃S SAMs discussed in the previous section give rise to different work functions. The adsorption of molecules in the bridge structure gives a substantial smaller shift of the work function than adsorption in the 1,3 hollow

structure or the reconstructed structure. Using eq. (4.4) we can interpret the changes in the work function in terms of molecular dipoles. This difference in work function shift between the structures can be related to the orientation of the molecular dipoles. Whereas in the bridge structure the molecular tails are tilted with respect to the surface normal, the tails of the two molecules that are adsorbed at hollow sites in the 1,3 hollow structure are almost perpendicular to the surface, see Table 4.1. The latter leads to larger dipole moments along the surface normal. All the molecular tails in the reconstructed structure are perpendicular to the surface, which leads to large dipole moments and a large work function shift. These results suggest that work function measurements might be a simple experimental way of distinguishing between the different structures.

As can be observed in Table 4.4, the work functions have a relatively weak dependence on the packing density. The local geometries of the thiolate molecules in the bridge structure are similar for the different packings, see e.g. Table 4.3. Hence one would expect the individual molecular dipoles to be similar. The weak dependence of the work functions on the packing density might seem somewhat surprising. Assuming fixed interface dipoles $\Delta\mu$ per molecule in eq. (4.4), the work functions should scale as $1/A$, where A is the surface area per molecule. Since this is clearly not the case, it means that $\Delta\mu$ depends on the packing density. In particular, the individual molecular dipoles increase with decreasing packing density.

Decreasing the packing density increases the distances between the molecules in the SAM. Hence it decreases the depolarizing field in the SAMs, or, in other words, the effective dielectric constant ε introduced in eq. (4.7) decreases with decreasing packing density. This effectively increases the molecular dipoles, which opposes the effect of a decreasing density of the molecules on the interface dipole. The net result is a weak dependence of the work function on the packing density in the range considered and in some cases even a nonmonotonic behavior, see Table 4.4.

In order to quantify this analysis we make use of the relations given by eqs. (4.4)–(4.7). We extract from the work function change an interface dipole per molecule $\Delta\mu$ and split $\Delta\mu$ into a contribution μ_{SAM} from the molecular dipole and a contribution μ_{chem} from the charge transfer between the molecule and the surface upon chemisorption. The results for each of the SAMs in the $\sqrt{7} \times \sqrt{7}$, $\sqrt{3} \times \sqrt{3}$ and $p(2 \times 2)$ structures are reported in Table 4.5. As we are explicitly interested in the influence of the packing density we continue to compare similar, i.e. bridge-like, structures.

μ_{SAM} is positive for fluorinated alkylthiolates, which means that the molecular dipoles point from the S atom to the CF_3 group. For the nonfluorinated alkylthiolates the absolute values of μ_{SAM} are larger, but the sign is negative, meaning that the dipoles point from the alkyl tails to the S atom. μ_{chem} is positive for all molecules. The latter contribution is associated with a dipole that points from the surface to the molecule. It is associated with a (partial) electron transfer from the surface to the molecule. Both contributions, μ_{SAM} and μ_{chem} , to the interface dipole $\Delta\mu$ are of comparable size. For the nonfluorinated molecules they are of opposite sign, which leads to moderate interface dipoles $\Delta\mu = -0.2$ to -0.3 D and work function changes ~ 0.5 eV. The contributions μ_{SAM} and μ_{chem} have the same sign for the fluorinated molecules, which gives large interface dipoles $\Delta\mu = 0.9$ – 1.3 D and large work function

structure		CH ₃ S	CH ₂ CH ₃ S	CF ₃ S	CF ₃ CH ₂ S
$\sqrt{7} \times \sqrt{7}$	$\Delta\mu$	-0.24	-0.27	0.83	0.96
	μ_{SAM}	-0.78	-0.79	0.39	0.43
	μ_{chem}	0.54	0.52	0.44	0.53
	ε	1.6	1.4	2.0	2.7
$\sqrt{3} \times \sqrt{3}$	$\Delta\mu$	-0.36	-0.31	0.95	1.04
	μ_{SAM}	-0.88	-0.79	0.44	0.50
	μ_{chem}	0.52	0.46	0.51	0.54
	ε	1.4	1.4	1.8	2.3
p(2×2)	$\Delta\mu$	-0.27	-0.36	1.17	1.38
	μ_{SAM}	-0.92	-1.01	0.50	0.71
	μ_{chem}	0.65	0.65	0.67	0.67
	ε	1.3	1.1	1.6	1.7

Table 4.5: Dipole per molecule $\Delta\mu$ from work function shift upon adsorption, the (perpendicular) molecular dipole moment μ_{SAM} in a free standing SAM and the chemisorption dipole moment μ_{chem} of the SAMs on Ag(111) surface. The values are in D. ε is the effective dielectric constant of the free standing SAM.

changes of up to 2.1 eV.

Comparing the results for the different packing densities in Table 4.5, we observe that the absolute value of μ_{SAM} increases if the packing density decreases. This can be understood by noting that the effective dielectric constant ε of the SAM decreases if the packing density decreases, as discussed above. We have calculated the dipole moment of the isolated alkylthiolate radical molecules, fixing the molecules in the geometries they attain in the SAM. The component μ_z along the surface normal in the adsorbed geometry is given in Table 4.6. From eq. (4.7) we then calculate the effective dielectric constant of the free standing SAM. The dielectric constants for fluorinated alkylthiolate SAMs are somewhat larger than those of their nonfluorinated counterparts. This might be expected since the polarizability of fluorinated molecules is larger and therefore screening in the SAM is larger. The results in Table 4.5 clearly

	CH ₃ S	CH ₂ CH ₃ S	CF ₃ S	CF ₃ CH ₂ S
EA	1.73	1.87	3.02	2.43
IP	9.20	8.95	10.79	9.82
χ_M	5.47	5.41	6.91	6.13
$ \mu_{\text{tot}} $	1.70	1.82	1.05	2.06
μ_z	-1.23	-1.14	0.79	1.17

Table 4.6: Electron affinity (EA), ionization potential (IP), Mulliken electronegativity (χ_M) in eV, total dipole moment $|\mu_{\text{tot}}|$ and dipole moment along the surface normal μ_z in D of isolated molecules in their adsorbed geometries.

show that the dielectric constants decrease with decreasing packing density.

μ_{chem} also increases with decreasing packing density. The origin of this effect is similar to that discussed in the previous paragraph; the screening of the dipoles in the layer decreases if the packing density decreases. An interesting observation is that at fixed packing density μ_{chem} shows little variation within the range of molecules. Apparently it is mainly determined by the S–Ag interaction and not so much by the molecular tails.

Upon adsorption electronic charge is transferred from the surface to the molecule. In order to visualize the charge transfer at the interface upon adsorption of the SAMs, we calculate the change in electron density Δn :

$$\Delta n = n_{\text{SAM-Ag}} - n_{\text{Ag}} - n_{\text{SAM}}, \quad (4.8)$$

where $n_{\text{SAM-Ag}}$, n_{Ag} and n_{SAM} are the electron densities of the SAM adsorbed on Ag(111), of the Ag(111) surface and of the free-standing SAM, respectively. The electron distributions are obtained on a real space grid from separate calculations on the adsorbed SAM, on the substrate and on the free-standing SAM, respectively. In the latter two calculations the substrate and the molecules are fixed in the adsorption geometries.

As examples, Fig. 4.4 shows the difference electron density Δn averaged in the xy plane along the surface normal of CH_3S and CF_3S SAMs adsorbed in the $\sqrt{7} \times \sqrt{7}$ structure and of $\text{CH}_3\text{CH}_2\text{S}$ and $\text{CF}_3\text{CH}_2\text{S}$ SAMs adsorbed in the $p(2 \times 2)$ structure. In addition 3-dimensional visualizations of Δn at the interface are presented. Only the region around the SAM/Ag(111) interface is shown, since in the substrate and the vacuum region $\Delta n \simeq 0$. The figures clearly demonstrate that Δn is localized at the interface, i.e., near the sulfur atoms and the top metal layer. Electronic density is transferred mainly from the top layer of silver atoms to the sulfur atoms, which results in a dipole moment μ_{chem} .

To check the consistency of this analysis, we can calculate the metal–sulfur dipoles from the difference electron density:

$$\mu'_{\text{chem}} = \iiint_{z_o}^{z_v} z \Delta n(x, y, z) dx dy dz, \quad (4.9)$$

where we choose z_o in the center between the second and the third metal layer of the substrate and z_v in the center of the vacuum. The metal–sulfur dipoles μ'_{chem} are within 10% of the values μ_{chem} listed in Table 4.5.

By integrating the peak of Δn on the sulfur atom, see Fig. 4.4, one can calculate the charge transfer from the substrate to the sulfur atom. A typical value over a range of structures is $q = (0.11 \pm 0.01)e$. Modeling the charge transfer dipole as $\mu_{\text{chem}} = qd$ gives $d = 1.1 \text{ \AA}$, assuming $\mu_{\text{chem}} = 0.6 \text{ D}$. The distance between the sulfur atoms and the top layer of silver atoms is $2.0 - 2.2 \text{ \AA}$, so this analysis is consistent with the interpretation of μ_{chem} as a metal–sulfur bond dipole.

The fact that this dipole moment hardly depends on the different molecular tails is slightly surprising, since the electronegativity of fluorinated tails is much higher than that of unfluorinated ones. The Mulliken electronegativity of a molecule is defined as:

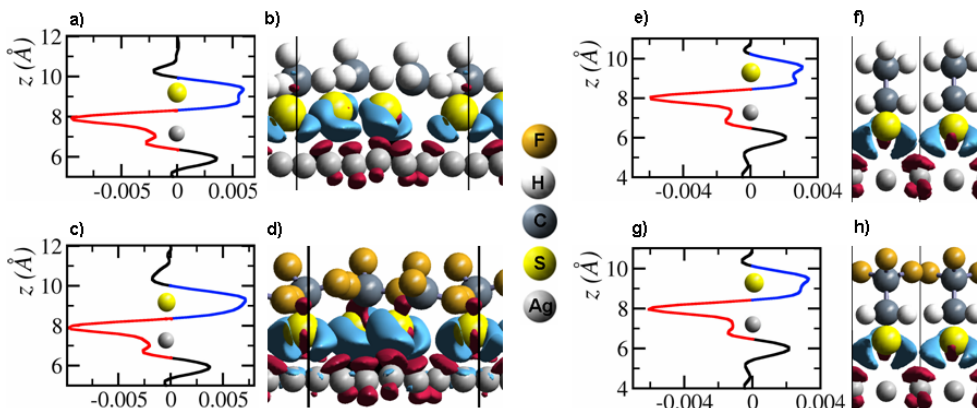


Figure 4.4: Difference electron density along the surface normal (z) averaged over the xy plane in units of \AA^{-3} and as isodensity surface. (a), (b) CH_3S and (c), (d) CF_3S in the $\sqrt{7} \times \sqrt{7}$ structure; (e), (f) $\text{CH}_3\text{CH}_2\text{S}$ and (g), (h) $\text{CF}_3\text{CH}_2\text{S}$ in the $p(2 \times 2)$ structure.

$$\chi_M = \frac{EA + IP}{2}, \quad (4.10)$$

where EA and IP are the electron affinity and ionization potential of the molecule. The EAs , IPs and Mulliken electronegativities of the molecules considered in this chapter (fixed in their adsorbed geometries) are given in Table 4.6.

One observes a considerable difference in the electronegativities χ_M of the molecules. The χ_M of both alkylthiolates is similar, but the χ_M of fluorinated alkylthiolates is much larger. The HOMO of the radical neutral molecules, which plays a role in determining the EA and IP, is stabilized by the electron withdrawing CF_3 group. This property is commonly associated with the attractive Coulomb field of the CF_3 group. The HOMO of the neutral molecules is localized mainly on the sulfur atom and one expects that the effect of the CF_3 group decreases if the distance between this group and the sulfur atom increases. Indeed one finds that the EA, IP and χ_M of CF_3S are significantly higher than those of $\text{CF}_3\text{CH}_2\text{S}$.

The electronegativity of a metal surface is given by its work function. From simple chemical reasoning one would assume that the charge transfer between a molecule and a surface would depend on the difference of their electronegativities. This is clearly not the case; the electronegativity of the molecule does not seem to influence the charge transfer. This suggests that the effects of the Coulomb field of the CF_3 group and the alkyl tails on the charge distribution at the sulfur–metal interface are screened by the metal.

4.4 Summary and conclusions

We have studied the interface dipole formation and work function changes produced by adsorption of CH_3S , $\text{CH}_3\text{CH}_2\text{S}$, CF_3S and $\text{CF}_3\text{CH}_2\text{S}$ SAMs on the Ag(111) surface by means of DFT calculations. Adsorption of the alkylthiolates CH_3S and $\text{CH}_3\text{CH}_2\text{S}$ decreases the work function as compared to the clean metal surface, whereas adsorption of the fluorinated alkylthiolates CF_3S and $\text{CF}_3\text{CH}_2\text{S}$ increases the work function.

In particular we have examined the influence of the structure and the packing density of the molecules in the SAM. CH_3S on Ag(111) in the unreconstructed $(\sqrt{7} \times \sqrt{7})\text{R}19.1^\circ$ structure with two of the three molecules in the unit cell adsorbed at a hollow site, leads to a work function shift of -0.8 eV. Adsorbing the CH_3S molecules on bridge sites stabilizes the structure by 0.10 eV/molecule and gives a work function shift of -0.5 eV. The recently proposed surface reconstruction induced by CH_3S adsorption yields an almost identical adsorption energy, and a work function shift of -1.0 eV. The difference between the work functions of these structures can be interpreted in terms of the difference in the orientation of the molecular dipoles.

These results are compared to the less densely packed $(\sqrt{3} \times \sqrt{3})\text{R}30^\circ$ and $\text{p}(2 \times 2)$ structures, which are more likely to occur for fluorinated alkylthiolate SAMs. Although the work function shift generally decreases for decreasing packing density, it is not simply proportional to the density of molecular dipoles. A partial compensating effect is caused by a decrease of the dielectric screening in the molecular layer.

Comparing the different molecules adsorbed in similar geometries shows that fluorinated alkylthiolates can increase the work function by up to 2 eV, which is much larger than the decrease in work function caused by (nonfluorinated) alkylthiolate adsorption. We explain this by separating the interface dipole into a contribution from the molecular dipoles and from the charge reordering at the metal-SAM interface. Electron transfer occurs from the Ag surface to the sulfur atoms of the thiolate molecules. The resulting dipole points in the same direction as the molecular dipole for fluorinated molecules. Addition of the two dipoles leads to a large interface dipole and a large work function shift. The direction of the molecular dipole of nonfluorinated molecules is opposite to the metal-sulfur bond dipole, resulting in a much smaller interface dipole and work function shift.

The electron transfer from the Ag surface to the molecules is remarkably independent of the electronegativity of the molecules. In good approximation the charge reordering only depends upon the metal-sulfur bond, which suggests that the influence of the molecular tails is screened by the metal substrate. In previous calculations we arrived at the same conclusion for adsorption of alkylthiolate SAMs on other noble metal surfaces, indicating that this result is more general [15, 48]. For adsorption on Ag(111) we find effective Ag-S dipoles $\mu_{\text{chem}} = 0.51 \pm 0.04$ D and 0.66 ± 0.01 D in the $(\sqrt{3} \times \sqrt{3})$ and $\text{p}(2 \times 2)$ structures, respectively.

For adsorption on Au(111) we have found very small Au-S dipoles $\mu_{\text{chem}} < 0.1$ D, indicating an apolar Au-S bond [15], whereas for adsorption on Pt(111) the Pt-S dipole is $\mu_{\text{chem}} = -0.45 \pm 0.03$ D [48]. The latter indicates an electron transfer from the sulfur atoms to the Pt surface. The metal-sulfur bonds formed upon SAM adsorption generate dipole moments that reduce the work function differences between the

clean metal surfaces, and can even reverse the order. The molecular dipole moments exhibit similar values for adsorption on Ag, Au and Pt, thus giving the possibility to design interface dipoles. By adding molecular and metal–sulfur bond dipoles the overall work function can be determined. It is possible to manipulate metal work functions considerably using SAMs. Work function shifts that can be as large as 2 eV.

Acknowledgments

This work is supported by “Prioriteits Programma Materialenonderzoek” (PPM), by the “Stichting voor Fundamenteel Onderzoek der Materie” (FOM), financially supported by the “Nederlandse Organisatie voor Wetenschappelijk Onderzoek” (NWO), and by “NanoNed”, a nanotechnology program of the Dutch Ministry of Economic Affairs. The use of supercomputer facilities was sponsored by the “Stichting Nationale Computer Faciliteiten” (NCF), financially supported by NWO.

Bibliography

- [1] J. K. Lee, K.-B. Lee, D. J. Kim, and I. S. Choi, *Langmuir* **19**, 8141 (2003).
- [2] J. D. Swalen *et al.*, *Langmuir* **3**, 932 (1987).
- [3] C. S. Chen, M. Mrksich, S. Huang, G. M. Whitesides, and D. E. Ingber, *Biotechnol. Prog.* **14**, 356 (1998).
- [4] I. D. Parker, *J. Appl. Phys.* **75**, 1656 (1994).
- [5] I. H. Campbell *et al.*, *Phys. Rev. B* **54**, 14321 (1996).
- [6] I. H. Campbell *et al.*, *Appl. Phys. Lett.* **71**, 3528 (1997).
- [7] B. de Boer, A. Hadipour, M. M. Mandoc, T. van Woudenberg, and P. W. M. Blom, *Adv. Mater.* **17**, 621 (2005).
- [8] G. E. Poirier, *Langmuir* **15**, 1167 (1999).
- [9] F. Schreiber, *Prog. Surf. Sci.* **65**, 151 (2000).
- [10] M. C. Vargas, P. Giannozzi, A. Selloni, and G. Scoles, *J. Phys. Chem. B* **105**, 9500 (2001).
- [11] Y. Morikawa, T. Hayashi, C. C. Liew, and H. Nozoye, *Surf. Sci.* **507**, 46 (2002).
- [12] V. D. Renzi *et al.*, *Phys. Rev. Lett.* **95**, 046804 (2005).
- [13] G. Heimel, L. Romaner, J.-L. Brédas, and E. Zojer, *Phys. Rev. Lett.* **96**, 196806 (2006).
- [14] R. Rousseau *et al.*, *J. Phys. Chem. B* **110**, 10862 (2006).

-
- [15] P. C. Rusu and G. Brocks, *J. Phys. Chem. B* **110**, 22628 (2006).
- [16] H. Rieley, G. K. Kendall, R. G. Jones, and D. P. Woodruff, *Langmuir* **15**, 8856 (1999).
- [17] M. Yu *et al.*, *J. Phys. Chem. B* **110**, 2164 (2006).
- [18] J. Neugebauer and M. Scheffler, *Phys. Rev. B* **46**, 16067 (1992).
- [19] P. Hohenberg and W. Kohn, *Phys. Rev.* **136**, B864 (1964).
- [20] J. P. Perdew *et al.*, *Phys. Rev. B* **46**, 6671 (1992).
- [21] G. Kresse and J. Hafner, *Phys. Rev. B* **47**, (R)558 (1993).
- [22] G. Kresse and J. Furthmüller, *Phys. Rev. B* **54**, 11169 (1996).
- [23] G. Kresse and D. Joubert, *Phys. Rev. B* **59**, 1758 (1999).
- [24] P. E. Blöchl, *Phys. Rev. B* **50**, 17953 (1994).
- [25] M. Methfessel and A. T. Paxton, *Phys. Rev. B* **40**, 3616 (1989).
- [26] P. E. Blöchl, O. Jepsen, and O. K. Andersen, *Phys. Rev. B* **49**, 16223 (1994).
- [27] G.-M. He, *Phys. Rev. B* **74**, 245421 (2006).
- [28] M.W.Schmidt *et al.*, *J. Comput. Chem.* **14**, 1347 (1993).
- [29] A. D. Becke, *J. Chem. Phys.* **98**, 5642 (1993).
- [30] P.J.Stephens, F.J.Devlin, C.F.Chabrowski, and M.J.Frisch, *J. Phys. Chem.* **98**, 11623 (1994).
- [31] C. J. Fall, N. Binggeli, and A. Baldereschi, *J. Phys.: Condens. Matter.* **11**, 2689 (1999).
- [32] A. Michaelides, P. Hu, M.-H. Lee, A. Alavi, and D. A. King, *Phys. Rev. Lett.* **90**, 246103 (2003).
- [33] F. Favot, A. D. Corso, and A. Baldereschi, *J. Chem. Phys.* **114**, 483 (2001).
- [34] J. D. Jackson, *Classical Electrodynamics* (Wiley, New York, 1975).
- [35] A. Dhirany, A. J. Hines, A. J. Fisher, O. Ismail, and P. Guyot-Sionnest, *Langmuir* **11**, 2609 (1995).
- [36] R. Heinz and J. P. Rabe, *Langmuir* **11**, 506 (1995).
- [37] P. Fenter *et al.*, *Langmuir* **7**, 2013 (1991).
- [38] M. Fonticelli *et al.*, *J. Phys. Chem. B* **108**, 1898 (2004).
- [39] M. Yu, S. M. Driver, and D. P. Woodruff, *Langmuir* **21**, 7285 (2005).

- [40] G. Parkinson *et al.*, Surf. Sci. **601**, 50 (2007).
- [41] D. Torres, P. Carro, R. C. Salvarezza, and F. Illas, Phys. Rev. Lett. **97**, 226103 (2006).
- [42] P. E. Laibinis *et al.*, J. Am. Chem. Soc. **113**, 7152 (1991).
- [43] G.-Y. Liu *et al.*, J. Chem. Phys. **101**, 4301 (1994).
- [44] C. A. Alves and M. D. Porter, Langmuir **9**, 3507 (1993).
- [45] J. Pflaum *et al.*, Surf. Sci. **89**, 498 (2002).
- [46] R. C. Monreal, L. Guillemot, and V. A. Esaulov, J. Phys.: Condens. Matter. **15**, 1165 (2003).
- [47] M. L. Bocquet, A. M. Rappe, and H. L. Dai, Mol. Phys. **103**, 883 (2005).
- [48] P. C. Rusu and G. Brocks, Phys. Rev. B **74**, 073414 (2006).

Part II

Interfaces formed by π -conjugated organic monolayers on metal surfaces

Chapter 5

Work function pinning at metal-organic interfaces

Despite the relatively weak interaction between organic molecules and metal surfaces, substantial dipoles are formed at metal-organic interfaces. We monitor interface dipoles by first-principles calculations of work function changes caused by adsorption of perylene and 3,4,9,10-perylene-tetra-carboxylic-di-anhydride monolayers. These changes are the result of two competing effects. Pauli repulsion pushes electrons into the surface, which decreases the work function. If the metal work function is sufficiently low, electrons are donated back from the surface to the molecule. In this regime the work function is effectively determined by pinning of the Fermi level at a molecular energy level.

The rapidly developing field of organic electronics has stimulated intensive research into the fundamental electronic properties of molecular organic semiconductors and their interfaces with metal electrodes [1, 2]. As the quality of molecular crystals increases, transport of charge carriers across the interfaces between metal electrodes and the organic material starts to determine the device performance [3, 4]. Often large dipoles are found at metal-organic interfaces (MOIs), which strongly influence the barrier for charge carrier injection [5, 6]. MOI dipoles are localized foremost at the first molecular layer and can be extracted from the change in the surface work function after deposition of an organic monolayer [2].

The large size of the MOI dipoles indicates a substantial charge reordering at the interface, which might seem surprising since often there is only a weak bonding between the metal surface and the molecular layer. Inert physisorbed atoms and molecules decrease the work function, which is interpreted using the Pauli repulsion between the molecular and surface electrons (the “pillow effect”) [7, 8]. Adsorption of π -conjugated molecules can lead to a substantial increase, as well as a decrease of the work function [2, 5, 6].

In this paper we use density functional theory (DFT) calculations to study the

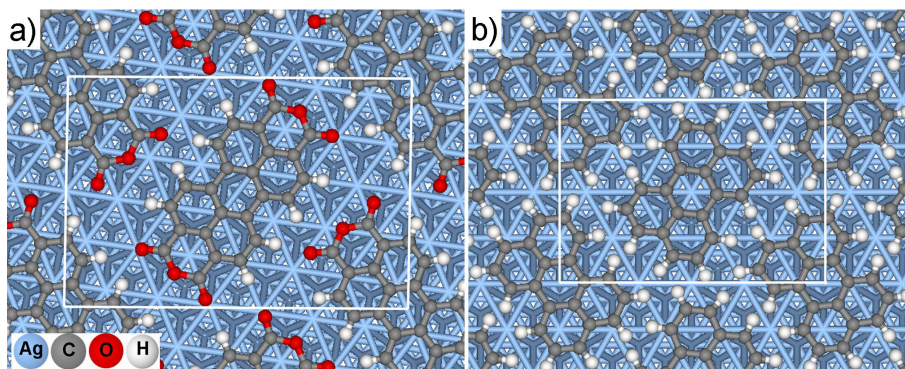


Figure 5.1: Herringbone structure of a monolayer of (a) PTCDA and (b) perylene on Ag(111).

work function change due to monolayers of the molecules PTCDA (3,4,9,10-perylene-tetra-carboxylic-di-anhydride) and perylene, adsorbed on metal surfaces with work functions ranging from 3.0 eV (Ca) to 5.3 eV (Au). For both molecules we find a cross-over from a regime in which the work function is reduced by the pillow effect to a regime in which the work function is pinned. The crossover value of the work function is higher for the systems with PTCDA overlayers (~ 4.7 eV, in agreement with experiments [5]) than for the systems with perylene overlayers (~ 3.7 eV). Pinning is interpreted from charge transfer to the lowest unoccupied molecular orbital (LUMO). The position of the cross-over from the pillow effect regime can be correlated with the position of the LUMO.

PTCDA adsorbed on noble metal (111) surfaces are experimental model systems for studying MOIs [9–12]. In a monolayer the PTCDA molecules are arranged in a herringbone structure with their planes parallel to the surface, see Fig. 5.1. The experimental distances between the monolayer and the metal surface are 2.9 and 3.3 Å for Ag(111) and Au(111), respectively [10, 13]. For Ag(111) DFT calculations have a problem to predict this distance, raising a discussion about the nature of the bonding between PTCDA and the surface [9, 10, 14]. Common DFT functionals describe strong chemical interactions well, but they fail to capture weaker (van der Waals) bonding correctly. Nevertheless for large molecules such bonding can be sizable, and the deficiency can lead to underestimating the binding energy and overestimating the bonding distance. For this reason we did not attempt to calculate the distance d between molecule and surface, but instead performed calculations for a range of distances $d = 3.0 - 3.6$ Å, close to the experimental values.

The results in this paper show that charge transfer at a PTCDA-metal interface and the resulting work function pinning are given accurately by DFT calculations. The charge distribution is mainly determined by electrostatics and short-range exchange-correlation, which are described well by common DFT functionals. A similar conclusion has been drawn for the charge transfer between molecules in an organic crystal [15].

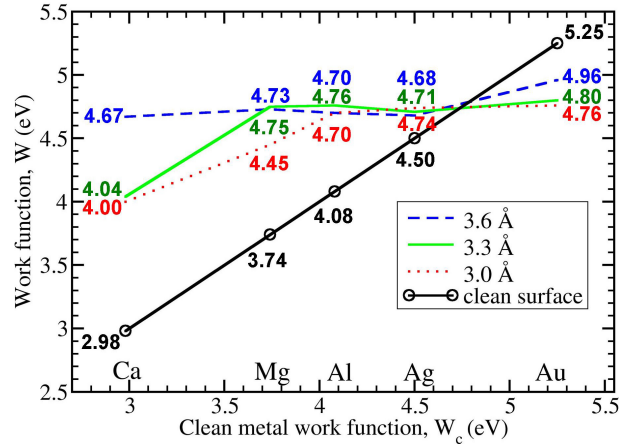


Figure 5.2: Work functions of a PTCDA monolayer on (111) metal surfaces [(0001) for Mg]. The clean metal work function is given along the x -axis. The numbers give the calculated values, the lines guide the eye. The bottom (black) curve refers to the clean metal surfaces. The top three curves are for different distances d between the PTCDA molecules and the surfaces.

Density functional theory (DFT) calculations are carried out using the VASP program [16, 17], with projector augmented waves (PAW) [18], a plane wave basis set and the PW91 functional. We use supercells containing a slab of at least three layers of metal atoms, a molecular monolayer adsorbed on one side of the slab, and a vacuum region of at least 10 Å. The surface Brillouin zone is sampled by a 5×5 k -point grid; the plane wave kinetic energy cutoff is 400 eV. To avoid interactions between periodic images of the slab, a dipole correction is applied [19]. Work functions are calculated as in Ref. [20]. Calculated work functions of clean metal surfaces are usually within ~ 0.2 eV of the experimental values.

Fig. 5.2 shows the calculated work functions of a PTCDA monolayer adsorbed on Ca, Mg, Al, Ag and Au. All metal surfaces are close-packed and the surface unit cells are chosen such that the PTCDA layer has a density of ~ 1 molecule per 120 \AA^2 . Adsorption of PTCDA on Au decreases the work function, whereas adsorption on the other metals increases it. At $d = 3.3 \text{ \AA}$ the work function is almost independent of the metal substrate and it is pinned at ~ 4.7 eV.

Adsorption on Ca is a somewhat exceptional case. The geometries of the molecule and of the surface are then severely distorted, which indicates a strong chemical interaction between PTCDA and Ca [21]. Weakening the interaction artificially by increasing the distance to $d = 3.6 \text{ \AA}$, also brings the work function of PTCDA on Ca to 4.7 eV. The work functions of PTCDA on Mg, Al and Ag are almost unchanged by increasing the distance to $d = 3.6 \text{ \AA}$. Only the value for PTCDA on Au is increased by 0.2 eV, which we attribute to a decrease of the pillow effect to be discussed below. Decreasing the distance to 3.0 \AA brings little changes to most of the work functions.

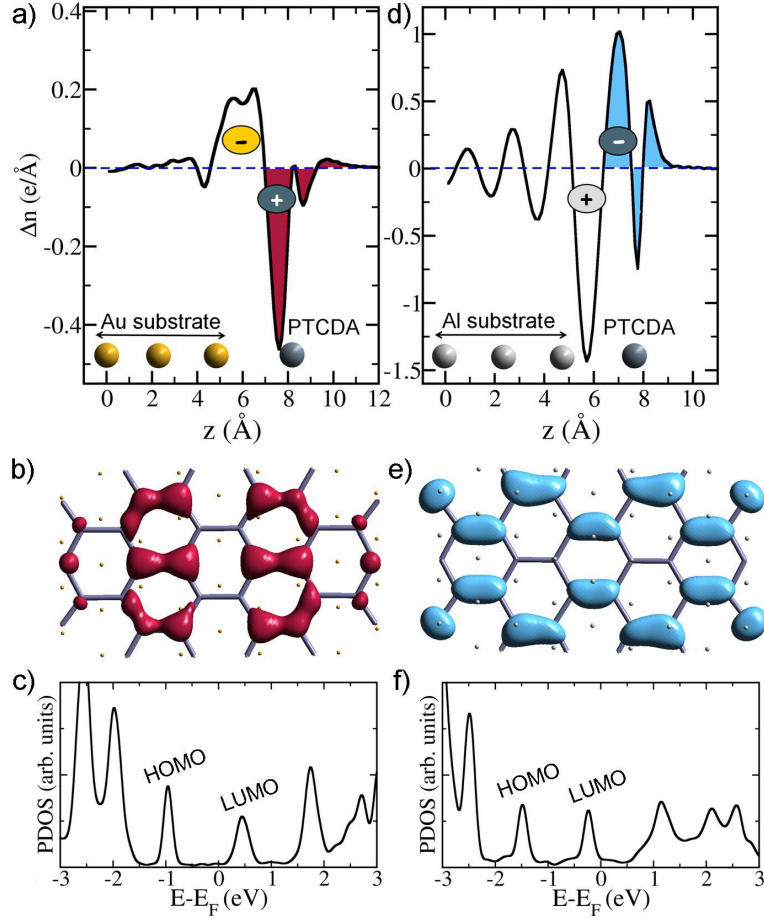


Figure 5.3: (a) Electron density difference per molecule Δn for PTCDA on Au(111) at $d = 3.3 \text{ \AA}$, as function of z , integrated over x, y . The \pm indicates the direction of the interface dipole; (b) isodensity surface of Δn close to the molecular plane; (c) projected density of states (PDOS) on PTCDA; (d) Δn for PTCDA on Al(111) at $d = 3.0 \text{ \AA}$; (e) isodensity surface; (f) PDOS; labels refer to the same peaks as in (c).

The largest effect is a decrease of 0.3 eV for Mg, accompanied by a geometrical distortion of molecule and surface [21].

In conclusion, for a range of distances and metal substrates the work function is remarkably constant at $\sim 4.7 \text{ eV}$. The fact that the work function is pinned by a PTCDA monolayer, as well as the energy of the pinning level, are in good agreement with experimental results [5]. "Unpinning" only occurs on very low work function metals, where one expects a strong chemical interaction between molecule and metal.

The work function change after adsorption results from the formation of an in-

interface dipole. This can be visualized by the (laterally averaged) electron density difference $\Delta n = n_{\text{PTCDA/met}} - n_{\text{met}} - n_{\text{PTCDA}}$, where the electron density of the clean surface n_{met} and that of the isolated molecular layer n_{PTCDA} are obtained in separate calculations. Examples of Δn are given in Fig. 5.3. Calculating the interface dipole as $\Delta\mu = \int z\Delta n(z)dz$ gives a good agreement with the interface dipole $e\Delta\mu = \Delta W\varepsilon_0 A$ extracted from the change in work function ΔW (with A the surface area per molecule).

Fig. 5.3 (a) shows Δn for PTCDA on Au to be localized at the PTCDA/Au interface. The net effect of orthogonalizing the molecular and the surface wave functions, is that electrons are pushed from the *molecular region* into the *metal*, called the pillow effect [7]. The resulting dipole layer is localized mainly between the PTCDA layer and the metal surface, and it decreases the work function. Since the pillow effect is sensitive to the overlap between the molecular and the surface wave functions, it decreases with an increasing molecule-surface distance. This is observed in Fig. 5.2 for PTCDA on Au. The charge depletion in the PTCDA region is shown in Fig. 5.3 (b). Its nodal pattern corresponds to the second highest occupied molecular π orbital of PTCDA. Modeling the interface dipole as a plane capacitor $\Delta\mu = q\delta$ and calculating the charge by integrating over the shaded peak in Fig. 5.3 (a) gives $q = 0.34e$ and $\delta = 1.05 \text{ \AA}$, which illustrates the strong localization of the dipole layer.

The dipole layer generates a potential step that lowers the molecular levels with respect to the Fermi level E_F of the substrate. For PTCDA on Au E_F lies below the LUMO, as is shown in the projected density of states (PDOS) of Fig. 5.3 (c). The fact that the occupied levels of PTCDA lie substantially below E_F indicates that the charge transfer from the molecular region to the surface is due to the pillow effect, and is not an electron donation from the highest occupied molecular orbital (HOMO) to the metal.

The change in electron density for PTCDA on lower work function metals is qualitatively different. An example for PTCDA on Al is shown in Fig. 5.3 (d-f). Electrons are transferred from the *metal* to the *molecule*. The distribution of Δn is much wider than for PTCDA on Au, although the maximum amplitude is still between the PTCDA layer and the metal surface. Into the Al substrate Δn shows Friedel oscillations that are typical of electrostatic screening in a metal of a charge outside the metal. On the molecule Δn has the nodal structure that is characteristic of the LUMO of PTCDA. Electronic charge has been transferred to the LUMO, in agreement with experimental observations [10–12], as is confirmed by the PDOS in Fig. 5.3 (f).

The Pauli repulsion between the molecular and surface states is operative for adsorption on any metal surface. In general the charge transfer is therefore the net result of pushing metal electrons out of the region of the occupied PTCDA orbitals into the metal (the pillow effect), plus an electron back-donation from the metal to the LUMO of PTCDA. At the point in Fig. 5.2 where the three upper curves cross the lowest curve (4.7 eV) the work function of a PTCDA covered surface is identical to that of a clean metal surface. At this point the interface dipole is zero and the pillow effect and back-donation are then exactly balanced. From Fig. 5.2 it can be observed that this point corresponds to the pinning level of the work function.

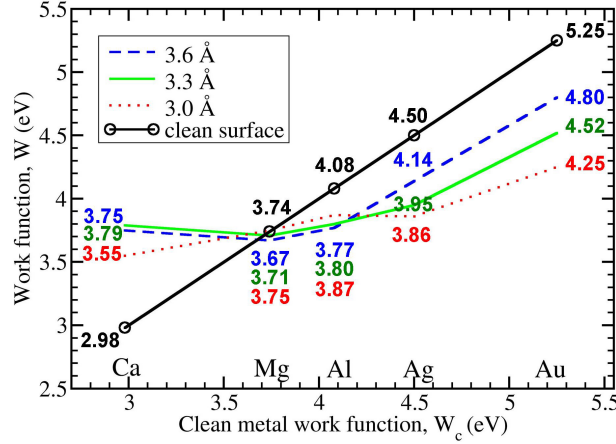


Figure 5.4: As Fig. 5.2, for a monolayer of perylene molecules.

Pinning at MOIs has been interpreted before in terms of a charge neutrality level (CNL), in analogy to a Schottky barrier model for conventional semiconductors [22, 23]. That model relies upon a large density of interface states (DOIS) in the fundamental gap of the semiconductor, which tends to pin the Fermi level of the metal. In a molecular semiconductor a large DOIS could result from a strong metal-molecule interaction, which would lead to a large broadening of the molecular levels. In our calculations we do not observe the very large broadening found in Refs. [22] and [23], see Fig. 5.3 (c),(f). The absence of a very large broadening is also observed in other calculations [24, 25]. In addition, the broadening, and the DOIS it induces, is sensitive to the molecule-surface distance and we find that the pinning effect is not sensitive to this distance. We propose that onset of pinning can be interpreted as a balance between the pillow effect and back-donation from the metal to the molecule. On most metals, PTCDA adsorption then leads to a partial occupation of the LUMO, as is observed in STM experiments [10–12].

The position of the LUMO energy level should have a large influence on the charge transfer. To test this we have calculated work functions for adsorbed monolayers of perylene molecules. The electronic structure of perylene is similar to that of PTCDA, but it has a smaller electronegativity, and its levels are shifted upwards compared to PTCDA. We use a full monolayer coverage of ~ 1 perylene molecule per $75 - 100 \text{ \AA}^2$, see Fig. 5.1. The work function results are shown in Fig. 5.4. Clearly two regimes can be distinguished. For perylene adsorption on high work function metals the pillow effect pushes electrons out of the molecular region into the surface, which reduces the work function. The effect is sensitive to the overlap between the perylene and metal wave functions, which is reflected in the work function changing with the distance between molecule and surface. The analysis of Δn gives a qualitatively similar result to that of PTCDA, see Fig. 5.3. The interface dipole is localized between the metal surface and the perylene layer.

The work function of perylene adsorbed on low work function metals is strongly pinned at ~ 3.7 eV. The analysis of Δn shows a net transfer of electrons from the metal to the LUMO of perylene. For adsorption on Mg the work function is close to that of the clean Mg surface. This marks the point where the pillow effect is exactly balanced by the back-donation from the metal to the LUMO. In the pinning regime the work function is insensitive to the distance between molecule and surface.

We suggest a simple phenomenological interpretation of our results. Neglecting the broadening of molecular levels, electrons are transferred from the metal to a molecular energy level $\epsilon_M(n)$, which depends upon the occupation number n . Following Slater's transition state idea [26], $\epsilon_M(n) = \epsilon_0 + Un$, with U the effective charging energy per electron of a molecule in the adsorbed monolayer, and ϵ_0 the LUMO energy [27]. The molecular layer is in equilibrium with the metal substrate, so $\epsilon_M(n) = E_F$, which determines the charge on the molecule. This charge and its screening by the metal result in a potential step nF , which yields a work function $W = W_c + nF = W(1 - A) - \epsilon_0 A$, with $A = F/U$, and $W_c = -E_F$ the work function of the clean metal surface. If we assume that U is determined by electrostatics only and approximate the charge distribution of the adsorbed molecular layer by a plane capacitor, then $A = 1$. The work function $W = -\epsilon_0$ is then pinned at the LUMO.

To include the pillow effect, W_c is replaced by $W_c - \Delta$, with Δ the work function shift induced by the pillow effect. Since the pillow effect creates an interface dipole that is localized between the surface and the molecules, it is consistent to apply the same shift to the molecular levels and replace ϵ_0 by $\epsilon_0 - \Delta$. Repeating the arguments of the previous paragraph then leads to a work function $W = (W_c - \Delta)(1 - A) - \epsilon_0 A$. The pinning is complete if $A = 1$, and the pinning level is not affected by the pillow effect, i.e. $W = -\epsilon_0$.

If $\epsilon_0 - \Delta > E_F$, there is no electron transfer to the LUMO. Only the pillow effect is operative and the work function is given by $W = W_c - \Delta$. Perylene adsorbed on Au and Ag falls in this regime, as does PTCDA on Au, see Figs. 5.2 and 5.4. If $\epsilon_0 - \Delta < E_F$, electrons are transferred to the LUMO, and the work function is pinned by the LUMO, independent of the size of the pillow effect. This is found for perylene on Mg and Ca, and for PTCDA on all metals except Au.

In conclusion, we have calculated the work functions of overlayers of PTCDA and perylene molecules adsorbed on metal surfaces. In contrast to previous models we do not find that molecular level broadening due to molecule-surface interaction plays a decisive role in determining the work function. The pillow effect describes the reduction of the work function if the Fermi level of the metal lies within the HOMO-LUMO gap of the molecules. If the Fermi level crosses a molecular level, the work function is pinned at this level.

Acknowledgments

The authors thank Héctor Vázquez for useful discussions. This work is supported by the "Stichting voor Fundamenteel Onderzoek der Materie (FOM)", and by "NanoNed", a nanotechnology program of the Dutch Ministry of Economic Affairs. The use of

supercomputer facilities was sponsored by the “Stichting Nationale Computer Faciliteiten (NCF)”

Bibliography

- [1] M. E. Gershenson, V. Podzorov, and A. F. Morpurgo, *Rev. Mod. Phys.* **78**, 973 (2006).
- [2] A. Kahn, N. Koch, and W. Gao, *J. Polym. Sci., Part B: Polym. Phys.* **41**, 2529 (2003).
- [3] N. Koch, S. Duhm, J. P. Rabe, A. Vollmer, and R. L. Johnson, *Phys. Rev. Lett.* **95**, 237601 (2005).
- [4] I. N. Hulea, S. Russo, A. Molinari, and A. F. Morpurgo, *Appl. Phys. Lett.* **88**, 113512 (2006).
- [5] I. G. Hill, A. Rajagopal, and A. Kahn, *Appl. Phys. Lett.* **73**, 662 (1998).
- [6] M. Knupfer and T. Schwieger, *Appl. Surf. Sci.* **252**, 77 (2005).
- [7] P. S. Bagus, V. Staemmler, and C. Wöll, *Phys. Rev. Lett.* **89**, 096104 (2002).
- [8] J. L. F. D. Silva, C. Stampfl, and M. Scheffler, *Phys. Rev. Lett.* **90**, 066014 (2003).
- [9] S. X. Du *et al.*, *Phys. Rev. Lett.* **97**, 156105 (2006).
- [10] A. Hauschild *et al.*, *Phys. Rev. Lett.* **94**, 036106 (2005).
- [11] A. Kraft *et al.*, *Phys. Rev. B* **74**, 041402(R) (2006).
- [12] R. Temirov, S. Soubatch, A. Luican, and F. S. Tautz, **444**, 350 (2006).
- [13] A. Gerlach, S. Sellner, F. Schreiber, N. Koch, and J. Zegenhagen, *Phys. Rev. B* **75**, 045401 (2007).
- [14] R. Rurali, N. Lorente, and P. Ordejon, *Phys. Rev. Lett.* **95**, 209601 (2005).
- [15] G. Brocks, *Phys. Rev. B* **55**, 6816 (1997).
- [16] G. Kresse and J. Hafner, *Phys. Rev. B* **47**, (R)558 (1993).
- [17] G. Kresse and J. Furthmüller, *Phys. Rev. B* **54**, 11169 (1996).
- [18] G. Kresse and D. Joubert, *Phys. Rev. B* **59**, 1758 (1999).
- [19] J. Neugebauer and M. Scheffler, *Phys. Rev. B* **46**, 16067 (1992).
- [20] C. J. Fall, N. Binggeli, and A. Baldereschi, *J. Phys.: Condens. Matter.* **11**, 2689 (1999).

- [21] To obtain the values given in Fig. 5.2 we prevented excessive geometry distortions. Fully optimizing the geometries does not change the work functions on Au, Ag and Al; it decreases the work function on Mg by 0.15 eV ($d = 3.3 \text{ \AA}$). The work function on Ca(111) is lowered to 3.3 eV, accompanied by a large bending of PTCDA [9, 10]. Ca atoms are pulled up from the surface, giving Ca–O distances of 2.3 \AA . We suggest that the Ca–PTCDA interface is chemically unstable with Ca atoms donating their valence electrons to PTCDA.
- [22] H. Vázquez *et al.*, Europhys. Lett. **65**, 802 (2004).
- [23] H. Vázquez *et al.*, Appl. Surf. Sci. **234**, 107 (2004).
- [24] S. Picozzi *et al.*, Phys. Rev. B. **68**, 195309 (2003).
- [25] K. Lee, J. Yu, and Y. Morikawa, Phys. Rev. B **75**, 045402 (2007).
- [26] J. C. Slater, *The Self-consistent Field for Molecules and Solids* (McGraw-Hill, New York, 1974).
- [27] Within Slater’s transition state approach the LUMO level does not correspond to the electron affinity (EA) of the molecule.

Chapter 6

Charge transfer and dipole formation at interfaces between metals and aromatic molecules

We study the dipole layer formed at metal-organic interfaces by means of first-principles calculations. Interface dipoles are monitored by calculating the work function change of Au, Ag, Al, Mg and Ca surfaces upon adsorption of a monolayer of PTCD (3,4,9,10-perylene-tetra-carboxylic-di-anhydride), perylene or benzene molecules. Adsorption of PTCD leads to pinning of the work function for a range of metal substrates. It gives interface dipoles that compensate for the difference in the clean metal work functions, leading to a nearly constant work function. In contrast, adsorption of benzene always results in a decrease of the work function, which is relatively constant for all metal substrates. Both effects are found in perylene, where adsorption on low work function metals gives work function pinning, whereas adsorption on high work function metals gives work function lowering. The work function changes upon adsorption are analyzed and interpreted in terms of two competing effects. If the molecule and substrate interact weakly, the molecule pushes electrons into the surface, which lowers the work function. If the metal work function is sufficiently low with respect to the unoccupied states of the molecule, electrons are donated into these states, which increases the binding and the work function.

6.1 Introduction

Applications of organic semiconductors in light-emitting diodes [1, 2], field-effect transistors [3, 4] and solar cells [5, 6] have stimulated research into the fundamental electronic properties of organic materials and their interfaces with metal electrodes [7, 8]. The weak forces between the molecules in an organic material lead to small band widths, which enhances the importance of electron-phonon and electron-electron in-

teractions [9, 10]. Nevertheless high charge carrier mobilities can be achieved in well-ordered molecular crystals [7]. As the quality of molecular crystals increases, transport of charge carriers across the interfaces between metal electrodes and the organic material starts to determine the performance of the devices [11]. Metal organic interfaces (MOIs) often give rise to a non-Ohmic behavior, indicating the existence of significant Schottky barriers.

Chemical bonding between molecules and metal surfaces modifies the charge distribution at a MOI. It results in an interface dipole layer, which strongly influences the Schottky barrier height [12–14]. This effect of chemical bonding is observed very clearly in self-assembled monolayers of thiolate molecules chemically bonded to noble metal surfaces [14–19]. Common organic semiconductors however consist of closed shell molecules, which are usually thought to bind weakly to metal surfaces. It has therefore been assumed for a long time that the charge reordering at such MOIs is insignificant and that no significant interface dipole is formed.

In absence of an interface dipole, the Schottky barrier at a MOI can be predicted by aligning the vacuum levels of the metal and the organic material, called the Schottky-Mott rule. Over the last decade, however, experimental studies have indicated the general breakdown of the vacuum alignment rule, and have demonstrated that significant interface dipoles are formed at MOIs [8, 20–24]. In addition such studies have shown that interface dipoles at MOIs are localized foremost at the first molecular layer covering the metal. The interface dipoles are not affected much by deposition of additional organic layers. Because MOI dipoles are localized at the interface, they can be extracted from the change in the surface work function after deposition of a single organic layer.

Apart from straightforward chemical bonding, other ideas have been put forward to explain large interface dipoles. Conventional semiconductors such as Si have reactive surfaces, which bind strongly to metal overlayers. A significant density of states is then created at the metal-semiconductor interface within the band gap of the semiconductor, the so-called metal induced gap states (MIGS) [25–27]. In this model, MIGS determine the charge distribution at the interface and hence the interface dipole. The MIGS model has also been applied to MOIs [28–30]. It requires a strong interaction between the metal and the organic material.

If molecules are physisorbed onto a metal surface, one expects a weak interaction between the molecular semiconductor and the metal. For physisorbed molecules interface dipoles at MOIs have been explained by the so-called pillow effect [31–35]. If a molecule approaches a metal surface, the electronic clouds of the molecule and the metal start to overlap. The Pauli exchange repulsion between these clouds leads to a spatial redistribution of electrons, which modifies the surface dipole. Since the electronic cloud of the metal is usually "softer" than that of the molecule, the net effect of Pauli repulsion is that electrons are pushed back into the metal. The result is an interface dipole that decreases the work function of the surface.

A decrease of the work function is commonly found if inert atoms or small molecules are adsorbed on a metal surface [31–36]. In contrast, adsorption of larger, π -conjugated molecules can lead to a substantial increase, as well as a decrease of the work function [8, 20–24]. The dependence of this work function shift and the associated interface

dipole on the molecules and the metal has been the subject of intensive study. If the work function W of a surface after coverage with a molecular layer is measured for a range of metal substrates with different initial work functions W_c , the results can be characterized by the parameter

$$S = \frac{dW}{dW_c}, \quad (6.1)$$

where W_c , W are the work functions of the clean metal surface and of the surface with the adsorbed organic layer, respectively.

The vacuum level alignment (Schottky-Mott) rule gives $S = 1$. One often assumes that the pillow effect does not depend strongly on the metal substrate. If this is the case, it gives a relatively constant decrease of the work function, leading to $S \approx 1$. Although this is observed for some molecules, very often S is significantly smaller than 1 [8]. Moreover, there is no a priori reason why S should be a constant. Indeed for some molecules several regimes can be distinguished, between which a transition from $S \approx 1$ to $S \approx 0$ is observed [37].

In this chapter we study the dipole formation at interfaces of molecular monolayers of PTCDA (3,4,9,10-perylene-tetra-carboxylic-di-anhydride), perylene and benzene adsorbed on close-packed metal surfaces of Au, Ag, Al, Mg and Ca by means of density functional theory (DFT) calculations. The work functions of the clean metal surfaces span a range from 3.0 eV (Ca) to 5.3 eV (Au). By studying a range of metal surfaces and using different molecules, the position of the metal Fermi level and the positions of the molecular levels can be varied. Their effect on the dipole layer formation at the MOIs can be analyzed.

Our choice for PTCDA is made because monolayers of PTCDA have been studied extensively, experimentally as well as theoretically. Deposition of PTCDA on (noble) metal surfaces can lead to well-ordered epitaxial overlayers [38]. In particular the structure and electronic structure of PTCDA on Ag(111) have been studied in detail [39–46]. Work function measurements have been performed for PTCDA adsorbed on a range of metal surfaces [8, 20]. These measurements show work function pinning, i.e. $S \approx 0$. PTCDA is a conjugated molecule with a relatively small electronic gap. Work function changes upon adsorption of the simple, large gap molecule benzene have been interpreted in terms of the pillow effect [35]. If this effect does not depend too strongly on the metal substrate, one would expect $S \approx 1$. The size and complexity of perylene is between that of benzene and PTCDA. Upon adsorption of perylene on metal surfaces, one might see a value of S between 0 and 1. Moreover, as mentioned above, S need not be constant.

This chapter is organized as follows. In the next section we give the technical details of our calculations. In Sec. 6.3 we present our results obtained for adsorption of PTCDA monolayers on different metal surfaces. A preliminary account has been given in the previous chapter. Here we compare results obtained with different density functionals, and study the influence of the packing density of the molecules on the surface. Section 6.4 gives the results obtained for adsorbed benzene and perylene monolayers. All results are discussed in Sec. 6.5 using a simple phenomenological model, and a short summary and conclusions are given in Sec. 6.6.

6.2 Computational details

The electronic structure is treated within density functional theory (DFT) [47, 48] using the local density approximation (LDA) [49, 50], or the generalized gradient approximation (GGA) with the PW91 exchange-correlation functional [51]. The calculations are performed with the VASP (Vienna *ab initio* simulation package) program [52, 53], which uses the projector augmented wave (PAW) method [54, 55]. For Au and Ag atoms the outer shell d and s electrons are treated as valence electrons, for Al the outer shell s and p electrons, and for Mg and Ca the outer shell s electrons. For atoms of first row elements the $2s$ and $2p$ electrons are treated as valence electrons. The valence pseudo wave functions are expanded in a basis set consisting of plane waves. All plane waves up to a kinetic energy cutoff of 400 eV are included.

To model the metal-molecule interface, we use a supercell containing a slab of at least three metal layers with one layer of molecules adsorbed on one surface, and a vacuum region of at least 10 Å. Periodic boundary conditions are applied and the atomic positions in the top metal layer and in the molecules are allowed to relax. A dipole correction is applied to avoid spurious interactions between dipoles of repeated slabs along the direction normal to the surface [56].

The electronic structure is calculated self-consistently using 5 to 13 \mathbf{k} -points in the irreducible surface Brillouin zone (SBZ) according to the Monkhorst-Pack scheme [57] and applying a Methfessel-Paxton smearing of 0.2 eV [58]. Five \mathbf{k} -points give well-converged results for PTCDA layers, because of the large size of the surface unit cell (see next section). For accurate calculations of total energies and densities of state (DOS) the charge densities are recalculated with 13 and 25 irreducible \mathbf{k} -points using the tetrahedron method [59]. DOSs are plotted using Gaussian smearing with a broadening parameter between 0.01 and 0.1 eV.

Work functions are evaluated from the following expression:

$$W = V(\infty) - E_F, \quad (6.2)$$

where $V(\infty)$ is the electrostatic potential in the vacuum region and E_F is the Fermi energy of the bulk metal. $V(\infty)$ is obtained from the potential averaged in the (x, y) plane

$$\bar{V}(z) = \frac{1}{A} \iint_{cell} V(x, y, z) dx dy, \quad (6.3)$$

where $V(x, y, z)$ is the electrostatic potential on a real space grid in the supercell. In practice $\bar{V}(z)$ reaches an asymptotic value $V(\infty)$ at a distance of a few Å from the surface [17, 19]. An accurate value of E_F is obtained from a separate bulk calculation, following the procedure described in Ref. [60].

Test calculations regarding slab thickness, vacuum thickness, \mathbf{k} -point sampling grid and plane waves kinetic energy cutoff are performed in order to estimate the convergence. From these tests we find that with the parameters given above, total energies are converged to within 0.01 eV and work functions to within 0.05 eV. The results for PTCDA on Ca(111) turn out to be the most sensitive with respect to vacuum thickness and \mathbf{k} -point sampling. So for this system the results have been

	Au	Ag	Al	Mg	Ca
GGA	2.94	2.93	2.86	3.19	3.92
LDA	2.87	2.84	2.82	3.13	3.78
exp.	2.88	2.89	2.86	3.21	3.95

Table 6.1: Optimized nearest neighbor distances in the bulk metals. All values are in Å.

obtained using 14 \mathbf{k} -points in the irreducible SBZ and a vacuum thickness of at least 14 Å.

To analyze our results we have also calculated some properties of isolated molecules, as will be discussed in Sec. 6.5. One molecular property we use is the electron affinity (EA), which is obtained from a Δ SCF calculation. Such calculations are quite cumbersome with programs that use periodic boundary conditions, such as VASP. Therefore, for calculations on isolated molecules we use the GAMESS program [61], and treat the electronic structure within DFT using the BLYP functional [62, 63]. We use the 6-31+G* basis set, which gives EAs for acenes that are converged on a scale of ~ 0.1 eV [64]. As in Ref. [64], we find that including a diffuse orbital in the basis set is important and that the smaller 6-31G* basis set does not give a sufficiently converged EA [65]. For PTCDA the EAs obtained using the 6-31G* and 6-31+G* bases differ by 0.4 eV. The DOSs of the isolated molecule calculated with VASP and GAMESS are very similar, so that in this respect the two can be used interchangeably.

6.3 PTCDA

Before discussing the results obtained for adsorbed layers, we benchmark our calculations on clean metal surfaces. We consider the close-packed (111) surfaces of fcc Au, Ag, Al, and Ca, and the (0001) surface of hcp Mg. The metals in this set are relatively simple, free-electron like and the set of surfaces spans a considerable range in work functions. Table 6.1 lists the optimized nearest neighbor distances of the bulk metals, calculated with GGA(PW91) and LDA(CA) functionals. As usual, the GGA values are larger than the LDA values, but both are generally in reasonable agreement with experiment. We use these optimized distances to construct the surface unit cells.

Table 6.2 lists the calculated work functions of the clean (111) surfaces (for Mg the (0001) surface), compared to experimental values and values obtained in previous calculations. Our results have been obtained using slabs consisting of six metal layers. A 25×25 \mathbf{k} -point sampling of the SBZ is applied, while allowing the top two metal layers to relax. The GGA values generally are within ~ 0.1 eV of the experimental values, whereas LDA tends to overestimate the work function somewhat. The exception is Al(111), where LDA gives a better value compared to experiment. Our results agree with those obtained in previous theoretical studies; the small differences can be attributed to differences in the computational parameters used, such as the DFT functional, the basis set, and the lattice parameter.

	Au	Ag	Al	Mg	Ca
GGA	5.25	4.50	4.08	3.74	2.98
LDA	5.52	4.90	4.21	3.93	3.08
exp.	5.26 ^a , 5.35 ^b	4.46 ^c , 4.50 ^d , 4.56 ^e	4.24 ^f	3.78 ^g	2.87 ^h
calc.	5.27 ⁱ , 5.35 ^b	4.42 ^j	4.25 ^k	3.76 ^l , 3.88 ^m	2.86 ⁿ

Table 6.2: Calculated work functions of clean (111) surfaces; (0001) for Mg. All values are in eV. ^a[66], ^b[15], ^c[67], ^d[68], ^e[69], ^f[70], ^g[71], ^hpolycrystalline value [72], ⁱGGA [73], ^jGGA [74], ^kLDA [75], ^lLDA [76], ^mLDA [77].

6.3.1 Structure of adsorbed monolayers

PTCDA monolayers adsorbed on Ag(111) and Au(111) surfaces have been studied in detail experimentally [39–46, 78–80]. In a close-packed monolayer the PTCDA molecules lie flat on the surface in a “herringbone” structure with the centers of the PTCDA molecules located on surface bridge sites [40]. The surface unit cell contains two PTCDA molecules, see Fig. 6.1 (b). The experimental distances between the carbon rings of the molecules and the surface atoms are 2.86 Å and 3.27 Å for adsorption on Ag(111) and Au(111), respectively [46, 81]. Experiments also indicate a weak interaction between PTCDA and Au(111), consistent with physisorption [41, 80], but a stronger interaction between PTCDA and Ag(111) [40–44]. PTCDA binds strongly to more open Ag surfaces and to surface steps [82]. We do not know of any detailed studies on the structure of PTCDA adsorbed on the other metal (111) surfaces. Depositing metals onto thin films of PTCDA often leads to interdiffusion and doping [83–87].

In our calculations we use the herringbone structure of PTCDA on Ag shown in Fig. 6.1 (b). The underlying Ag substrate contains 33 metal atoms per unit cell and our supercell contains 175 atoms in total. Since the lattice parameters of Au, Ag and Al are similar, see Table 6.1, we use a similar supercell for PTCDA on these surfaces. For Mg and Ca, we choose a herringbone structure that results in a packing density of PTCDA molecules similar to that on the other surfaces. This results in 30 and 20 atoms per metal layer for Mg and Ca, respectively.

To study the effect of the packing density of PTCDA molecules, we also perform calculations on the structure used by Picozzi *et al.* [88], see Fig. 6.1 (a). This surface unit cell contains one PTCDA molecule. We refer to this structures as the “simple” structure. The underlying Ag(111) surface then contains 36 atoms per unit cell, so that the coverage of PTCDA molecules is $\sim \frac{1}{2}$ ML. The surface unit cells for the other metal substrates are chosen such, that the coverage remains close to this value. As it is easier to vary the geometry of the molecule and substrate in the simple structure, as compared to the close-packed herringbone structure, we use the former to study the energetics of PTCDA adsorption. The optimized geometries of the PTCDA molecules in the two structures are very similar, as demonstrated by Table 6.3. The GGA or LDA optimized geometries are very similar.

Common DFT functionals describe strong chemical interactions well, but they fail to capture weaker (van der Waals) bonding correctly. This deficiency can lead

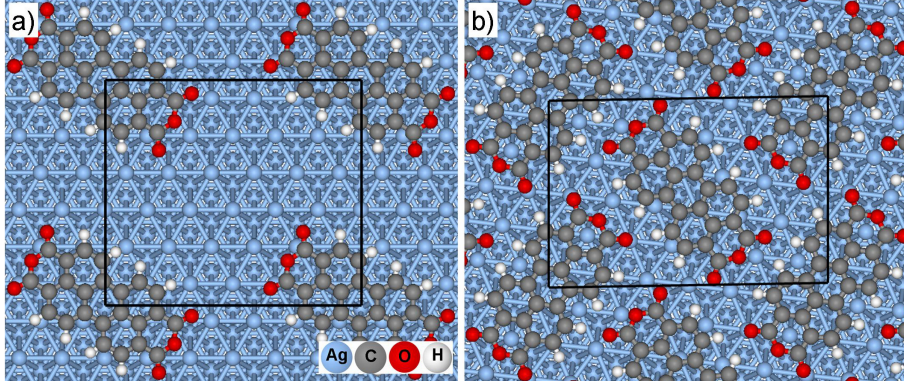


Figure 6.1: PTCDA monolayers on the Ag(111) surface. The rectangles denote the surface unit cells used in calculations (with area A); (a) the simple structure ($A = 268 \text{ \AA}^2$); (b) the herringbone structure ($A = 243 \text{ \AA}^2$).

to underestimating the binding energy and overestimating the bond distance between molecule and surface, if GGA functionals are used to describe the adsorption of closed-shell molecules on metal surfaces [34]. Using LDA functionals however can lead to a serious overbinding and a equilibrium distance that is too small [89]. Previous GGA calculations of the binding energy of PTCDA on Ag(111) gave slightly contradictory results, i.e. a moderate binding of $\sim 0.5 \text{ eV/molecule}$ [82], or a very weak binding of $\sim 0.1 \text{ eV/molecule}$ [44, 90, 91], or even a purely repulsive binding curve [88]. In the calculations where binding was obtained, the equilibrium distance ($\sim 3.4 \text{ \AA}$) was larger than the experimental equilibrium distance (2.9 \AA) [42, 46]. In contrast, LDA calculations on PTCDA on Ag(111) gave much shorter equilibrium distances of 2.8 \AA [88] and 2.7 \AA [44], and a very large binding energy ($\sim 3 \text{ eV/molecule}$ [44]).

Our results agree with this general trend in GGA and LDA calculations. Fig. 6.2 shows typical binding energy curves calculated with the simple structure, where we varied the distance between the PTCDA molecule and the surface and constrained the molecule to a planar geometry. The GGA results for PTCDA on Au lead to an

	LDA	GGA	GGA
	simple	simple	herringbone
C–H	1.10	1.09	1.09
C–C	1.42	1.43	1.43
C–O ^a	1.22	1.23	1.23
C–O ^b	1.38	1.40	1.40
C–O–C(°)	125.2	125.3	124.7

Table 6.3: Average bond lengths (in \AA) of PTCDA adsorbed on Ag(111). ^acarboxyl, ^banhydride.

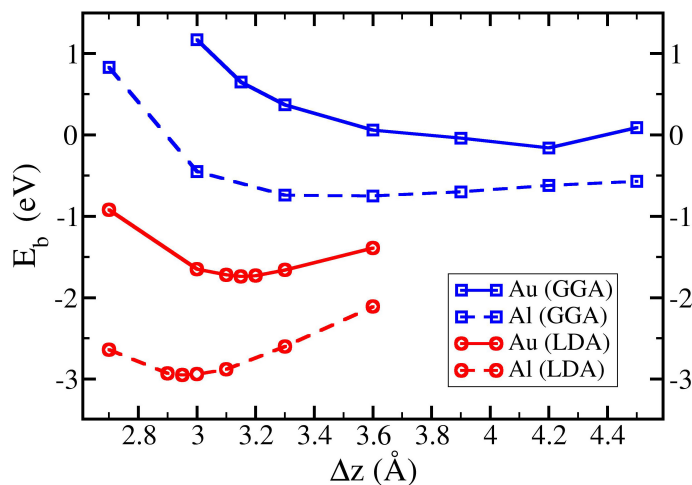


Figure 6.2: Binding curves for planar PTCDA on Au(111) (solid lines) and Al(111) (dashed lines). GGA and LDA values are indicated by the squares and circles, respectively.

extremely shallow binding curve with a minimum at a distance > 4 Å and a very small binding energy of ~ 0.1 eV/molecule. Using GGA for PTCDA on Al gives a sizable binding energy (~ 0.8 eV/molecule) and an equilibrium distance ~ 3.5 Å. The binding energy and equilibrium distance obtained for PTCDA on Ag (not shown in Fig. 6.2) are approximately halfway between those obtained for PTCDA on Al and PTCDA on Au. LDA calculations lead to much larger binding energies, i.e. 1.7 eV/molecule for PTCDA on Au and 3.0 eV/molecule for PTCDA on Al. The corresponding equilibrium distances are 3.15 Å and 2.95 Å, respectively. An LDA calculation for PTCDA on Ag gives an equilibrium distance of 2.75 Å, which is somewhat smaller than the experimental value.

In conclusion, neither GGA nor LDA gives a reliable description of the binding in weakly bonded systems such as PTCDA on Au(111). GGA leads to underbinding and a large equilibrium distance, whereas LDA gives overbinding and a small equilibrium distance. As the binding energy between the PTCDA molecule and the metal surface increases along the series Ag, Al, Mg and Ca, the differences between the GGA and the LDA equilibrium distances tend to become smaller and we expect the results to become more reliable. Moreover, if the binding energy increases, the PTCDA molecule loses its planar geometry.

If the interaction between the PTCDA molecule and the surface is large, the molecule has a tendency to arch as shown in Fig. 6.3. The extent of this geometry deformation depends upon the metal substrate. Optimizing the geometry of PTCDA on Ca with GGA, we find that the outer carbon atoms of the perylene core are 0.8 Å closer to the surface than the carbon atoms in the center. The latter have a distance of 2.6 Å to the surface. Such short distances are indicative of a strong interaction

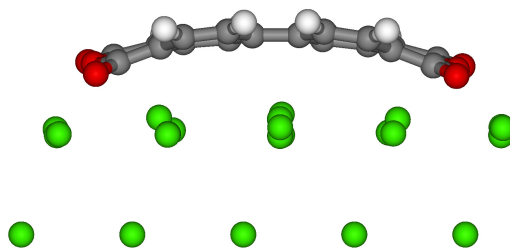


Figure 6.3: Optimized geometry of the arching PTCDA molecule on the Ca(111) surface.

between molecule and surface. A geometry deformation also occurs in the end groups of the PTCDA molecule, where the carboxyl oxygens move towards the surface, and the anhydride oxygen moves away from the surface, see Fig. 6.4. A strong deformation of the PTCDA molecule is accompanied by a rumpling of the surface, where metal atoms are lifted out of the surface, decreasing the distance with the molecule. For instance, the distances between the carboxyl oxygens and the nearest Ca atoms are 2.3 Å. Such short distances suggest the formation of bonds. Indeed PTCDA bonds strongly to a Ca(111) surfaces with a binding energy of 8.4 eV/molecule (calculated with GGA).

The deformation of the adsorbed PTCDA molecule and that of the metal substrate decrease through the series Ca, Mg, Al, Ag, and Au. This is accompanied by an increase of the mean distance between the molecule and the surface and a decrease of the binding energy. The binding energy between the PTCDA molecule and the Mg(0001) surface is 2.3 eV/molecule, which is much less than between PTCDA and Ca(111). Through the series Al, Ag and Au the binding energy decreases monotonically, as discussed above. The binding energy for PTCDA on Au(111) is vanishingly small and the molecule and surface have an undistorted, planar geometry.

The binding energy and the geometries of PTCDA on Al and Ag obtained in previous calculations follow the trends discussed above [82, 88, 90, 91]. As we will

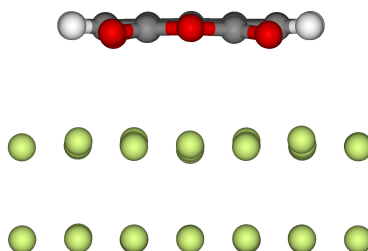


Figure 6.4: Side view of the optimized geometry of the PTCDA molecule on the Mg(0001) surface.

see in the next section, adsorption of PTCDA on the very electropositive Ca surface is accompanied by a large transfer of electrons from the surface to the molecule. This results in a strong molecule-surface bond, accompanied by a sizable geometry distortion. As the metal becomes more electronegative along the series Mg, Al, Ag and Au, the electron transfer decreases, as well as the bond strength and the geometry distortion.

6.3.2 Work functions

The calculations discussed in the previous section enable us to understand the trends in the bonding and in the geometry of PTCDA adsorbed on the different metal surfaces. However, there still remains an uncertainty about the absolute accuracy of the calculated results. Clearly for the weakly bonded cases GGA gives an underbinding and LDA gives an overbinding. In these cases neither GGA nor LDA can be expected to give an accurate equilibrium distance. Because of this uncertainty we investigate the formation of interface dipoles in a number of steps. We start with the simple structure and perform calculations for fixed molecule surface distances d in the range 3.0–3.6 Å. Results obtained with GGA and with LDA are then compared. In the second step we switch to the more densely packed herringbone structure that is observed experimentally, which allows us to study the effect of the packing density. Finally, we consider the effect of full geometry relaxation of the molecules and the surface.

Fig. 6.5 (a) shows the work functions for a layer of PTCDA molecules adsorbed in the simple structure on the different metal surfaces, calculated using the GGA functional. One immediate observation is that adsorption on Au(111) leads to a lowering of the work function as compared to the clean surface, whereas adsorption on the other metal surfaces leads to an increase of the work function. There is some

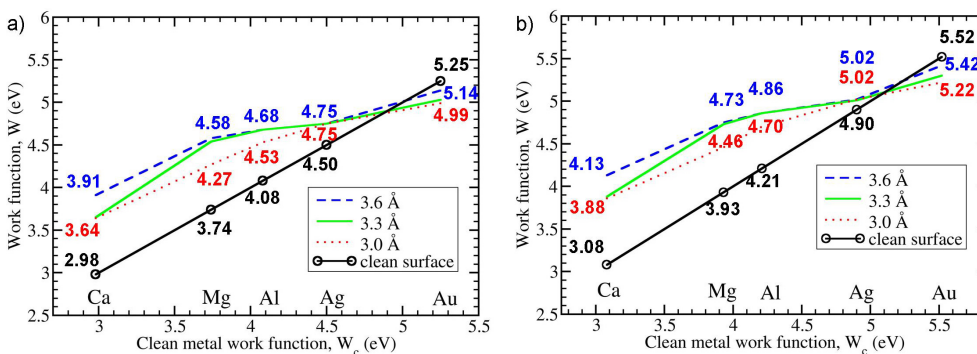


Figure 6.5: Work functions of a PTCDA monolayer on (111) metal surfaces [(0001) for Mg] in the simple structure, calculated using (a) the GGA and (b) the LDA functionals. The clean metal work function is given along the x -axis. The numbers give the calculated values, the lines guide the eye. The bottom (black) curve refers to the clean metal surfaces. The top three curves are for different distances d between the PTCDA molecules and the surfaces.

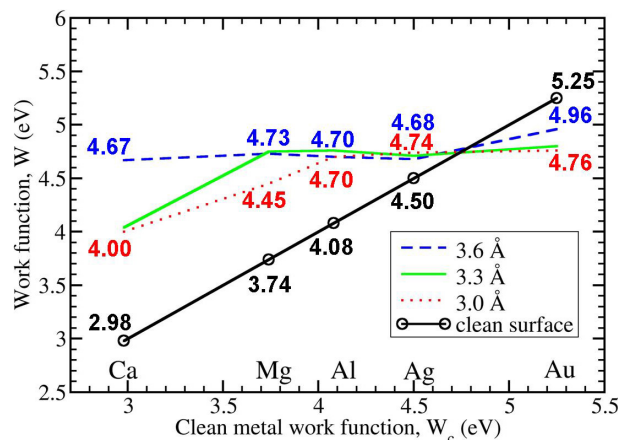


Figure 6.6: As Fig. 6.5 for PTCDA in the herringbone structure

dependence of the work function on the distance between the molecule and the surface, but it is not excessively large. By fitting a straight line through the curves in Fig. 6.5 (a) one obtains (see Eq. (6.1)) $S = 0.5$ at $d = 3.6$ Å, and $S = 0.6$ at $d = 3.0$ Å. These values are considerably lower than the $S = 1$ that follows from the Schottky-Mott rule, indicating that significant interface dipoles are formed upon adsorption. Since S increases somewhat upon decreasing the molecule-surface distance, the interface dipoles decrease with decreasing distance. The calculated values for S are much higher than the $S \approx 0$ obtained experimentally [8, 20]. We will show below that this discrepancy is resolved by increasing the packing density of the PTCDA molecules, which is only $\sim \frac{1}{2}$ ML in the simple structure.

To illustrate the effect of using a different functional, Fig. 6.5 (b) gives the work functions for the simple structure at fixed distances between the molecule and the substrates, calculated using the LDA functional. Compared to the GGA results of Fig. 6.5 (a), the LDA work functions are generally somewhat higher, as was also the case for the clean metal surfaces, see Table 6.2. The changes in the work functions upon adsorption calculated with LDA or GGA are comparable however (at the same molecule-surface distance). It means that, although the binding between the molecules and the surfaces as calculated with LDA or GGA can be considerably different, as discussed in the previous section, the charge redistribution upon adsorption is similar, if we consider the same molecule-surface distance. Since the GGA work functions of the clean metal surfaces are somewhat closer to the experimental values, see Table 6.2, we will also use GGA values for the adsorbed layers in the following.

Fig. 6.6 shows the work functions of the herringbone structure of PTCDA on metal surfaces, calculated using the GGA functional. As for the simple structure, Fig. 6.5 (a), adsorption on Au(111) lowers the work function, and on the other metal surfaces it increases the work function. In the herringbone structure the work function shifts are much larger however. Most strikingly, as one can observe in Fig. 6.6, the work

function of PTCDA on a metal surface is pinned at ~ 4.7 eV over a considerable range of metal substrates and molecule-surface distances. The pinning leads to $S \approx 0$, which is in agreement with experiment. Moreover, the value of the pinned work function is close to the value found experimentally [8, 20]. Deviations from pinning are observed only for low work function metals and short molecule-surface distances, i.e. $d \leq 3.3$ Å for Ca and $d = 3.0$ Å for Mg.

As a final step we completely optimize the geometry of the PTCDA molecule and the substrate as discussed in the previous section. Only on the electropositive metals this gives a sizeable change in the work function. Adsorption of PTCDA on Ca(111) leads to a geometry distortions of both the molecule and the substrate, which gives a lowering of the work function to 3.3 eV. On Mg the effect of geometry distortions is smaller, whereas on Al, Ag, and Au they have a negligible effect on the work function.

6.4 Benzene and perylene

Experiments give a lowering of the work function after adsorption of a benzene monolayer for several metal surfaces. Measured work function shifts are 0.18 eV on Al(111) [92], 0.3 eV [93] and 0.7 eV [94, 95] on Ag(111), 0.7 eV [96] and 1.05 eV [35] on Cu(111), and 1.10 eV [35] on Au(111). Previous DFT/GGA calculations for benzene on Al(111) gave an equilibrium distance of 3.7-3.8 Å [92]. Quantum chemical MP2 calculations for a single benzene molecule adsorbed on a cluster of metal atoms gave equilibrium distances of 3.8 Å for benzene on Au(111) and 4.0 Å for benzene on Cu(111) [35]. We calculate the work functions of an benzene monolayer adsorbed on different metal surfaces at a set of fixed distances in the same way as discussed in the previous section. A simple $(\sqrt{7} \times \sqrt{7})R19.1^\circ$ structure is used as in Ref. [92], which is somewhat less than close-packed.

The (GGA) results are given in Fig. 6.7. The most important observation is that adsorption of benzene leads to a decrease of the work function for all the surfaces studied. This is very different from the effect of PTCDA adsorption, see Figs. 6.5 and 6.6. Moreover, adsorption of benzene gives a work function lowering that is of a similar size for all surfaces (at the same molecule-surface distance). It leads to $S = 0.9$ at $d = 3.6$ Å, and $S = 0.8$ at $d = 3.0$ Å. These values are close to the Schottky-Mott limit. The size of the work function shift depends on the distance between the molecule and the surface. At $d = 3.0$ Å it is roughly twice as large as at $d = 3.6$ Å. The sign of the work function shift, its relative independence of the metal and its sensitivity to the molecule metal distance agree with an interpretation in terms of the pillow effect. The latter is determined by the Pauli repulsion between the molecular and surface electrons, which decreases the surface dipole and therefore the work function [32, 35, 97]. Pauli repulsion depends on the overlap between the molecular and surface wave functions and therefore on the distance between the molecule and the surface. Our GGA calculations and the results obtained in previous calculations [35, 92] suggest that the distances between the benzene molecule and the metal surfaces are rather large (i.e. > 3.5 Å). However, as discussed in the previous section, GGA does not give accurate equilibrium distances in case the bonding is weak.

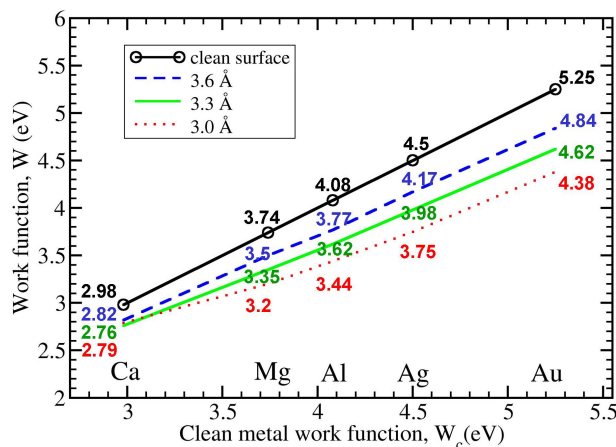


Figure 6.7: As Fig. 6.5 for benzene in a $(\sqrt{7} \times \sqrt{7})R19.1^\circ$ structure [92].

In conclusion, adsorption of the large PTCDA molecule leads to work function pinning ($S \approx 0$), see Fig. 6.6, and adsorption of the small benzene molecule gives an almost constant work function lowering ($S \approx 1$), see Fig. 6.7. It is interesting to study the adsorption of an intermediate sized molecule, such as perylene. The structure of a perylene monolayer on a metal surface is less well-established than that of a PTCDA monolayer. A herringbone structure similar to PTCDA is one of the structures proposed for a close-packed perylene monolayer on Ag(111) and Au(111) [41, 98, 99]. UPS measurements gave a decrease of the work function of perylene on Au and Ag by 0.8 eV and 0.6 eV, respectively, and an increase of the work function of perylene on Ca by 0.3 eV [100].

We perform calculations for a perylene monolayer adsorbed on different metal surfaces at a set of fixed distances. Analogous to PTCDA we use two different structures, i.e. a close-packed herringbone structure, and a simple structure with a packing density of $\sim \frac{1}{2}$ ML. The calculated work functions are shown in Fig. 6.8. Two regimes can be distinguished. For the high work function surfaces (Au, Ag) adsorption of perylene leads to a lowering of the work function, whereas for the low work function surface of Ca adsorption of perylene increases the work function. These results are in agreement with experiment. The curves in Fig. 6.8 show that the transition between these two regimes takes place in the range Mg – Al.

From these curves the transition between the two regimes can be quantified. Starting with the results obtained for the simple structure at a molecule-surface distance $d = 3.6$ Å, a line through the points for Ca, Mg and Al gives $S = 0.3$, whereas a line through the points for Al, Ag and Au leads to $S = 1.0$. For the herringbone structure the same procedure for $d = 3.6$ Å gives $S = 0$ and $S = 0.9$, respectively. It is instructive to compare these S values to the values obtained for benzene and PTCDA. It suggests that for Ca, Mg and Al one obtains pinning of the work function upon perylene adsorption, similar to PTCDA, see Fig. 6.6, whereas for Ag and Au

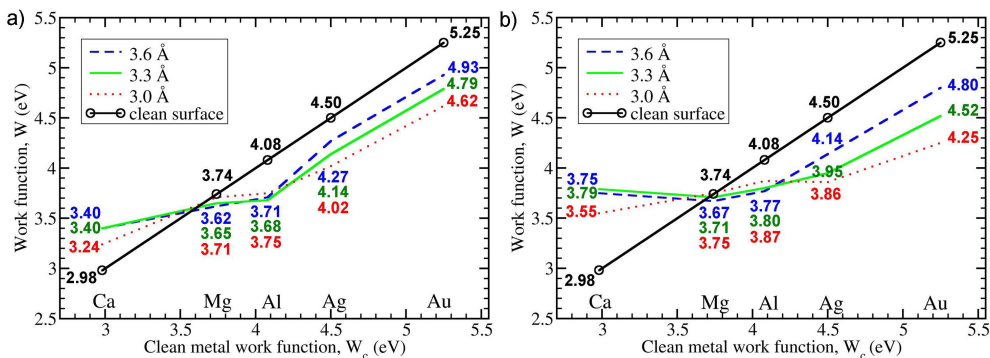


Figure 6.8: As Fig. 6.5 for perylene in (a) the simple structure and (b) the herringbone structure.

one finds a consistent work function decrease, similar to benzene, see Fig. 6.7. Upon decreasing the distance between the perylene molecules and the surfaces the S values in the high and low work function regimes become somewhat closer and the transition between the two regimes becomes less sharp. Note that the distance dependence in the low work function regime resembles the distance dependence of the PTCDA case, whereas in the high work function regime it resembles the benzene case.

In order to be able to identify the two regimes and the transition between them, one needs a series of metal surfaces that cover a range of work functions. Experimentally a transition between the $S \approx 0$ to $S \approx 1$ regimes is observed for Alq₃ adsorbed on different surfaces [37].

6.5 Discussion

The results presented in Fig. 6.6 show that adsorption of a PTDCA monolayer pins the work functions at ~ 4.7 eV for a broad range of distances. The fact that one gets pinning, as well as the value of the pinning level, are in good agreement with experimental observations. The results obtained for benzene and perylene adsorption are in qualitative agreement with available experimental results, i.e. adsorption of benzene leads to a lowering of the work function in all cases, and adsorption of perylene gives a work function decrease for high work function metals and a work function increase for low work function metals. In order to analyze the behavior of the work function we first focus on the density of states, then we look explicitly to the charge transfer at the molecule-substrate interface, and finally we consider a simple phenomenological model.

6.5.1 Density of states

Figure 6.9 gives the Kohn-Sham (KS) density of states (DOS) of an isolated PTCDA molecule, calculated using the GGA functional. The energies of the highest occupied

molecular orbital (HOMO) and the lowest unoccupied molecular orbital (LUMO) are at -6.24 eV respectively -4.64 eV with respect to the vacuum level. The KS spectrum is similar to that obtained in previous DFT calculations [28, 84, 101, 102]. The GGA HOMO-LUMO gap of 1.60 eV also agrees with the value found in other GGA calculations [28, 88].

The interpretation of KS energy levels is the subject of a long-standing debate. From calculations with advanced functionals it is argued that the KS energies of all occupied molecular orbitals correspond to vertical ionization potentials (IPs) [103, 104]. The latter can be extracted from a photoemission spectrum, for instance. Approximative functionals such as GGA give a reasonable ionization spectrum, but it is shifted to a higher energy by approximately a constant. The lowest experimental IP of PTCDA is 8.15 eV, as quoted in Ref. [101]. The equivalent of the lowest IP of an extended system is the work function. Even approximative functionals such as GGA or LDA usually give work functions that are close to the experimental values, as is illustrated by Table 6.2. Results of a similar quality are obtained for work functions of adsorbed atomic and molecular layers. The results for PTCDA on metal surfaces discussed in Sec. 6.3.2 illustrate this.

The KS levels of unoccupied molecular orbitals generally do not have such a simple interpretation. In particular, the energy of the DFT LUMO (ϵ_0) does not give the electron affinity (EA). From calculations with accurate functionals it is shown that $\epsilon_0 < -\text{EA}$, both for molecules [105], as well as for extended systems [106, 107]. The difference between $|\epsilon_0|$ and the EA can be several eV's. The same is of course true for GGA functionals.

For approximative functionals such as GGA, Slater's transition state model [108] allows for a simple estimate of the EA. Define $\epsilon_M(1)$, ϵ_0 as the KS energies of the singly occupied HOMO of the PTCDA^- ion, and of the LUMO of the neutral PTCDA^0 molecule, respectively. Assuming that one can fractionally occupy the level ϵ_M with N electrons, one can parameterize

$$\epsilon_M(N) = \epsilon_0 + UN, \quad (6.4)$$

where U is the charging energy per electron [109]. Slater's transition state model then gives $\text{EA} \approx -\epsilon_M(\frac{1}{2})$. From separate SCF calculations on PTCDA^0 and PTCDA^- we extract ϵ_0 and $\epsilon_M(1)$, and calculate $U = \epsilon_M(1) - \epsilon_0 = 3.31$ eV. This procedure gives results that agree with charging energies for isolated conjugated molecules extracted from total energy calculations [10]. Using the LUMO energy given above, we then find $\text{EA} = 2.98$ eV. This value is in agreement with the value $\text{EA} = 2.96$ eV we extract from a ΔSCF total energy difference calculation. (The almost exact agreement is of course somewhat fortuitous). Slater's transition state model can also be used to calculate the IP. Assuming that the charging energy for holes on PTCDA is the same as for electrons and using the HOMO energy given above, then yields $\text{IP} = 7.90$ eV, which is in fair agreement with the experimental value.

If a molecule is embedded in a crystal, its charging energy U is reduced drastically because of screening by the surrounding crystal [10, 110]. Using the screening energy of 1.82 eV calculated in Ref. [110], we obtain an effective charging energy of a PTCDA molecule in a crystal $U_{\text{cryst}} = 3.31 - 1.82 = 1.49$ eV. Slater's transition state model

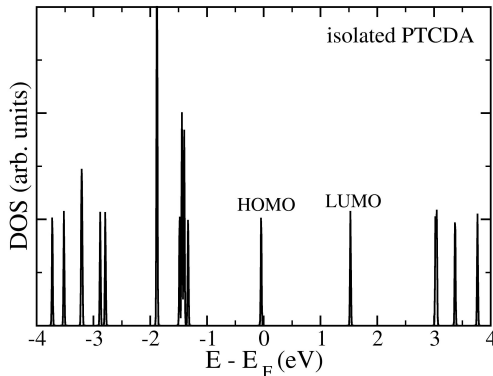


Figure 6.9: Total DOS of an isolated PTCDA molecule calculated using a Gaussian broadening of 0.01 eV. The highest occupied molecular orbital (HOMO) and the lowest unoccupied molecular orbital (LUMO) are indicated. The energy is set to zero at the position of the HOMO. With respect to the vacuum level the HOMO and LUMO levels are at -6.24 eV and -4.64 eV, respectively.

then gives $EA_{\text{cryst}} = 3.90$ eV and $IP_{\text{cryst}} = 6.99$ eV for the EA and IP of a PTCDA molecule in a crystal. This leads to a transport gap $E_t = IP_{\text{cryst}} - EA_{\text{cryst}} = 3.09$ eV. The values of the IP and E_t are in fair agreement with the values extracted from experiment, i.e. 6.7 ± 0.2 eV and 3.2 ± 0.4 eV, respectively [111].

In conclusion, a KS DOS calculated with GGA should be interpreted with care. The energies of the molecular levels depend upon their occupancy, see eq. (6.4). The effective charging energy U that enters this expression, strongly depends upon the environment of the molecule, because of screening. The latter is affected by the presence of a metal substrate, for instance [110, 111].

We now turn to the DOS of PTCDA monolayers adsorbed on metal surfaces. Since the DOS is usually dominated by the metal substrate, we look at the DOS projected on the atoms of the molecule (PDOS) to identify the molecular levels. Fig. 6.10 gives the PDOS on a PTCDA molecule adsorbed on metal surfaces at distances of $d = 3.0$ and $d = 3.6$ Å. We apply a Gaussian broadening of 0.1 eV to avoid a “spiky” appearance of the PDOS. Comparison to Fig. 6.9 allows us to identify the molecular levels, in particular the HOMO and LUMO.

The results show that PTCDA adsorption leads to a broadening of the molecular levels due to the interaction between the molecule and the surfaces. The extend of the broadening is moderate. At $d = 3.6$ Å the typical width at half height of the HOMO and LUMO peaks is ~ 0.2 eV. The widths become somewhat larger at shorter distances (~ 0.3 eV). These widths agree with those found in previous DFT calculations of adsorbed PTCDA [88], as well as with widths typically found for other adsorbed molecules such as pentacene [89]. They are however much smaller than the widths found in the calculations of Refs. [28] and [29].

Comparing the two columns in Fig. 6.10, one observes that the PDOSs at the two distances are qualitatively similar, but that the spectrum at $d = 3.0$ Å is shifted

towards lower energy as compared to the spectrum at $d = 3.6 \text{ \AA}$ by up to 0.5 eV, depending upon the metal substrate. This is caused by the pillow effect, as we will discuss in Sec. 6.5.3. The GGA HOMO-LUMO gap of PTCDA decreases somewhat upon adsorption, from 1.6 eV in the isolated molecule to ~ 1.4 eV for the weakly interacting PTCDA on Au and ~ 1.1 eV for the strongly interacting PTCDA on Ca.

An important observation that can be made by comparing Figs. 6.6 and 6.10 is that work function pinning occurs when the Fermi level crosses the level of the LUMO. For PTCDA on Au the LUMO is still unoccupied, but already for PTCDA on Ag

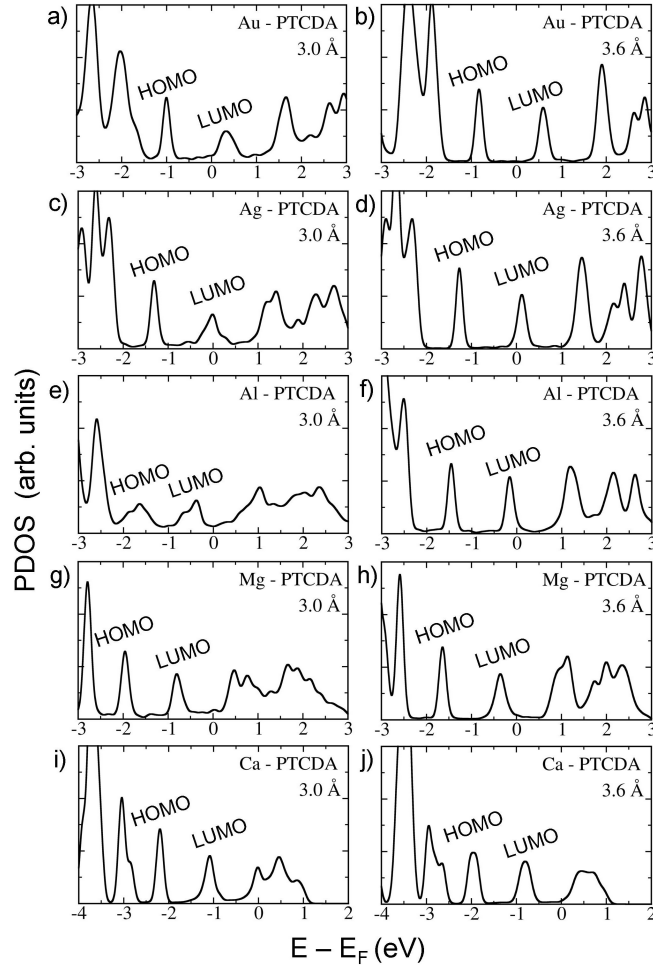


Figure 6.10: Projected density of states (PDOS) of the PTCDA molecule adsorbed on metal surfaces at a fixed distance d in the herringbone structure, calculated using a Gaussian broadening of 0.1 eV; left: $d = 3.0 \text{ \AA}$; right: $d = 3.6 \text{ \AA}$. The peaks corresponding to the molecular HOMO and LUMO levels are labeled.

the LUMO is partially occupied. This implies that electron transfer takes place from the metal substrate to the molecule. The amount of electron transfer increases along the series Ag, Al, Mg, and Ca, judging from the upwards shift of the Fermi level, see along the columns of Fig. 6.10. As long as the Fermi level is inside the LUMO peak, the work function is pinned, compare Fig. 6.6. At the short molecule-surface distance of 3.0 Å between PTCDA and Ca, the Fermi level jumps to the next peak, i.e. the LUMO+1, see Fig. 6.10 (i). This is accompanied by an “unpinning” of the work function, compare Fig. 6.6.

Detailed experiments have been performed for PTCDA on Ag(111). In UPS and STM experiments a state is observed at the Fermi level that is identified as the LUMO of the PTCDA molecule, whereas the HOMO is found at ~ -1.6 eV with respect to

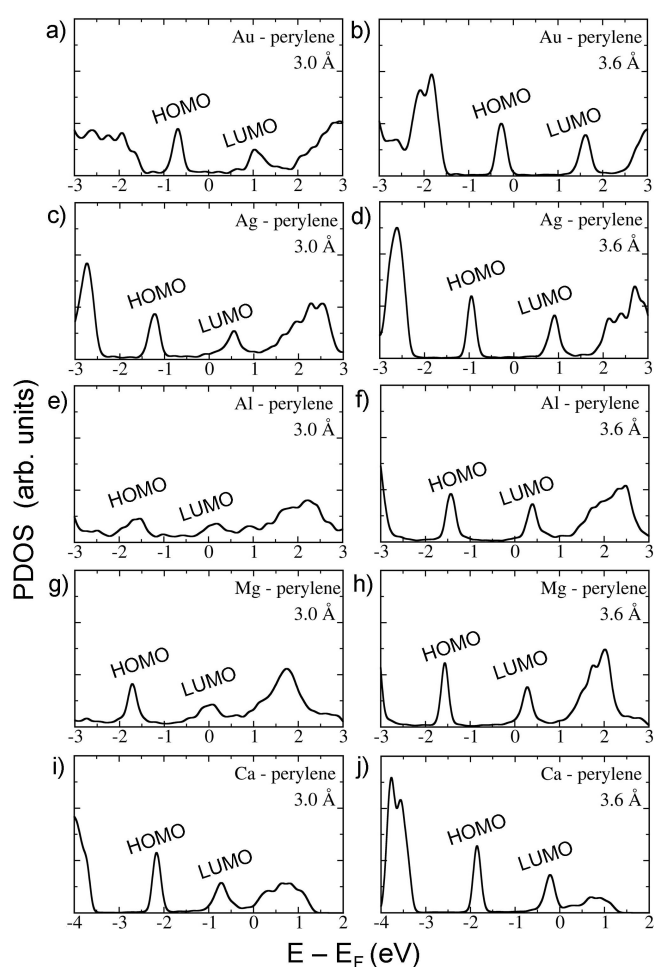


Figure 6.11: As Fig. 6.10 for perylene adsorbed on metal surfaces.

the Fermi level [43–45]. In Fig. 6.10 (c), where the distance between PTCDA and the Ag surface is close to the experimental value, we find the HOMO at -1.3 eV and the LUMO at the Fermi level, in agreement with the experimental analysis. The binding energy of PTCDA on a metal substrate increases along the series Ag, Al, Mg, and Ca, which would suggest that the GGA DOSs become increasingly reliable. Only for the weakly bonded PTCDA on Au is the LUMO unoccupied, see Figs. 6.10 (a), (b). In STM experiments the LUMO of PTCDA on Au(111) is observed clearly above the Fermi level [80, 110, 112]. Applying an analysis similar to that following eq. (6.4) and using the polarization energy calculated in Ref. [110], shifts our LUMO up by ~ 1 eV, which brings it close to experiment.

Pinning of the work function at MOIs has been interpreted in terms of a charge neutrality level (CNL) [28–30], in analogy to Schottky barrier models for conventional semiconductors [27, 113, 114]. The CNL model relies on having a large continuum DOS at the metal-semiconductor interface, which fills the energy gap of the semiconductor. The Fermi level is then pinned by these metal induced gap states (MIGS) [25]. Conventional semiconductors such as Si or GaAs have quite reactive surfaces with surface atoms carrying dangling bonds. The energies of these dangling bond states are within the semiconductor gap. Bonding at a metal-semiconductor interface leads to broadening of these states, which generates a large continuum DOS at the interface in the semiconductor gap [115, 116]. Closed shell molecules such as PTCDA do not have dangling bond states within the HOMO-LUMO gap. The creation of a large DOS at a MOI within the HOMO-LUMO gap then depends upon a large broadening of the molecular levels. We do not observe such a large broadening.

The DOS of an isolated perylene molecule resembles that of PTCDA. The GGA HOMO-LUMO gap of 1.8 eV is slightly larger than that of PTCDA. Fig. 6.11 gives the PDOS on a perylene molecule adsorbed on metal surfaces at distances of $d = 3.0$ and $d = 3.6$ Å. Comparison to Fig. 6.8 (b) shows that pinning of the work function sets in as the Fermi level reaches the LUMO. In other words, as for PTCDA, the work function is pinned by the LUMO of the molecule. The pinning level for adsorbed perylene is ~ 3.7 eV, which is 1 eV lower than for PTCDA.

6.5.2 Charge transfer and interface dipole

The charge transfer at the PTCDA-metal interface can be visualized directly by calculating the laterally averaged electron density difference

$$\Delta\bar{n}(z) = \bar{n}_{\text{PTCDA/metal}}(z) - \bar{n}_{\text{metal}}(z) - \bar{n}_{\text{PTCDA}}(z). \quad (6.5)$$

The electron density \bar{n}_{metal} and \bar{n}_{PTCDA} of the metal substrate and the molecule are obtained in separate calculations with the substrate and the molecule frozen in the adsorption geometry, using the same unit cell. The lateral averaging is done as in eq. (6.3). Examples of $\Delta\bar{n}(z)$ are shown in Fig. 6.12.

Fig. 6.12 (a)–(c) clearly show the formation of interface dipoles that are localized at the PTCDA/metal interface. Note that the sign of the interface dipole moment of PTCDA on Au is opposite to that of PTCDA on the other metal surfaces. For PTCDA on Au electrons are displaced from the molecular region into the metal,

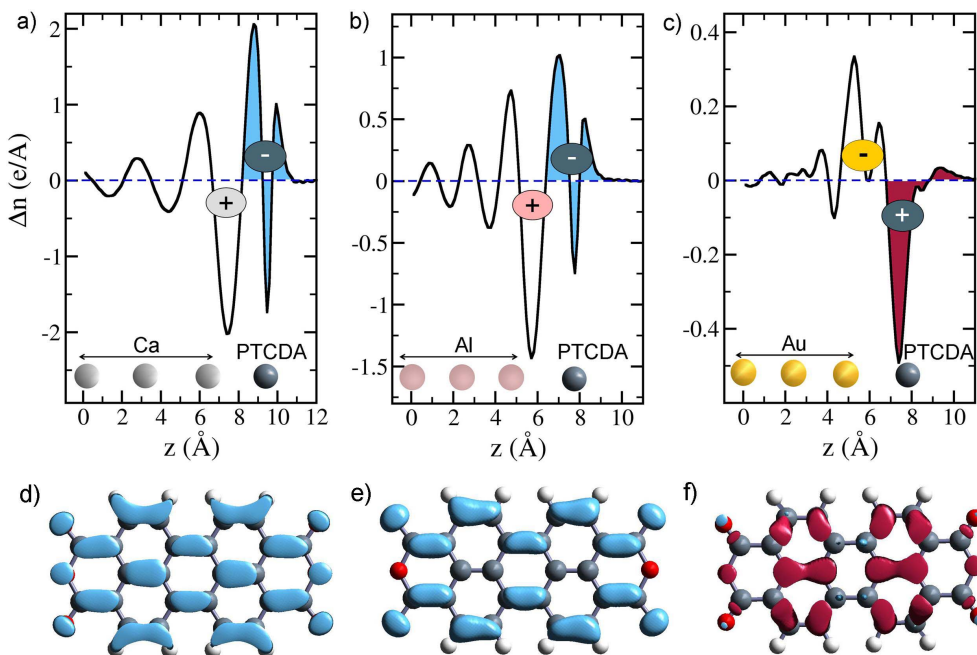


Figure 6.12: Laterally averaged electron density difference $\Delta\bar{n}(z)$ for PTCDA adsorbed on (a) Ca(111), (b) Al(111), and (c) Au(111) at a fixed distance $d = 3.0 \text{ \AA}$. The $+/-$ indicate the direction of the interface dipole. The charge on the molecule is estimated by integrating over the shaded areas (see text). (d–f) Isodensity surface of $\Delta n(x, y, z)$ close to the molecular plane.

whereas for PTCDA on other metals electrons are displaced from the metal to the molecule. According to the PDOSs shown in Figs. 6.10 (c)–(j) the latter can be interpreted as electron transfer from the metal to the LUMO of the molecule. In contrast, the displacement of electrons for PTCDA on Au cannot straightforwardly be related to the transfer of electrons to or from a molecular level, as can be observed from the PDOSs shown Figs. 6.10 (a), (b).

This charge displacement for PTCDA on Au can be interpreted in terms of the pillow effect [32, 35]. If the interaction between the molecule and the surface is not too strong, then the wave function of the system can be written in good approximation as an anti-symmetrized product of the wave functions of the separate molecule and the substrate. Anti-symmetrization introduces the effects of exchange between the molecular and substrate electrons, which leads to a repulsive interaction in case of a closed shell molecule, the so-called Pauli repulsion. The electronic cloud of the molecule is usually “harder” than that of the metallic substrate, i.e. it is less easily deformed. The net effect of Pauli repulsion is then that the electronic cloud, which originally spilled out somewhat from the metal surface, is pushed back into the metal by the molecular electronic cloud, as if the molecule lands on a pillow. The push

back of electrons into the metal can be observed in Fig. 6.12 (c). It lowers the surface dipole, and therefore it lowers the work function.

One would expect that the spatial distribution of the displaced electrons reflect the shape of the molecule. The pattern of electron depletion in the molecular region can be visualized by plotting $\Delta n(x, y, z)$, as is shown in Fig. 6.12 (f). The nodal pattern roughly corresponds to the second highest occupied molecular π orbital of PTCDA (HOMO-5 in Ref. [102]). It confirms the conclusion drawn from the PDOSs of Figs. 6.10 (a), (b) that the electron depletion is not due to a transfer of electrons from the highest occupied state of the molecule to the Au surface.

The change in electron density for PTCDA on other metals is qualitatively different from that of PTCDA on Au. Electrons are transferred from the metal to states of the molecule, which is clearly demonstrated by plotting $\Delta n(x, y, z)$. The nodal pattern of $\Delta n(x, y, z)$ for PTCDA on Al, Fig. 6.12 (e), corresponds to the LUMO of PTCDA, indicating that electrons are transferred to this state, in agreement with Fig. 6.10(d). For PTCDA on Ca, Fig. 6.12 (e), the nodal pattern shows both features of the LUMO and of the LUMO+1 [84]. This agrees with Fig. 6.10 (i), which shows that electrons are transferred to both these states.

One can calculate the interface dipole per adsorbed molecule as $\Delta\mu = eA \int z\Delta\bar{n}(z)dz$, with A the surface area of the adsorbed molecule. Alternatively the interface dipole is extracted from the change in the work function ΔW upon adsorption of the molecules [117]

$$\Delta\mu = \frac{\varepsilon_0 A}{e} \Delta W. \quad (6.6)$$

The results are given in Table 6.4. The total charge q on the molecule can be estimated by

$$q = -e \int_{z_0}^{z_v} \Delta\bar{n}(z)dz, \quad (6.7)$$

where z_0 is the point between the molecule and the surface where $\Delta\bar{n}(z_0) = 0$ and z_v is a point in the vacuum. The integration is indicated by shaded areas in Figs. 6.12 (a)–(c). Provided q is not zero, a parameter that characterizes the charge distribution can be defined as

$$z_d = -\frac{\Delta\mu}{q}. \quad (6.8)$$

It is the effective distance between the sheets of positive and negative charge, if the interface dipole would be represented as a plane capacitor.

Comparing the values for Ag to Ca in Table 6.4, one notices an increase in the interface dipole and in the number of electrons transferred from the metal surface to the molecule. This is consistent with the change in the work function upon adsorption and with the PDOSs, see Figs. 6.6 and 6.9. The charge distributions of the interface dipole on Ag, Al, Mg, and Ca are similar, as characterized by a similar value of z_d for these cases. The distributions shown in Figs. 6.12 (a, b) can be interpreted as electronic charge placed in a π -orbital on the PTCDA molecule, which is screened by electrons in the metal, which leads to the characteristic Friedel oscillations in the metal substrate.

metal	$\Delta\mu$ (D)	q (e)	z_d (Å)
Au	-1.58	+0.34	0.99
Ag	0.77	-0.31	0.52
Al	2.00	-0.82	0.51
Mg	2.29	-0.84	0.57
Ca	3.29	-1.34	0.51

Table 6.4: Interface dipole per molecule $\Delta\mu$ (eq. (6.6)), total molecular charge q (eq. (6.7)), and effective distance z_d (eq. (6.8)) for PTCDA on metal surfaces. The distance between the molecules and the surface is fixed at 3.0 Å.

Adsorption of PTCDA on Au is qualitatively different from adsorption on the other metal surfaces, as can be judged from the signs of the interface dipoles and the charges and the different value of z_d . The charge distribution of PTCDA on Au, Fig. 6.12 (c), is also qualitatively different. It is more localized in the region between the molecule and the surface, as can be expected if it is due to Pauli repulsion (i.e. the pillow effect), since the latter is active in the region where the molecular and the surface wave functions overlap.

Since this overlap decreases with increasing distance between the molecule and the surface, one expects the charge displacement to decrease accordingly. Indeed the charge on PTCDA adsorbed on Au, calculated using eq. (6.7), at a distance $d = 3.6$ Å is 0.23 e , as compared to 0.34 e at $d = 3.0$ Å, see Table 6.4. The pillow effect is a very general mechanism that should be operative for any adsorbed closed shell molecule, even if electrons are transferred from the substrate to the LUMO, as for PTCDA adsorbed on other metal surfaces. One would expect that this leads to an interface dipole that depends strongly on the molecule-surface distance. However, Fig. 6.6 shows that for PTCDA on Ag and Al (and to a lesser extent also for PTCDA on Mg), the work function, and therefore the interface dipole, is independent of the distance over a considerable range.

6.5.3 Model

The pinning of the work function and the (lack of) distance dependence can be clarified by a simple qualitative model. Although the interaction between the molecule and the surface leads to broadening of molecular levels, see Fig. 6.9, we neglect the broadening for reason of simplicity. We assume that electrons can be transferred to the LUMO, whose energy $\epsilon_M(N)$ depends on the occupation number N , as in eq. (6.4). The charging energy U depends upon the environment of the molecule. All molecules in a monolayer have the same occupation number and in calculating U the electrostatic interactions between all molecules should be taken into account, as well as the interactions with the screening charges induced in the metal substrate.

If the molecular layer is in equilibrium with the metal substrate, $\epsilon_M(N) = E_F$,

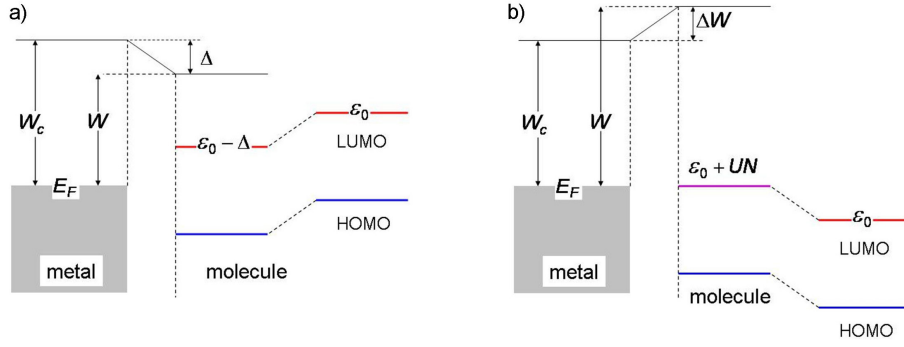


Figure 6.13: (a) The pillow effect results in a potential step Δ , which lowers the molecular levels close to the interface. (b) Charge transfer to the LUMO rises the molecular levels and pins the Fermi level.

with E_F the Fermi level of the metal. This determines the occupation number

$$N = \frac{E_F - \epsilon_0}{U}. \quad (6.9)$$

The idea is illustrated by Fig 6.13 (b). One has of course the additional requirement that $0 \leq N \leq 2$. If $N \neq 0$, the molecular layer is charged and with the screening counter charge in the metal this leads to a dipole layer. It results in a potential step at the interface, which we parameterize as NF with F the potential step normalized per electron transferred to a molecule. The work function then becomes $W = W_c + NF$, with $W_c = -E_F$ the work function of the clean metal surface.

So far we have not yet taken the pillow effect into account, which lowers the work function of the clean metal surface from W_c to $W_c - \Delta$. Since according to Fig. 6.12 (c) the pillow effect leads to an interface dipole that is localized mainly between the surface and the molecule, it is consistent to apply this potential step also to the molecular levels. One replaces ϵ_0 by $\epsilon_0 - \Delta$ in eq. (6.9). The idea is illustrated by Fig 6.13 (a). From $W = W_c - \Delta + NF$ one obtains expressions for the work function and the S parameter (eq. (6.1)):

$$\begin{aligned} W &= (W_c - \Delta)\left(1 - \frac{F}{U}\right) - \epsilon_0 \frac{F}{U}, \\ S &= 1 - \frac{F}{U}. \end{aligned} \quad (6.10)$$

Since $0 \leq N \leq 2$, these expressions are valid if $\Delta - \epsilon_0 - 2U \leq W_c \leq \Delta - \epsilon_0$. If the clean metal work function falls outside these bounds, one has

$$W = W_c - \Delta; \quad S = 1, \quad (6.11)$$

for $W_c > \Delta - \epsilon_0$. The molecular level is then unoccupied, i.e. $N = 0$ and only the pillow effect is operative. If $W_c < \Delta - \epsilon_0 - 2U$, one has $N = 2$. The molecular level

is fully occupied, which leads to:

$$W = W_c - \Delta + 2F; S = 1. \quad (6.12)$$

From purely electrostatic considerations one has $F \leq U$, which leads to $S \leq 1$. Moreover, if the charge on the molecular layer and its counter charge in the substrate are modeled by a plane capacitor, then $U = F = e^2/C$, where C is the ‘‘capacitance’’ of the molecule [109]. In this simple limit eq. (6.10) becomes:

$$W = -\epsilon_0; S = 0. \quad (6.13)$$

Note that in this limit one has perfect pinning, i.e. the work function is determined by the molecular level only. It is independent of the metal and of the pillow effect.

This simple model can be used to qualitatively describe the work functions in Figs. 6.5 – 6.8. The simplest case is when $W_c > \Delta - \epsilon_0$, i.e. when the work functions of all the metals considered are too high with respect to the position of the LUMO level. W and S are then given by eq. (6.11), i.e. the work function is simply shifted with respect to the work function of the clean metal surface. Benzene adsorbed on metal surfaces is such a case, see Fig. 6.7. Since the work function shift is determined by the pillow effect, one expects it to be sensitive the distance between the molecule and the surface, which can be observed in Fig. 6.7.

If $W_c \leq \Delta - \epsilon_0$, the LUMO reaches the Fermi level of the metal. W and S are given by eq. (6.10), and in the simple plane capacitor model by eq. (6.13). A close-packed monolayer of planar molecules, such as in the herringbone structure of PTCDA (Fig. 6.1 (b)), comes closest to a plane capacitor. Fig. 6.6 shows that indeed the work function is pinned at ~ 4.7 eV over a considerable range of metal work functions and molecule-surface distances. If $W_c < \Delta - \epsilon_0 - 2U$, the LUMO becomes fully occupied. W and S are given by eq. (6.12) and the work function becomes ‘‘unpinned’’.

The energy at which this occurs depends upon the molecule-surface distance. Decreasing the distance increases the pillow effect, i.e. it increases Δ . Moreover it decreases U , since at a shorter distance the screening by the metal substrate is larger. In the plane capacitor model $U \propto 1/d$, where d is the molecule-surface distance. The distance dependence of the unpinning of the work function is observed in Fig. 6.6. At $d = 3.6$ Å the work function is fully pinned, at $d = 3.3$ Å it becomes unpinned for Ca, and at $d = 3.0$ Å it is unpinned for Ca and Mg.

The simple structure for PTCDA has only $\sim \frac{1}{2}$ ML coverage (Fig. 6.1 (a)). It makes sense that this situation cannot be describe by a simple plane capacitor, and one has to use eq. (6.10). It gives a linear dependence of W on W_c with a slope $0 < S < 1$, which can be observed in Fig. 6.5.

The behavior of perylene is consistent with the model given above. If $W_c > \Delta - \epsilon_0$, only the pillow effect is operative and the LUMO is unoccupied, see eq. (6.11). This holds for Au and Ag in Figs. 6.8 (a) and (b). If $W_c \leq \Delta - \epsilon_0$, we observe pinning. For a close-packed monolayer the plane capacitor model explains the pinning (eq. (6.13)) observed for Mg and Ca in Fig. 6.8 (b). For the simple structure with $\sim \frac{1}{2}$ ML packing density, eq. (6.10) can be used to describe the behavior for adsorption on the low work function metals.

6.6 Summary and conclusions

We study the interface dipole formation at interfaces formed by a monolayers of PTCDA, benzene and perylene molecules with the Au, Ag, Al, and Ca(111) and the Mg(0001) surfaces, using first-principles DFT calculations. The interface dipoles are monitored by calculating the change of the surface work function upon adsorption of the molecular layer. Molecular packing densities corresponding to $\frac{1}{2}$ ML and 1 ML coverage are considered and the distance between the molecules and the surfaces is varied to establish the dependence of the work function on these parameters.

Adsorption of PTCDA in a densely pack structure leads to pinning ($S \approx 0$) of the work function at ~ 4.7 eV for a range of metal substrates and molecule-substrate distances in good agreement with experimental observations. The interface dipoles that are created upon adsorption compensate for the differences between the work functions of the different clean metal surfaces. Along the series Ag, Al, Mg, Ca the interface dipole generated by PTCDA adsorption increases, which is consistent with an increasing transfer of electrons from the substrate to the PTCDA molecules. This can be visualized by the electron density difference created by PTCDA adsorption. The increased electron transfer also leads to a stronger bond between the molecule and the surface. Decreasing the packing density of the PTCDA molecules to $\frac{1}{2}$ ML decreases the pinning effect, but it still gives a linear dependence between the work function of the adsorbed layer and that of the clean metal surfaces ($S \approx 0.5$). Adsorption of PTCDA on Au(111) leads to a very weak bond and an interface dipole that has an opposite sign, as compared to the other surfaces. Here the pillow effect is dominant, which pushes the electrons into the metal substrate.

Adsorption of benzene results in a reduction of the work function, irrespective of the substrate, in agreement with experiments. This reduction is in the range 0.2 – 0.8 eV, depending upon the distance between the molecule and the surface. At a fixed distance $S \approx 0.9$. In the case of benzene adsorption only the pillow effect is operative. The latter, as well as the effect of charge transfer to the molecule are observed in adsorption of perylene. Adsorption of a full ML of perylene molecules on low work function metals gives work function pinning ($S = 0$) at ~ 3.7 eV. Adsorption on high work function metals gives the work function reduction characteristic of the pillow effect with $S \approx 0.9$. The transition between the two regimes takes place for substrate work functions in the range Mg-Al. Decreasing the packing density decreases the pinning in the low work function regime.

The work function changes upon adsorption are analyzed and interpreted by means of the projected density of states on the molecules and the charge density difference induced by adsorption of the molecules. The work function changes of surfaces in the low work function regime are entirely consistent with a transfer of electrons from the substrate to the LUMO of the molecules. In the low work function regime they are consistent with the pillow effect pushing electrons into the substrate. A simple model inspired by Slater's transition state approach allows us to describe the changes in the work function upon adsorption qualitatively.

Bibliography

- [1] C. W. Tang and S. A. VanSlyke, *Appl. Phys. Lett.* **51**, 913 (1987).
- [2] J. H. Burroughes *et al.*, *Nature* **347**, 539 (1990).
- [3] A. Tsumura, H. Koezuka, and T. Ando, *Appl. Phys. Lett.* **49**, 1210 (1986).
- [4] F. Garnier, R. Hajlaoui, A. Yassar, and P. Srivastava, *Science* **265**, 1684 (1994).
- [5] N. S. Sariciftci, L. Smilowitz, A. J. Heeger, and F. Wudl, *Science* **258**, 1474 (1992).
- [6] G. Yu, J. Wang, J. McElvain, and A. J. Heeger, *Adv. Mater.* **10**, 1431 (1998).
- [7] M. E. Gershenson, V. Podzorov, and A. F. Morpurgo, *Rev. Mod. Phys.* **78**, 973 (2006).
- [8] A. Kahn, N. Koch, and W. Gao, *J. Polym. Sci., Part B: Polym. Phys.* **41**, 2529 (2003).
- [9] G. Brocks, *Synth. Met.* **102**, 914 (1999).
- [10] G. Brocks, J. van den Brink, and A. F. Morpurgo, *Phys. Rev. Lett.* **93**, 146405 (2004).
- [11] I. N. Hulea, S. Russo, A. Molinari, and A. F. Morpurgo, *Appl. Phys. Lett.* **88**, 113512 (2006).
- [12] R. T. Tung, *Phys. Rev. Lett.* **84**, 6078 (2000).
- [13] R. T. Tung, *Phys. Rev. B* **64**, 205310 (2001).
- [14] P. C. Rusu and G. Brocks, *Phys. Rev. B* **74**, 073414 (2006).
- [15] V. D. Renzi *et al.*, *Phys. Rev. Lett.* **95**, 046804 (2005).
- [16] G. Heimel, L. Romaner, J.-L. Brédas, and E. Zojer, *Phys. Rev. Lett.* **96**, 196806 (2006).
- [17] P. C. Rusu and G. Brocks, *J. Phys. Chem. B* **110**, 22628 (2006).
- [18] G. Heimel, L. Romaner, E. Zojer, and J.-L. Brédas, *Nanolett.* **7**, 933 (2007).
- [19] P. C. Rusu, G. Giovannetti, and G. Brocks, *jpcc* (2007).
- [20] I. G. Hill, A. Rajagopal, and A. Kahn, *Appl. Phys. Lett.* **73**, 662 (1998).
- [21] H. Ishii, K. Sugiyama, E. Ito, and K. Seki, *Adv. Mater.* **11**, 605 (1999).
- [22] N. Koch, S. Duhm, J. P. Rabe, A. Vollmer, and R. L. Johnson, *Phys. Rev. Lett.* **95**, 237601 (2005).

- [23] M. Knupfer and T. Schwieger, *Appl. Surf. Sci.* **252**, 77 (2005).
- [24] H. Ishii *et al.*, *Phys. Rev. B* **201**, 1075 (2004).
- [25] V. Heine, *Phys. Rev.* **138**, A1689 (1965).
- [26] S. G. Louie, J. R. Chelikowsky, and M. L. Cohen, *Phys. Rev. B* **15**, 2154 (1977).
- [27] C. Tejedor, F. Flores, and E. Louis, *J. Phys. C: Sol. State Phys.* **10**, 2163 (1977).
- [28] H. Vázquez *et al.*, *Europhys. Lett.* **65**, 802 (2004).
- [29] H. Vázquez *et al.*, *Appl. Surf. Sci.* **234**, 107 (2004).
- [30] H. Vázquez, Y. J. Dappe, J. Ortega, and F. Flores, *J. Chem. Phys.* **125**, 144703 (2007).
- [31] J. L. F. D. Silva, C. Stampfl, and M. Scheffler, *Phys. Rev. Lett.* **90**, 066104 (2003).
- [32] P. S. Bagus, V. Staemmler, and C. Wöll, *Phys. Rev. Lett.* **89**, 096104 (2002).
- [33] X. Crispin *et al.*, *J. Am. Chem. Soc.* **124**, 8131 (2002).
- [34] Y. Morikawa, H. Ishii, and K. Seki, *Phys. Rev. B* **69**, 041403(R) (2004).
- [35] G. Witte, S. Lukas, P. S. Bagus, and C. Wöll, *Appl. Phys. Lett.* **87**, 263502 (2005).
- [36] Y. C. Chen, J. E. Cunningham, and C. P. Flynn, *Phys. Rev. B* **30**, 7317 (1984).
- [37] J. Tang, C. Lee, S. Lee, and Y. Xu, *Chem. Phys. Lett.* **396**, 92 (2004).
- [38] S. R. Forrest, *Chem. Rev.* **97**, 1793 (1997).
- [39] E. Umbach, K. Glöckler, and M. Sokolowski, *Surf. Sci.* **402-404**, 20 (1998).
- [40] M. Eremtchenko, J. A. Schaefer, and F. S. Tautz, *Nature* **425**, 602 (2003).
- [41] M. Eremtchenko, D. Bauer, J. A. Schaefer, and F. S. Tautz, *New J. Phys* **6** (2004).
- [42] A. Hauschild *et al.*, *Phys. Rev. Lett.* **94**, 036106 (2005).
- [43] Y. Zou *et al.*, *Surf. Sci.* **600**, 1240 (2006).
- [44] A. Kraft *et al.*, *Phys. Rev. B* **74**, 041402(R) (2006).
- [45] R. Temirov, S. Soubatch, A. Luican, and F. S. Tautz, *Phys. Rev. Lett.* **444**, 350 (2006).
- [46] A. Gerlach, S. Sellner, F. Schreiber, N. Koch, and J. Zegenhagen, *Phys. Rev. B* **75**, 045401 (2007).
- [47] P. Hohenberg and W. Kohn, *Phys. Rev.* **136**, B864 (1964).

- [48] W. Kohn and L. J. Sham, *Phys. Rev.* **140**, A1133 (1965).
- [49] J. P. Perdew and A. Zunger, *Phys. Rev. B* **23**, 5048 (1981).
- [50] D. M. Ceperley and B. J. Alder, *Phys. Rev. Lett.* **45**, 566 (1980).
- [51] J. P. Perdew *et al.*, *Phys. Rev. B* **46**, 6671 (1992).
- [52] G. Kresse and J. Hafner, *Phys. Rev. B* **47**, (R)558 (1993).
- [53] G. Kresse and J. Furthmüller, *Phys. Rev. B* **54**, 11169 (1996).
- [54] G. Kresse and D. Joubert, *Phys. Rev. B* **59**, 1758 (1999).
- [55] P. E. Blöchl, *Phys. Rev. B* **50**, 17953 (1994).
- [56] J. Neugebauer and M. Scheffler, *Phys. Rev. B* **46**, 16067 (1992).
- [57] H. J. Monkhorst, and J. D. Pack, *Phys. Rev. B* **13**, 5188 (1976).
- [58] M. Methfessel and A. T. Paxton, *Phys. Rev. B* **40**, 3616 (1989).
- [59] P. Blöchl, O. Jepsen, and O. Andersen., preprint (1993).
- [60] C. J. Fall, N. Binggeli, and A. Baldereschi, *J. Phys.: Condens. Matter.* **11**, 2689 (1999).
- [61] M. W. Schmidt *et al.*, *J. Comput. Chem.* **14**, 1347 (1993).
- [62] A. D. Becke, *Phys. Rev. A* **38**, 3098 (1988).
- [63] C. Lee, W. Yang, and R. G. Parr, *Phys. Rev. B* **37**, 785 (1988).
- [64] A. Modelli, L. Mussoni, and D. Fabbri, *J. Phys. Chem. A* **110**, 6482 (2006).
- [65] M. Andrzejak, G. Mazur, and P. Petelenz, *J. Mol. Struct. (Theochem)* **527**, 91 (2000).
- [66] G. V. Hansson and S. A. Flodstrom, *Phys. Rev. B* **18**, 1572 (1978).
- [67] M. Chelvayohan and C. H. B. Mee, *J. Phys. C: Solis State Phys.* **15**, 2305 (1982).
- [68] R. C. Monreal, L. Guillemot, and V. A. Esaulov, *J. Phys.: Condens. Matter.* **15**, 1165 (2003).
- [69] K. Giesen *et al.*, *Phys. Rev. B* **35**, 975 (1987).
- [70] J. K. Grepstad, P. P. Gartland, and B. J. Slagsvold, *Surf. Sci.* **35**, 348 (1976).
- [71] P. A. Anderson, *Phys. Rev.* **54**, 753 (1938).
- [72] H. B. Michaelson, *J. Appl. Phys.* **48**, 4729 (1977).

- [73] S. Piccinin, A. Selloni, S. Scandolo, R. Car, and G. Scoles, *J. Chem. Phys.* **119**, 6729 (2003).
- [74] M. L. Bocquet, A. M. Rappe, and H. L. Dai, *Mol. Phys.* **103**, 883 (2005).
- [75] A. Curioni and W. Andreoni, *IBM J. RES. DEV.* **45**, 101 (2001).
- [76] E. Wachowicz and A. Kiejna, *J. Phys.: Condens. Matter* **13**, 10767 (2001).
- [77] H. L. Skriver and N. M. Rosengaard, *Phys. Rev. B* **46**, 7157 (1992).
- [78] T. Schmitz-Hübsch, T. Fritz, F. Sellam, R. Staub, and K. Leo, *Phys. Rev. B* **55**, 7972 (1997).
- [79] P. Fenter, F. Schreiber, L. Zhou, P. Eisenberger, and S. R. Forrest, *Phys. Rev. B* **56**, 3046 (1997).
- [80] N. Nicoara, E. Román, J. M. Gómez-Rodríguez, J. A. Martín-Gago, and J. Méndez, *Org. Elec.* **7**, 287 (2006).
- [81] B. Krause, A. C. Dürr, F. Schreiber, and H. Dosch, *J. Chem. Phys.* **119**, 3429 (2003).
- [82] S. X. Du *et al.*, *Phys. Rev. Lett.* **97**, 156105 (2006).
- [83] Y. Hirose *et al.*, *Phys. Rev. B* **54**, 13748 (1996).
- [84] S. Kera *et al.*, *Phys. Rev. B* **63**, 115204 (2001).
- [85] T. Kampen, A. Das, S. Park, W. Hoyer, and D. Zahn, *Appl. Surf. Sci.* **234**, 333 (2004).
- [86] G. Gavrila, D. R. T. Zahn, and W. Braun, *Appl. Phys. Lett.* **89**, 162102 (2006).
- [87] G. Fuentes and M. Knupfer, *Appl. Phys. A* **84**, 329 (2006).
- [88] S. Picozzi *et al.*, *Phys. Rev. B.* **68**, 195309 (2003).
- [89] K. Lee, J. Yu, and Y. Morikawa, *Phys. Rev. B* **75**, 045402 (2007).
- [90] R. Rurali, N. Lorente, and P. Ordejo'n, *Phys. Rev. Lett.* **95**, 209601 (2005).
- [91] A. Hauschild *et al.*, *Phys. Rev. Lett.* **95**, 209602 (2005).
- [92] R. Duschek *et al.*, *Chem. Phys. Lett.* **318**, 43 (2000).
- [93] R. Dudde, K.-H. Frank, and E.-E. Koch, *Surf. Sci.* **225**, 267 (1990).
- [94] X.-L. Zhou, M. Castro, and J. White, *Surf. Sci.* **238**, 215 (1990).
- [95] K. Gaffney *et al.*, *Chem. Phys.* **251**, 99 (2000).
- [96] D. Velic, A. Hotzel, M. Wolf, and G. Ertl, *J. Chem. Phys.* **109**, 9155 (1998).

- [97] J. L. F. D. Silva, C. Stampfl, and M. Scheffler, *Phys. Rev. Lett.* **90**, 066014 (2003).
- [98] C. Seidel, R. Ellerbrake, L. Gross, and H. Fuchs, *Phys. Rev. B* **64**, 195418 (2001).
- [99] M. Eremtchenko, D. Bauer, J. Schaefer, and F. Tautz, *J. Mater. Res.* **19**, 2028 (2004).
- [100] L. Yan, N. J. Watkins, S. Zorba, Y. Gao, and C. W. Tang, *Appl. Phys. Lett.* **81**, 2752 (2002).
- [101] H. Vázquez, Ph.D. thesis (2006).
- [102] N. Dori *et al.*, *Phys. Rev. B* **75**, 195208 (2006).
- [103] D. P. Chong, O. V. Gritsenko, and E. J. Baerends, *J. Chem. Phys.* **116**, 1760 (2002).
- [104] O. V. Gritsenko, B. Braïda, and E. J. Baerends, *J. Chem. Phys.* **119**, 1937 (2003).
- [105] M. Grüning, O. V. Gritsenko, S. J. A. van Gisbergen, and E. J. Baerends, *J. Chem. Phys.* **116**, 9591 (2002).
- [106] Y. M. Niquet and X. Gonze, *Phys. Rev. B* **70**, 245115 (2004).
- [107] M. Grüning, A. Marini, and A. Rubio, *J. Chem. Phys.* **124**, 154108 (2006).
- [108] J. C. Slater, *The Self-consistent Field for Molecules and Solids* (McGraw-Hill, New York, 1974).
- [109] J. R. Sabin, S. B. Trickey, S. P. Apell, and J. Oddershede, *Int. J. Quant. Chem.* **77**, 358 (2000).
- [110] E. V. Tsiper, Z. G. Soos, W. Gao, and A. Kahn, *Chem. Phys. Lett.* **360**, 47 (2002).
- [111] I. Hill, A. Kahn, Z. Soos, and J. R.A. Pascal, *Chem. Phys. Lett.* **327**, 181 (2000).
- [112] J. Kröger, H. Jensen, R. Berndt, R. Rurali, and N. Lorente, *Chem. Phys. Lett.* **438**, 249 (2007).
- [113] J. Tersoff, *Phys. Rev. Lett.* **52**, 465 (1984).
- [114] J. Tersoff, *Phys. Rev. B* **32**, 6968 (1985).
- [115] S. G. Louie and M. L. Cohen, *Phys. Rev. B* **13**, 2461 (1976).
- [116] N. D. Lang and A. R. Williams, *Phys. Rev. B* **18**, 616 (1978).
- [117] J. D. Jackson, *Classical Electrodynamics*, Wiley, New York (1975).

Summary

The rapidly developing field of organic electronics has stimulated intensive research into the fundamental electronic properties of molecular organic semiconductors and their interfaces with metal electrodes as well as insulating substrates. Theoretical and experimental studies are driven by potential applications where organic molecules constitute active materials in a wide range of electronic devices such as light-emitting diodes (LEDs), field-effect transistors (FETs), solar cells or biosensors. The thesis is motivated by the modeling of charge injection barriers from metallic contacts into organic materials. Experiments indicate that the energy barriers of electron or hole injection are determined by the formation of an interface dipole layer localized at first molecular layer. Such barriers can be extracted by monitoring the change in the work function, produced upon the deposition of the organic layer. We calculate such work functions using density functional theory (DFT).

The **Introduction** starts with a description of the main theoretical tool used for calculations, namely DFT. Then we present general ideas behind the pseudopotential and plane waves basis set approach, used to represent the Kohn-Sham DFT wave functions. The need for understanding electronic properties at metal-organic interfaces is motivated by a short description of a polymer light emitting diode (polyLED), as used in flat-panel displays. A discussion on interface Schottky barriers concludes the first chapter, defining the parameters that are used in later chapters.

Other general concepts or tools that are used to analyze the electronic properties of metal-organic interfaces, such as interface dipole layer, work function, adsorption energy, electron density difference or density of states, are explained throughout the following chapters.

The thesis is organized in two main parts. In **Part I** we study interfaces formed by self-assembled monolayers (SAMs) on metal surfaces, whereas in **Part II** we focus on interfaces formed by monolayers of π -conjugated molecules adsorbed on metal surfaces.

In **Chapter 2** we study interfaces formed by short chain alkylthiolate and fluorinated alkylthiolate monolayers of CH_3S , $\text{CH}_3\text{CH}_2\text{S}$ and CF_3S , $\text{CF}_3\text{CH}_2\text{S}$ respectively, chemisorbed on noble (111) metal surfaces of Ag, Au and Pt. The results show that adsorption of alkylthiolates decreases the work function, whereas adsorption of the fluorinated counterparts gives an increase in the metal work function. We show that the change in surface dipole that occurs upon adsorption of a self-assembled monolayer (SAM) is the result of two nearly independent contributions.

Bonds between the thiolate molecules and the metal surface generate an interface dipole μ_{chem} which is nearly independent of the molecule, but is a function of the metal. We find that in the case of a Ag substrate electron transfer occurs from the silver surface to the sulfur atoms of the SAMs. In the case of a Pt substrate, the electron transfer is opposite, i.e from the sulfur atoms to the Pt surface, whereas for the Au substrate very little electron transfer occurs. The interface dipole μ_{chem} tends to compensate for the difference between the work functions of the clean metal surfaces. A second contribution to the surface dipole is due to individual molecular dipoles, μ_{SAM} . The overall work function is thus determined by summing up these two contributions. The results show that it is possible to tune metal work functions using SAMs and that the work function shifts produced upon molecular adsorption can be as large as 2 eV.

Chapters 3 and 4 focuses on SAMs on Au and Ag surfaces respectively, where several structures and different packing densities are discussed. The work functions show a relatively weak dependence on the packing density. We show that increasing the packing density of the SAMs on the metal surface gives rise to a higher depolarization field in the SAMs. The effect is modeled as an effective dielectric constant in the molecular layer and opposes the increase in the metal work function due to the increase in the packing density. The main conclusions emphasized in **Chapter 2** also hold for these more complex structures.

In the second part of the thesis we study interfaces formed by π -conjugated organic molecules adsorbed on close-packed metal surfaces of Ca, Mg, Al, Ag and Au. Such molecules do not have a permanent dipole moment. By studying a range of metal surfaces and using different molecules, the position of the metal Fermi level and the positions of the molecular levels can be varied. Thus, their effect on the dipole layer formation at metal-organic interfaces can be analyzed. We find that the size and sign of the interface dipole is the result of two competing effects. A typical "pillow effect" due to the overlap of molecular and surface electrons wave functions is operative for adsorption of molecules on any metal surface pushing metal electrons out from the region of the occupied molecular orbitals into the metal, which reduces the work function. If the resulting work function is lower than the molecular LUMO level, electrons are donated from the metal surface to the molecule, populating the molecular LUMO level and pinning the work function at a constant value for a range of metal surfaces. Such effect gives a increase in the metal work function. The overall work function is determined by the balance between the two effects.

In **Chapter 5** we focus on PTCDA ($C_{22}H_8O_6$) and perylene ($C_{20}H_{12}$) molecules. For both molecules we find a crossover from a regime in which the work function is reduced by the pillow effect to a regime in which the work functions are pinned. Pinning is interpreted from electron transfer to the lowest unoccupied molecular orbital (LUMO) level, whereas the position of the crossover can be correlated with the position of the molecular LUMO. The study encompasses a theoretical model to describe the pinning behavior at metal-organic interfaces. Unpinning occurs in the case of very low work function metals when electrons are transferred from the metal surface up to the next unoccupied molecular orbital.

In **Chapter 6**, the interfaces formed by PTCDA, perylene and benzene on metal

surfaces are discussed in more detail. In particular, we find that the size of the interface dipoles is nearly independent of the exchange and correlation functionals used in calculations, namely GGA and LDA. We also evaluate the influence of the packing density of the molecules on the work function and find that this dependence is not negligible. The pillow effect discussed for the cases of PTCDA on Au and perylene on Au and Ag is demonstrated for interfaces formed by benzene (C_6H_6) monolayers adsorbed on surfaces ranging from the low metal work function of Ca (3.0 eV) to the high metal work function of Au (5.3 eV).

From the work done on several systems, we conclude that large interface dipoles can be formed at interfaces formed by π -conjugated organic molecules and metal surfaces. The interface dipoles influence the size of charge injection barriers. For good electron injection, small work function interfaces are required, whereas for small hole injection barriers, higher metal-organic work function systems are desirable.

List of publications

[1] Work functions of self-assembled monolayers on metal surfaces by first-principles calculations (**Chapter 2**)
P. C. Rusu and G. Brocks
Phys. Rev. B **74**, 073414 (2006)

[2] Surface dipoles and work functions of alkylthiolates and fluorinated alkylthiolates on Au(111) (**Chapter 3**)
P. C. Rusu and G. Brocks
J. Phys. Chem. B **110**, 22628 (2006)

[3] Dipole Formation at Interfaces of Alkylthiolate Self-assembled Monolayers and Ag(111) (**Chapter 4**)
P. C. Rusu, G. Giovannetti and G. Brocks
J. Phys. Chem. C **111**, 14448 (2007)

[4] Work function pinning at metal-organic interfaces (**Chapter 5**)
P. C. Rusu, G. Giovannetti, C. Weijtens, R. Coehoorn and G. Brocks
Phys. Rev. Lett. (submitted, 2007)

[5] Charge transfer and dipole formation at interfaces between metals and aromatic molecules (**Chapter 6**)
P. C. Rusu, G. Giovannetti, C. Weijtens, R. Coehoorn and G. Brocks
Phys. Rev. B (to be submitted)

Acknowledgments

There are a lot of factors and people who contributed to my path towards this Ph.D. thesis. Here I would like in few words to express my gratitude to the people who made this happening and to the people who made the last four and a half years enjoyable.

First I would like to thank the person who helped me the most and guided me through this Ph.D. project. Thank you Geert for always being there for me! Thank you for the discussions, for suggestions, for helping me out in papers, listening to my rehearsals or for posters. One of the things that I always liked is the way you look at things. You always mentioned first the positive points of my work, and then you nicely transferred the discussion, with a positive criticism, towards what needs to be done in order to improve it. I also want to say that I enjoyed every discussion we had regarding the work, sport or daily life. I remember that waiting more than an hour in the car during a traffic jam in Eindhoven was not so bad at all, but only funny. Thank you for everything.

I would like to thank you Paul for the chance you offered me by working in your group, in a nice and international environment. I'm so glad that I could meet so many nationalities. Thank you for your time that you spent listening to my talk rehearsals, thank you for your advices and the support that I have received from you from the beginning. I especially enjoyed the events that your wife Andrea and you organized in the beginning of each year or when you have welcomed a new CMS guy. Those evening were all very nice and I felt myself very welcome.

Next, I would like to thank Els, Gerrit, Enno and Theo. It was very nice to know all of you. Thank you Els for your help to get through the Dutch birocracy and much more. It was quite tough for couple of times when it came to the resident permit. Luckily the situation changed very favorable for me in the last year. I particularly enjoyed talking with you Gerrit. Because of you I managed to break my record in riding a bicycle. It happened when you took us for a barbecue that you organized. It was a very dangerous and winded road, not to mention that we climbed up to the highest point in Twente. Thus, an overall of 40 km that day, couple of beers and nice food ended with a muscular fever for a couple of days afterwards. :) Thank you Enno for helping me with the computer and the printer and for taking care of the cluster. Thank you Theo for advices and discussions.

It's been some time since I came to the CMS group. Meanwhile some people left, some fresh members came to the group this year, people that I've started to know

better and better. It's been a good time for me here and I want to thank you guys for everything. In the order that I met you... Thank you Victor, Mohand, Petr, Maciej, Anton, Illya, Volodymyr, Gianluca, Suleyman, Danny, Tulika, Pengxiang, Qinfang, Zhicheng, Dharendra and Sanjeev.

Particularly, I want to thank you Mohand for helping me with tons of linux problems, :) Victor for discussions regarding DFT codes and Petr for scientific and daily discussions. It's nice to share the same office with you. Spasiba!

Thanks Gianluca for helping me with several molecular calculations. Thank you Danny for VASP discussions and also for your help for the many times I bothered you regarding Dutch translations and Anton for making the cluster working and keeping it alive. I would also want to thank all of you for the times we played football or basketball or the times that we drank beers together!

I would like to thank the members of the PPM project who greatly helped me during this Ph.D. with discussions, advices and new ideas. I would like to thank Rob de Grot, Gilles de Wijs, Matthé Uijtewaal, Peter Bobbert, Chris Meisel, Christ Weijtens and Reinder Coehoorn. Although it's hard to think about this, I would like to mention that Chris Meisel who started his project in Eindhoven at the same time with me in 2003 tragically lost his life in 2005. I remember him as being a very open and friendly person. This was by far the worst news during my Ph.D.

I would also like to thank my former teachers and professors from Craiova who largely contributed to my professional carrier.

Many thanks to three families that I met during my stay in Enschede: Mohand & Dalila & Masin, Victor & Andreea & Vlad and Dela & Loredana. Thanks guys for the nice evenings that we spent together! Thank you for your friendship! I really enjoyed the tennis, basketball or football games that I played with you or against you Dela, the F1 races or the football games that we watched together. Thank you Mohand and Victor for the concerts we've been together. All of these made the time spent here so nice!

I would specially like to thank my good old friends for not letting the distance to stay in our way. It's not all about work so thank you for the time we spent together during week-ends or holidays. Thanks to the Internet I could be very much in touch with you whether you live in Netherlands, Germany, Belgium or Romania. Thank you for your friendship! I have to say that I feel very lucky to have such good friends. Many thanks to Silviu and Irina, Mircea, Vasi, Robert and Marcela, Adi, Fred.

For sure I couldn't be here without the permanent support and love of my parents and my brother. I can not thank you enough for everything! (Cu siguranta nu as fi ajuns aici fara iubirea si suportul permanent al parintilor si fratelui meu. Nu pot sa va multumesc indeajuns pentru tot!)

In the end, I would like to thank my girlfriend Luiza. Thank you for the priceless support and love that you've offered me from the very beginning. You've made my life so special! Besides you everything becomes easier to realize.

Enschede, September 2007

Paul Rusu

Curriculum Vitae

Name: Paul Constantin Rusu
Date of birth: April 3, 1979
Place of birth: Cetate, Dolj, Romania

EDUCATION

- 2003–2007:** **Ph.D.** in Computational Solid State Physics,
University of Twente, The Netherlands
Research project: "Metal - Organic Interfaces"
Computational Materials Science group (CMS),
Faculty of Science and Technology
Supervision: dr. G. Brocks and prof. dr. P. J. Kelly
- 2002:** **Postgraduate Program:** "Advanced Studies in Applied Computer
Science", Free University of Brussels, Belgium
- 2001:** Scholarship in the framework of Socrates/Erasmus Program,
Catholic University of Leuven, Belgium
Research project: "Neutrino oscillations, atmospheric neutrinos and
Super-Kamiokande experiment"
Faculty of Physics, Department of Particle Physics
Supervision: prof. dr. Raymond Gastmans
- 1997–2001:** **Bachelor of Science (B.Sc.)** in Physics,
University of Craiova, Romania